

A dissertation submitted to the
BAYREUTH GRADUATE SCHOOL OF MATHEMATICAL AND NATURAL SCIENCES
UNIVERSITY OF BAYREUTH

to attain the academic degree of
DOCTOR OF NATURAL SCIENCE (DR. RER. NAT.)

**Ecosystem-atmosphere exchange
of carbon dioxide and water vapour
in typical East-Asian croplands**

PENG ZHAO
M.Sc. Environmental Sciences

born 7 April, 1979
in Hebi, China

Bayreuth, 2014

supervised by DR. JOHANNES LÜERS

**Ecosystem-atmosphere exchange
of carbon dioxide and water vapour
in typical East-Asian croplands**

PENG ZHAO

supervised by DR. JOHANNES LÜERS

This doctoral thesis was prepared at the Department of Micrometeorology at the University of Bayreuth from July 2009 until March 2014. It was supervised by Dr. Johannes Lüers.

This is a full reprint of the dissertation submitted to obtain the academic degree of Doctor of Natural Sciences (Dr. rer. nat.) and approved by the Bayreuth Graduate School of Mathematical and Natural Sciences (BayNAT) of the University of Bayreuth.

Date of submission: 28.03.2014

Date of defence: 09.07.2014

Acting director: Prof. Dr. Franz Xaver Schmid

Doctoral committee:

PD Dr. Johannes Lüers	(1st reviewer)
Prof. Dr. Andreas Held	(2nd reviewer)
Prof. Dr. Bernd Huwe	(chairman)
Prof. John Tenhunen, Ph.D.	

Acknowledgement

I would like to greatly thank those people who have provided me their supports during my PhD study.

First of all I express my heartfelt gratitude to my mentors, who are:

my supervisor, Dr. Johannes Lüers, for stimulating my interest in this research topic, for his persistent interests in the results and countless productive discussions with enthusiasm besides giving me lots of freedom to develop my own ideas;

Prof. Dr. Thomas Foken, for all the knowledge he has generously shared with me, and for his invaluable comments and discussions on my publications and dissertation;

Prof. Dr. John Tenhunen, for his great supports on the activities including field campaigns, workshops, and excursions, which expanded my scientific horizon.

I would like to extend my appreciation to my colleagues in the Department of Micrometeorology, Univ. Bayreuth, especially Johannes Olesch for his technical support, Dr. Wolfgang Babel for his translation of the summary chapter into German, Michael Riederer, Dr. Doojdao Charuchittipan, Dr. Rafael Eigenmann, Dr. Andrei Serafimovich, Tobias Biermann, Jörg Hübner, Dr. Katharina Köck, Dr. Lukas Siebicke, for sharing their programming scripts; and my colleagues in TERRECO project, especially Bora Lee, Miloslav Belorid, Steve Lindner, Margarete Wartinger, and Dr. Jea-Chul Kim for their help in the field campaigns, and Bumsuk Seo for providing GIS data. Financial support funded by the German Research Foundation (DFG), as well as the Graduate School and the Department of Micrometeorology, Univ. Bayreuth, is greatly appreciated.

Last but not the least, I would like to thank my family — Lei, Ruhan, and Ruxuan, for their love, encouragement, and patience.

Summary

Agricultural areas comprise a large portion of the land surface of the earth. Under the current climate and environmental changes, the role of cropland ecosystems in the surface-atmosphere energy and matter exchange has drawn a lot of attention. This thesis investigated the potential change on ecosystem-atmosphere exchange of heat, water vapour and carbon dioxide if crop species planted or irrigation management is changed in croplands. Improvement of the Penman-Monteith model to simulate evapotranspiration and light-response model to simulate carbon dioxide flux for croplands is studied. Field campaigns were carried out in an irrigated rice field and a non-irrigated potato field in an intensively managed agricultural area in Korea Peninsula in 2010 and 2011. The eddy-covariance technique was used to observe net ecosystem carbon dioxide exchange and energy fluxes of sensible and latent heat with additional measurements of meteorological variables and biomass change.

Results show that the conventional Penman-Monteith approach which estimates the stomatal resistance as a function of single leaf stomatal resistance and leaf area index performs well for the estimation of evapotranspiration when the vegetation is fully developed in the potato field. In the case of evaporation-dominated croplands, i.e. the rice field with standing water or the potato field with small leaf area index in this study, it is shown that the stomatal resistance should be estimated as a function of meteorological variables rather than leaf area index.

The study on the light response function indicates that the primary cause of seasonal change in gross primary productivity was the change in leaf area index during the whole growing season under the summer monsoonal condition. Thus, a site-specific time window approach could significantly improve the model performance. In its standard form, however, the light response function does not account for leaf area index changes. In order to simulate longer time series, which is needed for filling large gaps in the observations, a new leaf-light response function is proposed.

A significant change in ecosystem-atmosphere exchange of heat, water vapour and carbon dioxide is found if irrigation management is changed. The non-irrigated potato field had 140 % more sensible heat and 30 % less latent heat than the nearby irrigated rice field. The difference in evapotranspiration between these two fields was mostly attributed to less evaporation (rather than transpiration) in the potato field than in the rice field. The seasonal sum of carbon dioxide flux was 12 % less for gross primary productivity, 7 % less for ecosystem respiration, and 20% less for net ecosystem exchange in the potato field than in the rice field. The rice field acted as a sink of carbon dioxide through the whole season, while the potato field turned from a sink to a slight source at the late growing stage when the above-ground green biomass disappeared. Besides the decline in solar radiation and the warm conditions in summer monsoon, the enhancement of ecosystem respiration caused by the large amount and the rapid growth rate of the biomass is suggested to be a cause of the mid-season depression in net ecosystem exchange.

Zusammenfassung

Landwirtschaftliche Nutzflächen nehmen einen großen Teil der Landoberfläche der Erde ein. Im Hinblick auf den gegenwärtigen globalen Wandel steht vor allem das Ackerland als Ökosystem durch seinen Einfluss auf den Energie- und Stoffaustausch zwischen Landoberfläche und Atmosphäre im Fokus. Diese Arbeit untersucht die Auswirkungen des Anbaus verschiedener Feldfrüchte auf den Austausch von Wärme, Wasser sowie Kohlendioxid zwischen Oberfläche und Atmosphäre unter Berücksichtigung des Bewässerungsmanagements. Dabei wurden Verbesserungen am Penman-Monteith Modell zur Simulation der Verdunstung sowie an der gebräuchlichen Michaelis-Menten-Beziehung zwischen Photosynthese und Einstrahlung zur Modellierung der Kohlendioxid-Aufnahme der Kulturpflanzen vorgenommen. Die Ergebnisse beruhen auf Messkampagnen, die 2010 und 2011 über einem bewässerten Reisfeld sowie einem unbewässerten Kartoffelacker in einem landwirtschaftlich intensiv genutzten Gebiet auf der koreanischen Halbinsel durchgeführt wurden. Hierbei wurden der fühlbare Wärmestrom, die Verdunstung und der Netto-Ökosystem-Austausch (net ecosystem exchange) mit der Eddy-Kovarianz-Methode bestimmt, sowie zusätzliche meteorologische Standardgrößen und Daten zur Biomasse erhoben.

Es konnte gezeigt werden, dass der übliche Ansatz bei Penman-Monteith, den stomatären Gesamtwiderstand als Widerstand des Einzelblattes, skaliert durch den Blattflächenindex zu parametrisieren, bei voll ausgebildetem Bewuchs im Kartoffelfeld eine gute Abschätzung der Verdunstung (Evapotranspiration) liefert. Überwiegt aber die Evaporation, wie zum Beispiel über der stehenden Wasserfläche des Reisfeldes, sowie über dem Kartoffelacker bei geringem Bewuchs, ist der Blattflächenindex kein geeigneter Parameter mehr. Dieses Problem kann behoben werden, wenn der stomatäre Widerstand durch meteorologische Größen bestimmt wird.

Die Untersuchung der Photosynthese-Einstrahlungs-Beziehung zeigte, dass der Trend der Bruttoprimärproduktion während der Vegetationsperiode unter monsunischem Einfluss durch den Blattflächenindex bestimmt wird. Dies wird in der gebräuchlichen Form der Beziehung

nicht berücksichtigt. Durch standort-spezifische Anpassung des Zeitfensters für die Bestimmung der Modellparameter können die Ergebnisse der Modellierung jedoch signifikant verbessert werden. Zur Modellierung längerer Zeiträume, wie es beim Füllen größerer Datenlücken notwendig ist, wird daher eine veränderte Blattfläche-Photosynthese-Einstrahlungs-Beziehung vorgeschlagen.

Eine Veränderung im Management der Bewässerung ruft eine signifikante Änderung im Austausch von Wärme, Wasser und Kohlendioxid hervor. Der unbewässerte Kartoffelacker zeigt gegenüber dem bewässerten Reisfeld einen um 140 % erhöhten fühlbaren Wärmestrom und eine um 30 % verringerte Verdunstung, was in erster Linie auf eine Verringerung der Evaporation, nicht der Transpiration zurückzuführen ist. In der Summe über die Wachstumsperiode ist der Kohlendioxidaustausch auf dem Kartoffelfeld geringer, und zwar um 12 % für die Bruttoprimärproduktion, um 7 % für die Respiration, und um 20 % für den Netto-Ökosystem-Austausch. Während das Reisfeld über die gesamte Wachstumsperiode eine Kohlenstoffsенке darstellt, wandelt sich der Kartoffelacker von einer Senke zu einer Quelle, sobald die oberirdische Biomasse abstirbt. Neben verringerter Globalstrahlung und den warmen Bedingungen während des Sommer-Monsuns wird der gezeigte Einbruch des Netto-Ökosystem-Austausches in der Mitte der Monsunzeit durch eine erhöhte Respiration aufgrund der hohen vorhandenen Biomasse, sowie der hohen Wachstumsraten verursacht.

Contents

Acknowledgement	iii
Summary	v
Zusammenfassung	vii
Nomenclature	xiv
1 Introduction	1
1.1 Background	1
1.2 Motivation	2
1.2.1 Croplands	2
1.2.2 Ecosystem evapotranspiration in croplands	5
1.2.3 Carbon dioxide flux in croplands	6
1.3 Objectives	8
2 Materials and Methods	11
2.1 Research sites	11
2.1.1 Location	11
2.1.2 Land-use of the study area	13
2.1.3 Field campaigns	14
2.2 Measurement methods	16
2.2.1 Weather observation	16
2.2.2 Biomass measurement	17
2.2.3 Eddy-covariance measurement	18
2.3 Data processing	19
2.3.1 Data quality control	19
2.3.2 Data gap-filling	21
2.3.3 Canopy energy components	22

2.3.4	Correction for energy balance closure	23
2.3.5	Partitioning of evapotranspiration	25
2.4	Models	25
2.4.1	Penman-Monteith equation	25
2.4.2	Parameterization of the stomatal resistance	26
2.4.3	Sensitivity test	28
2.4.4	Partitioning of NEE	29
2.4.5	Temperature-dependence function of ecosystem respiration	30
2.4.6	Leaf and light response of GPP	30
2.4.7	Evaluation of simulations	32
3	Meteorological and surface parameters	34
3.1	Weather conditions	34
3.2	Internal boundary layer and footprint	36
3.3	Biomass development	39
4	Ecosystem evapotranspiration and energy components	42
4.1	Energy balance	42
4.2	Diurnal variation	45
4.3	Seasonal variation	46
4.4	Penman-Monteith model and stomatal resistance	50
4.4.1	Sensitivity coefficients	50
4.4.2	PM-FAO model	52
4.4.3	PM-KP model	56
5	Carbon dioxide exchange	60
5.1	Time courses	60
5.2	Respiration	63
5.3	Photosynthetic assimilation	65
5.3.1	Light impact and time window approach	65
5.3.2	New leaf-light response function	68
5.3.3	Sky condition impact	72
5.3.4	Temperature impact	74
5.3.5	Humidity impact	77
6	Conclusions	79

List of Figures

2.1	Research sites at Haeon Basin on the Korean Peninsula.	12
2.2	Variations of monthly meteorological variables in Haeon Basin.	13
2.3	Photographs of the research sites.	14
3.1	Meteorological observations during the crop growing seasons in 2010 and 2011.	34
3.2	Footprint analysis for the research sites in 2010.	37
3.3	Biomass development of rice and potato.	40
3.4	Panoramas of the research sites.	41
4.1	Hovmöller diagrams of observed mesoscale fluxes of sensible heat and latent heat.	43
4.2	Wavelet cross-scalogram of sensible and latent heat fluxes at the rice and potato sites.	44
4.3	Diurnal courses of net radiation, ground heat flux, sensible and latent heat fluxes.	45
4.4	Seasonal variation of daily net radiation, latent heat flux, precipitation, and Bowen ratio in 2010.	47
4.5	Seasonal variation of daily evapotranspiration, evaporation, and transpiration in the potato field.	48
4.6	Diurnal and seasonal patterns of Penman-Monteith model sensitivity coefficients.	51
4.7	Sensitivity graphs for PM-FAO modelled Q_E to modifications in r_s , p_m , and p_h	53
4.8	Performance of PM-FAO model in the potato field.	54
4.9	Performance of PM-FAO model in the rice field.	55
4.10	Statistical distribution of the regression coefficients of the KP equation.	57
4.11	Sensitivity graphs for PM-KP modelled Q_E to modifications in KP coefficients.	58
4.12	Performance of PM-KP model in the potato field.	59
5.1	Hovmöller diagrams of GPP, R_{eco} , and NEE in the growing season.	61
5.2	Seasonal course of R_{ref} , dry weight, and growth rate of above-ground biomass.	64
5.3	Taylor diagrams for the performances of simulations for GPP applying the time-window scheme.	66

5.4	Relationship of the coefficients α and β against LAI.	67
5.5	Leaf-light response of GPP in the potato field.	70
5.6	Comparison between derived GPP (from observed NEE and simulated R_{eco}) and simulated GPP (by the leaf-light response function).	71
5.7	Taylor diagrams for the performances of simulations for GPP applying the temperature binning scheme.	75
5.8	Temporal distribution of temperature measurements within temperature classes.	76
5.9	Mean diurnal cycles of solar radiation, VPD, derived GPP and simulated GPP by the time-window scheme without VPD and with VPD-factor for the potato field during the early growing season.	77
5.10	Boxplot of VPD during each measurement period.	78

List of Tables

1.1	Literature about the most common gap-filling routines for NEE.	7
2.1	Information about the research sites.	15
2.2	Water depth in the rice field.	15
2.3	Biomass sampling dates and sample numbers.	18
3.1	Flux contribution from the target land use type in wind direction and stability classes.	38
4.1	Partitioning of evapotranspiration.	49
4.2	Calibration coefficients of KP model.	57
5.1	Comparison between the simulation and observation of NEE, including MAE, RMSE, I , and R	67
5.2	Modelled parameters of the light response function in LAI intervals.	69
5.3	Modelled parameters of the LAI response function in solar radiation intervals.	69
6.1	Application of the PM-FAO model and the PM-KP model for croplands.	80
6.2	Seasonal budgets of energy, water and carbon dioxide exchange of irrigated crop and non-irrigated crop.	82

Nomenclature

Abbreviations

AGC	automatic gain control
DAP	day after planting/transplanting
DOY	day of the year: DOY 1 = Jan. 1
EBC	energy balance closure
EBC-Bo	energy balance correction with Bowen ratio approach
EBC-HB	energy balance correction with buoyancy flux ratio approach
EC	eddy-covariance
ET	evapotranspiration
EV	evaporation
FAO	Food and Agriculture Organization
GLUE	Generalized Likelihood Uncertainty Estimation
GPP	gross primary productivity
KP	Katerji-Perrier
LAI	leaf area index
MAE	mean absolute error
NEE	net ecosystem exchange of carbon dioxide
NRMSE	normalized root mean square error
PM	Penman-Monteith
RH	relative humidity
RMSE	root mean square error
SD	standard deviation
SE	standard error
TR	transpiration
TW	time window
VPD	vapour pressure deficit

Symbols

a_1, a_2, \dots, a_n	model coefficients (general)
Bo	Bowen ratio, dimensionless
c_p	specific heat of air, $\text{J kg}^{-1} \text{K}^{-1}$
c_w	specific heat capacity of water, $\text{J kg}^{-1} \text{K}^{-1}$
d	displacement height, m
E_0	temperature sensitivity of Lloyd-Taylor function, K
e_s	saturated vapour pressure, hPa
f	function (general)
h	vegetation height, m
I	index of agreement, dimensionless
k	light distinct coefficient, dimensionless
n_r	random number, dimensionless
p_G	empirical ratio between ground heat flux and net radiation, dimensionless
Q_A	available energy flux, W m^{-2}
Q_E	latent heat flux, W m^{-2}
Q_G	ground heat flux, W m^{-2}
Q_H	sensible heat flux, W m^{-2}
ΔQ	stored energy in the canopy, W m^{-2}
R	correlation coefficient, dimensionless
R^2	coefficient of determination, dimensionless
R_{eco}	ecosystem respiratory flux, $\mu\text{mol m}^{-2} \text{s}^{-1}$
Res	residual energy, W m^{-2}
R_g	global radiation, W m^{-2}
R_n	net radiation, W m^{-2}
R_{ref}	ecosystem respiratory flux at a reference temperature, $\mu\text{mol m}^{-2} \text{s}^{-1}$
r_a	aerodynamic resistance, s m^{-1}
r_s	stomatal resistance, s m^{-1}
r_{si}	stomatal resistance of a single well-illuminated leaf, s m^{-1}
S_i	non-dimensional relative sensitivity coefficient for the i -th variable
s_c	temperature dependence of specific humidity at saturation, $\text{kg kg}^{-1} \text{K}^{-1}$
T	temperature (general), K
T_{ref}	reference temperature, K

NOMENCLATURE

T_w	water temperature, °C
t	temperature (general), °C
u	wind speed, m s^{-1}
u^*	friction velocity, m s^{-1}
x	fetch, m
z	measurement height, m
z_{oh}	roughness height for water vapour, m
z_{om}	roughness height for momentum, m
z_w	water depth, m
α	initial slope of Michaelis-Menten function, $\mu\text{mol s}^{-1} \text{W}^{-1}$
α'	initial slope of leaf-light response function, $\mu\text{mol s}^{-1} \text{W}^{-1}$
β	saturated carbon dioxide uptake rate, $\mu\text{mol m}^{-2} \text{s}^{-1}$
β'	specific saturated carbon dioxide uptake rate, $\mu\text{mol m}^{-2} \text{s}^{-1}$
γ	psychrometric constant, hPa K^{-1}
λ	heat of evaporation for water, J kg^{-1}
κ	Von-Kármán constant, dimensionless
ρ	air density, kg m^{-3}
ρ_w	water density, kg m^{-3}
ζ	stability parameter, dimensionless

1 Introduction

1.1 Background

The increase of the world economic activities nowadays results in the rising of carbon dioxide and other green house gases, which contributes significantly to climate change (IPCC, 2013). Meanwhile, the increasing human demand for life leads to land surface changes (e.g. many forests changed into croplands and croplands into suburbs). These changes can have substantial influence on the capacity of terrestrial ecosystems to assimilate carbon and to evapotranspire water, and can disturb other biogeochemical cycles by changes in leaf area, surface albedo, roughness, net radiation, and Bowen ratio (Foley et al., 2005). Furthermore, these biogeophysical effects can undoubtedly have feedback to the climate system. Studies on the ecosystem-atmosphere exchanges of carbon dioxide and water vapour, and their interactions with the physical climate and physiological functioning of plants and ecosystems have therefore drawn a lot of attention (Baldocchi et al., 2001).

As a useful and effective tool, the eddy-covariance (EC) technique has been used to continuously and directly quantify land surface fluxes of heat, water vapour, and carbon dioxide (Baldocchi, 2003). The EC method was proposed in the mid-twentieth century (Montgomery, 1948), developed rapidly in the 1980s, and became widely utilized since the 1990s (Foken et al., 2012a). It is applied across all major climate classes of terrestrial surface and biomes including forests, grasslands, wetlands, tundra, and croplands (Baldocchi et al., 2001). The EC technique provides the information of how momentum, energy and matter are transported between surface and atmosphere. Therefore, many disciplines (e.g. meteorology, biology, and geology) in natural sciences are intersected in the study on the EC method (Oliphant, 2012). Nowadays, studies on related topics, such as the energy balance closure, the quality control, flux partitioning and gap-filling, are still in progress (Baldocchi, 2003). As continuous temporal and spatial observation is difficult and expensive, determination of major controls on ecosystem exchange of carbon dioxide and water is important and necessary to establish eco-

logical and hydrological models. Performances of these models must be evaluated and their parameters must be calibrated (Sumner and Jacobs, 2005).

1.2 Motivation

1.2.1 Croplands

Contemporary cultivated areas comprise 24 % of the terrestrial surface of the earth (Millennium Ecosystem Assessment, 2005). In order to meet the demand of the increasing human population, the intensification of crop cultivation is inevitable and has been causing rapid land use and cover change for economic development (Alberto et al., 2009). The world grain harvest has doubled in the past four decades owing to the changing land-use practices including a 12 % increase in world cropland area with a 70 % increase in irrigated cropland area (Foley et al., 2005). On the other hand, irrigation has played a major role in the improvement of global food production. 51 % of the world rice area is occupied by irrigated rice with 75 % of world rice production (IRRI, 2009). Nevertheless, a lot of difficulties, such as the generally profligate use of water in irrigation, appear in irrigated agriculture (Walker, 1989). The irrigation management is threatened by the declining availability and the increasing scarcity of water due to more frequent occurrence of extreme heat and drought, resulting in the rise of irrigation costs (Alberto et al., 2009). This can have marked influence on farmers' decisions on irrigation methods or crop species for irrigated and non-irrigated croplands. As agricultural management practices have changed markedly during the past four decades (Cassman et al., 2002), the shift of land use from permanently flooded to aerobic or dry conditions will have profound effects on the energy and matter exchanges in croplands.

These managed croplands have great potential to impart wide-ranging changes to the global climate system and global biogeochemical cycles. However, the representation of varied crop dynamics is often approximated rather than precisely estimated in many biosphere-atmosphere modelling efforts (Kucharik and Twine, 2007). Other proxy potential vegetation biomes, such as grasslands, are commonly used based on their structural and physiological similarities, along with comparable growing seasons (Osborne et al., 2007). The carbon estimate for croplands is more uncertain than for other land-use types (Janssens et al., 2003; Ciais et al., 2010). The understanding of ecosystem-atmosphere exchange is limited partly due to missing data and the choice of gap-filling algorithms (Falge et al., 2001). Croplands

must therefore be further studied and included in efforts to estimate, interpret and regulate the global carbon cycle and terrestrial energy budget.

Unlike other managed ecosystems such as forests, a cropland ecosystem has its own special features and requires different considerations to explain carbon dioxide and water vapour exchange.

Firstly, crops have short growing seasons. The strong seasonal dependence on environmental conditions (e.g. net radiation, temperature) is one of the major factors that limit the crop growth (Osborne et al., 2010). Compared with evergreen forests, one entire year of observation in annual croplands can provide a flux data-set containing growth information for only several months or even shorter, resulting in less flux data for different crop species.

Secondly, vegetation in croplands changes rapidly over the course of the growing season. The patterns of the seasonal change in croplands are much more irregular and fluctuate than those of many natural ecosystems with stable vegetation cover (Kutsch et al., 2010). For example, rice paddies can have almost nothing of living biomass at the beginning of the growing season, but can have a LAI of six in the middle, which decreases to two at the end (Saito et al., 2005). The fast change of surface vegetation can have great impacts on the variation of energy and matter exchange, which introduces difficulties to the observation and simulation, especially to the gap-filling for the completeness of observation that is important for the estimation of daily and annual sum (Papale, 2012).

Thirdly, croplands are highly disturbed by human activities. According to environmental, economic, political or regulatory considerations, the grown species can vary significantly from year to year, and the fallow period is largely dependent on the species and seasons. Croplands are intensively managed with a wide diversity of cultivation practices (e.g. planting or transplanting, plowing, irrigation, manure amendment, and harvest) and manipulated by farmers' decisions across both regions and time. These human activities can greatly influence the energy and matter exchange between the ecosystem and the atmosphere, and make it difficult to find a universal strategy encompassing the site-specific year-to-year variation. Land use change in croplands has also a great influence on the budget of energy, water and carbon due to changes in land cover conditions and vegetation species. Currently, only a few studies have focused on the effect of land use change on the ecosystem-atmosphere exchange in croplands. Sakai et al. (2004) reported the strong influence on the diurnal and seasonal variation in heat, water and carbon exchange when land use was converted from pasture to rice field in an Amazonian agricultural field. A study in northeastern China by Zhao et al. (2008) found that

the land use change of marshland to rice field leads to an enhancement in evapotranspiration and decrease in sensible heat flux, while the effects of the change to dryland soybean has a strong dependence on environmental and biological conditions such as net radiation, leaf area index (LAI), air temperature, and vapour pressure deficit (VPD). As advanced water-saving techniques are developed, comparisons between the traditional flooded rice and the aerobic rice (a new type of rice variety planted in non-flooded soil condition) showed that the aerobic rice had 45 – 48 % more sensible heat flux while the flooded rice field had 19 – 20 % more latent heat flux and 50 % more GPP in the Philippines, and suggested that more studies are needed to clarify carbon flux dynamics of different crop systems (Alberto et al., 2009, 2011). Therefore, it could be expected that the shift of farmers' decision on crop species and irrigation management would have impacts on the surface energy and matter budget. The lack of detailed comparisons between irrigated and non-irrigated crops requires further research on the influencing factors of agroecosystem-atmosphere exchange.

Fourthly, croplands are normally patchy with a mixture of crop species. Fundamental differences in plant physiology and development for various species results in mixed information of the energy and matter exchange captured by eddy- covariance observation. The difficulty in selecting research site locations and separating crop species limits the understanding of the behaviours of individual crop species.

Lastly, croplands encompass a broad geographic area including various soil conditions and climate zones. The controlling factors of the energy and matter exchange are complex and difficult to study even for the same crop species. It is often required to adopt site-specific approaches for estimating the energy and matter exchange because of these differences (Osborne et al., 2010).

While the eddy-covariance technique is mostly deployed at forest sites and also frequently used in savannah and grasslands, only a few studies have focused on croplands (Béziat et al., 2009). In Asia, only a few observations employing the eddy-covariance technique were carried out at irrigated rice fields in Japan (Saito et al., 2005; Miyata et al., 2000, 2005), southern Korea (Moon et al., 2003), Bangladesh (Hossen et al., 2007), and Philippines (Alberto et al., 2009) to study the seasonal and inter-annual variations in carbon dioxide fluxes. The fluxes of carbon dioxide and water in general from croplands are less understood than those from other ecosystems such as forests and grasslands (Prescher et al., 2010).

1.2.2 Ecosystem evapotranspiration in croplands

Ecosystem evapotranspiration (ET) comprises of soil/water surface evaporation, plant transpiration, and the evaporation from intercepted rainfall. Studies on ET could help understand the water cycle on the earth. As a majority share (over 90 %) of the water budget in agricultural ecosystems is typically contributed by ET, accurate quantification of crop ET by observation or models is critical for the improvement of irrigation scheduling and water resource planning (Kang et al., 2008; Rana and Katerji, 2000; Ding et al., 2013).

Many models have been developed for the estimation of ET (see the review by Wang and Dickinson, 2012). As an accurate calculation, Penman-Monteith (PM) function (Monteith, 1965) has been commonly used as a well-known method. Most required inputs of the PM method, such as the available energy, the water vapour pressure deficit, air temperature, and aerodynamic resistance, can be measured or derived from the routine weather observation and eddy-covariance measurement, except the surface resistance (r_s), which is an effective parameter that controls the evaporation from the soil and transpiration from the plant canopy.

The determination of the surface resistance is one of the major difficulties in application of the PM method (Cleugh et al., 2007; Wang and Dickinson, 2012). For simplicity's sake, the Food and Agriculture Organization (FAO) suggested that the surface resistance can be estimated as a quotient of mean stomatal resistance and active LAI (Allen et al., 1998), which is widely applied. This FAO approach takes r_s as a constant when LAI does not change. However, different opinions exist in the community, because it does not take into consideration the dependence of r_s on meteorological variables (e.g. Katerji and Rana, 2006). Therefore, Katerji and Perrier (1983) proposed a simple linear model (KP approach) accounting for the influence of meteorological variables and aerodynamic resistance on r_s . Compared with other methods, the KP approach has the advantage of its simplicity (i.e. the calibration requires no more data than the routine weather observation and eddy-covariance measurement) and its good performance across a variety of croplands. Alves and Pereira (2000) noted that the KP approach performs well for well-watered crops and for short periods of time within which the surface vegetation and weather do not change much, but Katerji and Rana (2006) reported that the KP approach has also been adapted to soil water stress conditions and to the surface fully and partially covered by crops. It could be a good practice to compare PM-FAO and PM-KP approaches in irrigated and non-irrigated crops to find a more robust method to estimate ET for croplands under other climate conditions.

1.2.3 Carbon dioxide flux in croplands

Agricultural activities have a rising contribution to the global anthropogenic emissions of greenhouse gases (IPCC, 2013). The increase in crop yields leads to the change in the carbon dioxide exchange of agro-ecosystems. The net ecosystem exchange of carbon dioxide (NEE) between croplands and atmosphere is comprised of the fluxes of photosynthetic assimilation (gross primary productivity, GPP) and respiratory efflux (R_{eco}). Accurate observation of NEE is very important to estimate the ecosystem carbon balance, from which R_{eco} and GPP can be partitioned. These components are influenced by different environmental conditions, such as the growing stages of crops, the light response of crops, air or soil temperature, vapour pressure deficit (VPD), and soil water availability, which are considered in many statistical and empirical approaches especially for the data gap-filling (Greco and Baldocchi, 1996; Falge et al., 2001).

As light is the key external driver of photosynthesis assimilation, light response functions are often applied to the estimation of daytime GPP or NEE. Many (including linear, parabolic and hyperbolic) types of light response functions exist, among which the Michaelis-Menten function shows the best overall performance for daytime estimation (Falge et al., 2001). The Michaelis-Menten function (Michaelis and Menten, 1913) is a hyperbolic function, describing the potential shapes of ecosystem light response semi-empirically. It has been used in many studies for data gap-filling of ecosystem carbon dioxide exchange (e.g. Falge et al., 2001; Ruppert et al., 2006; Moffat et al., 2007; Lasslop et al., 2010).

However, only the light response is insufficient to simulate GPP due to the complicated influence by other factors such as temperature, humidity, and vegetation condition, which are therefore included to improve the performance of the simulation. For instance, measurements could be grouped into temperature classes to determine individual light response parameters in each class in order to test the influence of temperature on GPP (Falge et al., 2001; Ruppert et al., 2006). This temperature grouping approach is less frequently used nowadays but the reason has not been addressed. Vapour pressure deficit (VPD) is suggested to be introduced into Michaelis-Menten function to account for the dependence of GPP on air humidity (Lasslop et al., 2010), but in humid areas this influence might play a minor role. The time window approach is a standard approach, often used not only in the light response function, but also in most of existing gap-filling techniques, such as mean diurnal variation and look-up table (see Table 1.1). It segments the whole season into growing stages by a certain time window. The vegetation is assumed to be constant within each stage so that the parameterization

Table 1.1: Literature about the most common gap-filling routines for NEE.

References	Surface type	Site location	Binning approaches	Vegetation development	Site number	Data-set length
Falge et al. (2001)	forests, crops (wheat, soybean), and forest	Europe, America	time window (2 or 3 months), temperature binning	N.A.	19	1 to 2 years
Hollinger et al. (2004)	forest	America	time window (1 month)	N.A.	2	7 years
Desai et al. (2005)	forest	America	time window (> 1 month)	LAI = 5.3	2	2 years
Reichstein et al. (2005)	forests, shrub, and crops (corn, soy-bean)	Europe, America	time window (± 7 or ± 14 days)	N.A.	16	1 year
Papale et al. (2006)	forests	Europe	time window (± 7 or ± 14 days)	N.A.	8	1 to 2 years
Ruppert et al. (2006)	forest	Europe	temperature binning	PAI = 5.2	1	1 year
Stoy et al. (2006)	forests, grass	America	time window (1 month)	LAI < 7	3	5 years
Anmann et al. (2007)	grassland (rapid change)	Europe	time window (5 days)	LAI ≤ 7	1	3 years
Moffat et al. (2007)	forests	Europe	time window (1 or 2 months)	N.A.	6	1 to 2 years
Noormets et al. (2007)	forests	America	time window (1 month)	LAI = 0.2 to 3.86	5	0.5 year
Richardson and Hollinger (2007)	forests	Europe, America	time window (1 month)	N.A.	6	1 to 9 years
Xing et al. (2007)	forests	America	time window (9 days)	LAI = 2.1 to 8.4	8	growing seasons within 1 year
Lasslop et al. (2010)	forests, crops (corn or soybean), grass, and wet Savanna	Europe, America, Africa	time window (4 days)	N.A.	8	1 year
Wu et al. (2012) this study	forest croplands (potato, rice)	Europe Asia	time window (4 days) time window (4 days for potato, 8 days for rice), temperature binning	N.A. LAI = 0 to 5.7 (potato) LAI = 0.1 to 3.2 (rice)	1 2	13 years growing seasons within 1 year

can be simplified. However, the width of the time windows has been determined empirically, ranging from days to months. Further investigation on the optimal time window could possibly improve the simulation by the Michaelis-Menten function for croplands.

The time window approach works well for forest and meadow sites where biomass develops slowly during growing season and long-term measurements have been conducted. However, it could cause problems if there is no long-time dataset or if the plants such as crops develop rapidly and the growing season is very short. Large gaps in the data streams may be more problematic (Osborne et al., 2010). Analysis of biomass change is suggested to study how crops respond to the physical environment as carbon dioxide exchange rate is positively correlated with both photosynthesis and biomass accumulation (Campbell et al., 2001). The essential role of the surface vegetation calls for an adequate consideration for the change in biomass of croplands in the estimation of NEE, especially for the completeness of data that is important for the daily and annual sum (Papale, 2012). Although the relationship between the light use efficiency for GPP and LAI was reported (e.g. Otieno et al., 2009), LAI has not been widely involved in the commonly used gap-filling routines (Moffat et al., 2007). The consideration of LAI in the Michaelis-Menten function will have the potential to better track the surface vegetation change for the estimation of GPP.

1.3 Objectives

The mentioned current scientific problems to correctly address the ecosystem evapotranspiration (see Chapter 1.2.2) and the carbon dioxide flux (see Chapter 1.2.3) for fast growing crops lead to the main objectives of this study. This thesis will explore the applicability and potential improvement of the Michaelis-Menten model and the Penman-Monteith model, for a better understanding of the interactions between ecosystem and atmosphere in croplands. This study addresses the following hypotheses:

Hypothesis 1: PM-KP method could be a better alternative than PM-FAO model for the estimation of ET for croplands.

Hypothesis 2: Michaelis-Menten model could be improved for the simulation of carbon dioxide flux and therefore for the gap-filling of NEE or GPP data.

Hypothesis 3: The land-use change between flooded and non-irrigated crops could result in great differences in energy and matter exchange in croplands.

In order to verify these hypotheses, this study conducted the field work in major crop species on Korea Peninsula. The reasons why studying in Korea are as follows:

Firstly, Korea Peninsula is featured as an intensive agricultural area, which makes it easy to compare crop species growing in the same climate zone, but with different irrigation managements. This thesis managed to find two major croplands in this region for study. One is rice, well-known as a primary food source for half the world's population. The greatest number of paddy fields in the world, which is 79 million ha of irrigated rice fields, exists in Asia with the contribution of more than 75 % of the world's total rice supply (Cabangon et al., 2002). Rice fields are characterized by standing water during most of its cultivation period (Campbell et al., 2001). The peculiar irrigation management of the rice paddy ecosystem provides a unique opportunity for the study of energy and matter exchange different from those of non-irrigated croplands and forest ecosystems (Tsai et al., 2010). The other crop is potato, which ranks the fourth largest among the world's agricultural products in production volume and the leading non-grain commodity in the global food system (Fabeiro et al., 2001). The selected potato field was rain-fed without manual irrigation, featured by plasticulture system with plastic Polyethylene mulch. The comparison between these two crop species in the same region will provide insights into the differences in energy and matter exchange between irrigated and non-irrigated crops.

Secondly, Korea Peninsula is a typical region affected by the East Asian monsoon, which is different from European or American regions in the world. The East Asian monsoon is a seasonal flow driven by temperature differences between the Pacific Ocean and the East Asian continent (Chang, 2004). The living area of one third of the global population is influenced by the East Asian monsoon. Seasonal reversal of the large-scale atmospheric circulation divides the East Asian monsoon into warm wet summer and cold dry winter. Many regions in East Asia are characterized by summer monsoonal rainfall (Jo et al., 2010), which has been suggested to have great influence on the carbon cycle and energy budget in ecosystems. The summer monsoon is well known as Changma (in Korea), Meiyu (in China), and Baiu (in Japan) for intensive seasonal or intraseasonal rainfall with two peaks in subseasonal rainfall structures, such as Changma from late June to mid-July and post-Changma from mid-August to early September (Ha et al., 2012). Precipitation is intensified, clouds in the sky are enhanced during the summer monsoon. Total photosynthetic photon flux density, diffuse radiation, and VPD are reported to be the main controlling factors of the daytime carbon response (Moffat et al., 2010). Weather conditions are also key controls on ET in addition to field management such as irrigation and mulching (Allen et al., 1998; Tolk et al., 1998; Kang et al., 2003; Zhao

et al., 2010; Ding et al., 2013). During the summer monsoon, the decline of the solar radiation results in a substantial decrease in NEE in croplands, which was first reported by Kwon et al. (2009). This mid-season depression is found to be reproduced each year with variability of timing, which is caused by both meteorological conditions such as solar radiation, and human activities such as cultivation (Kwon et al., 2010). However, studies on mid-season depression of NEE in various crop species are rare in literature, which is possibly because the fluxes of carbon dioxide and water from croplands are generally less well understood than those from the other ecosystems such as forests and grasslands (Prescher et al., 2010). Furthermore, studies are limited by the confounding effects from other influencing factors and the data gaps caused by intensive precipitation (Kwon et al., 2009). Climate modelling studies have also indicated that the monsoonal precipitation in East Asia could be increased and the duration of monsoon could change in the future under the global warming (Yun et al., 2008; Jo et al., 2010). For example, it was reported that the maximum rainfall shifted in the recent decades from July to August in Korea (Lee et al., 2010). The complicated interaction between the environmental factors (e.g. precipitation, radiation, temperature, humidity) and crop managements (e.g. irrigation, fertilization, tillage) requires further studies on the ecosystem-atmosphere exchange of carbon dioxide and water vapour.

Thirdly, this study is in the framework of TERRECO (Complex TERRain and ECOlogical Heterogeneity) program, which is a joint project between several research institutes and departments in Germany and Korea, focusing on the linkage between ecosystem performance patterns in complex terrain and derived ecosystem services critical for human well-being. This study has contributions to the assessment of the influence of shifts in climate, land use and social response on ecosystem services.

In general, based on observations conducted in the growing seasons of two major cropping systems (both irrigated and non-irrigated) in Korea, this study is aimed to quantify the energy and carbon dioxide exchange between typical Asian agroecosystems and the atmosphere, to understand the pattern of the diurnal and seasonal variation of NEE, GPP, R_{eco} , and ET, and to explore the responses of these processes to environmental and biological drivers.

2 Materials and Methods

2.1 Research sites

2.1.1 Location

The research sites of this study were located in croplands at Haeon Basin (also called the Punchbowl) in Yanggu-gun, Kangwon-do, South Korea (Fig. 2.1). Haeon Basin is located at the northern border of South Korea, several kilometres south of the demilitarized zone between South and North Korea with longitude $128^{\circ} 5'$ to $128^{\circ} 11'E$, latitude $38^{\circ} 13'$ to $38^{\circ} 20'N$. This catchment is one of the primary agricultural areas in the region of Soyang Lake, a major source of drinking water for urban areas and the capital city of Seoul. As a bowl-shaped mountainous basin, Haeon has an elevation of 339 m and 1320 m above sea level at the valley and the mountain ridges, respectively.

Haeon Basin has a temperate climate with four clearly distinguishable seasons strongly influenced by East Asian monsoon. In spring (usually from late March to May), the seasonal mean temperature stays around $10^{\circ}C$ and the air is dry with seasonal mean relative humidity below 70 % (Fig. 2.2). Summer (usually from June to mid-September) is the warmest and moistest season with hourly temperature up to over $30^{\circ}C$ due to the warm prevailing winds from the Pacific Ocean, and with intensified rainfall brought by the summer monsoon called Changma or Jangma, resulting in high daily mean humidity up to 100 %. Although the research region has the longest daytime when the sun reaches its greatest height in the north hemisphere in summer, a depression in solar radiation occurs in June and July. Close to the coast, this region is usually influenced by several days of tropical storms (typhoons) in late summer. In autumn (from late September to November) the weather is normally dry and clear. Winter is cold and dry due to the Siberian wind, with daily mean temperature below $0^{\circ}C$ and humidity around 70 %. In the last 11 years (1999 - 2009) before this study the annual mean air temperature is $8.5^{\circ}C$, and the annual precipitation is averagely 1577

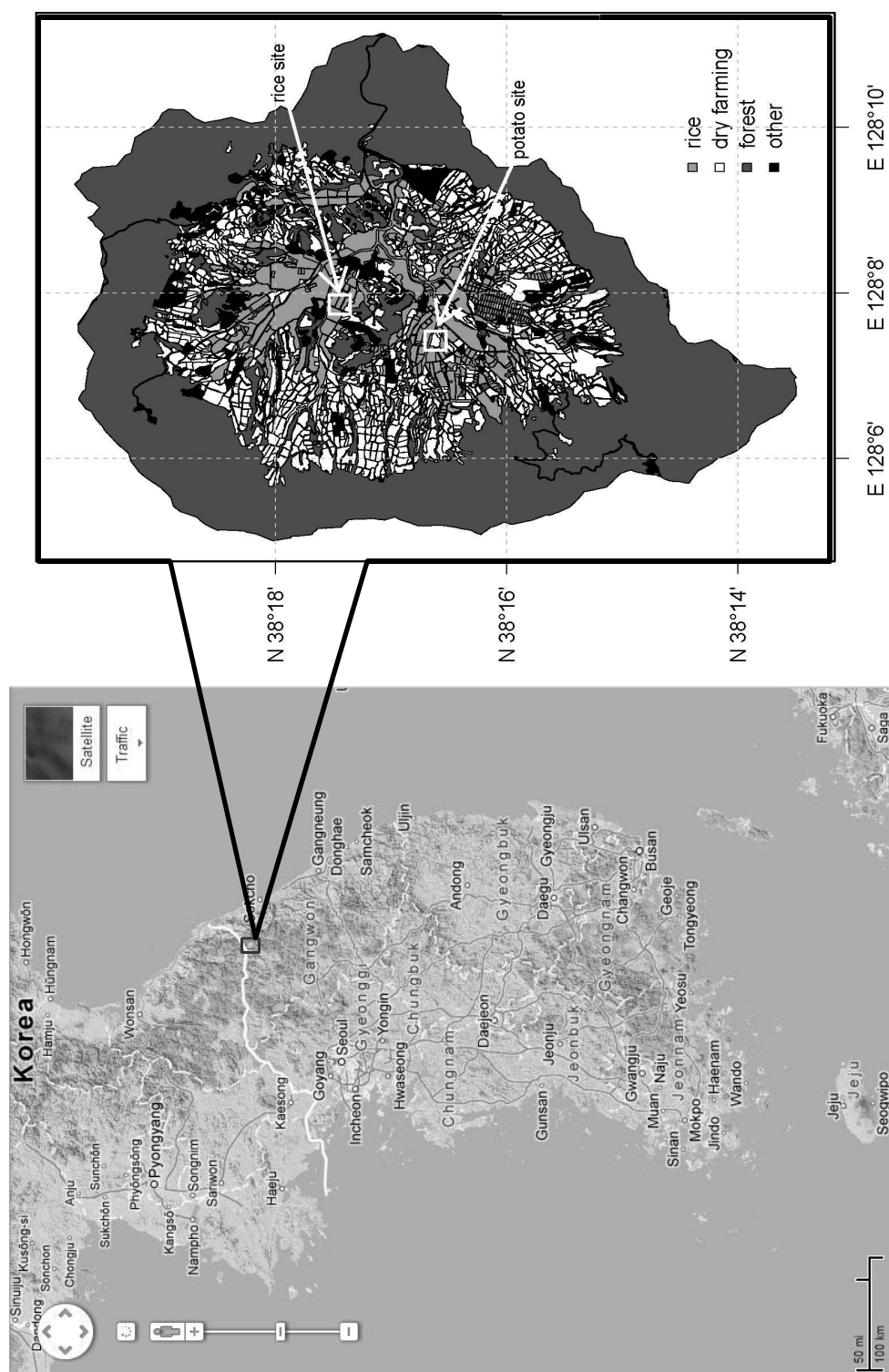


Figure 2.1: Research sites at Haeian Basin on the Korean Peninsula.

mm with year-to-year variation ranging from 1000 mm to over 2000 mm. 70 % of the annual precipitation falls in summer, in some years with subsequent typhoons in early autumn.

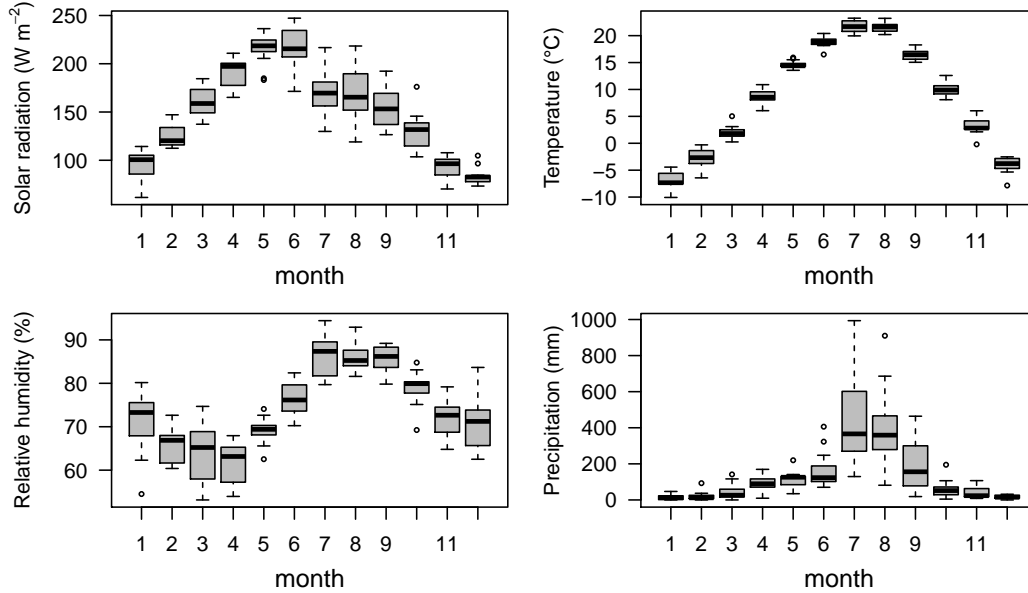


Figure 2.2: Variations of 11-year (1999 – 2009) averaged monthly solar radiation, air temperature, relative humidity, and precipitation in Haean Basin. The boxplot is composed of the median (solid line), the lower quartile and upper quartile (i.e. the 25th and 75th percentile, grey box), the lowest value still within 1.5 times of interquartile range (IQR) of the lower quartile, and the highest value still within 1.5 IQR of the upper quartile (markers).

2.1.2 Land-use of the study area

The whole area of Haean Basin is 62.7 km^2 . Agriculture has been expanded rapidly in Haean during the recent decades and this region has become an intensively managed agricultural region owing to the sufficient rainfall provided by the summer monsoon. Agricultural fields, mostly distributed at the flat bottom of the basin (Fig. 2.1), cover 27.5 % of Haean Basin.

A variety of crop species are planted in Haean Basin. The top three dominant crop species in Haean are rice paddy (501 ha), radish (412 ha), and potato (178 ha). The irrigation in rice fields is characterized by flooded water in the growing season. Non-irrigated crops, grown in plasticulture systems with plastic polyethylene mulch, are mostly patchy on slope lands where irrigation is difficult. The combination of ridge cultivation and plastic mulch induces a high spatial variability in soil moisture in the non-irrigated fields and amplifies the water

movement by slope direction and gravity especially during the rainy season (Ruidisch et al., 2013).

2.1.3 Field campaigns

A rice field and a potato field (Fig. 2.3) were chosen as representatives of typical irrigated and non-irrigated croplands in this study, because rice and potato are two of the top three dominating crop species, covering 34 % and 12 % of the whole cultivation area, respectively. The field campaigns were carried out in the growing seasons of the crops in 2010 and 2011 (Table 2.1). The research sites at the rice field ($38^{\circ} 17' \text{ N}$, $128^{\circ} 08' \text{ E}$, 457 m above sea level) and at the potato field ($38^{\circ} 17' \text{ N}$, $128^{\circ} 07' \text{ E}$, 455 m above sea level) were located at the bottom of Haeon catchment (Fig. 2.1) with a terrain slope of approximately 3° .

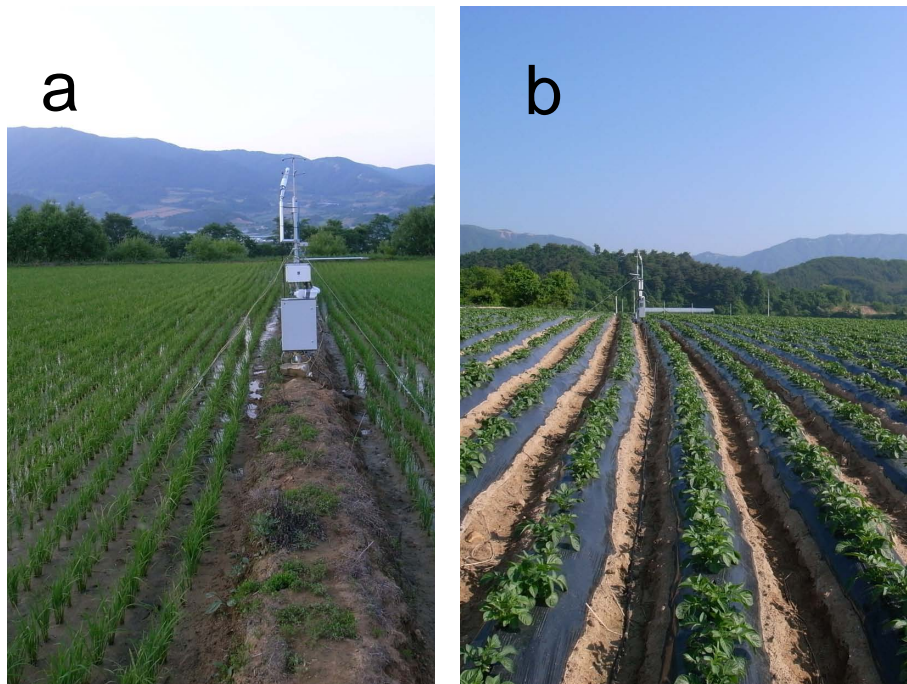


Figure 2.3: Photographs of the research sites (a: the rice field on 28 June, 2010; b: the potato field on 5 June, 2010). Photographs by Peng Zhao.

Table 2.1: Information about the research sites.

	Rice site	Potato site
Latitude	38 ° 17' 27.6" N	38 ° 16' 37.8" N
Longitude	128 ° 07' 52.0" E	128 ° 07' 28.5" E
Altitude	457 m above sea level	455 m above sea level
Density	36 plants m ⁻²	4 plants m ⁻²
Growing periods	24 May (transplanting)	26 April (planting)
	to 17 October, 2010 (harvest)	to 30 September, 2010 (harvest)
	20 May (transplanting)	
	to 14 October, 2011 (harvest)	

The flooded rice field, larger than 6 ha, was uniformly planted with a single rice variety and the area was surrounded by similarly flooded rice fields planted with the same species. Around the plot there were 5-m-wide footpaths and 0.6-m-wide field ridges with short wild grass and sparse trees growing on them. Rice seedlings were transplanted with a plant density of 36 plants m⁻² in late May and harvested in mid October with a growing season of nearly five months. The rice field was permanently flooded with water depth of 1 to 10 cm throughout the growing season (Table 2.2).

Table 2.2: Water depth in the rice field.

Date	Water depth (cm)
5 July 2010	2
27 July 2010	2
1 August 2010	2
3 August 2010	5
7 August 2010	10
10 August 2010	5
31 August 2010	7
30 September 2010	2
2 June 2011	7
11 June 2011	6
17 June 2011	5
24 June 2011	5
13 July 2011	4
22 July 2011	3
3 August 2011	3
22 August 2011	1
9 September 2011	2

The potato field was flat with an area of approximately 2.6 ha, on the west side of which there was a bean field nearby. There was a 2.5-m-wide field path in the potato field and a river along the north border of the plot. Potatoes were planted with a density of 4 plants m^{-2} in late April. The dry potato field was rainfed without irrigation under the plastic mulched ridge cultivation. The potato plants grew on ridges which were approximately 40 cm wide and 25 cm high. The ridges were covered with impermeable black polyethylene films as thin as micrometers. The films had poking holes with 5-cm diameter and at regular intervals with a plant spacing of 28 cm. They were used for maintaining constant temperature and humidity of the soil and preventing weed growth. Bare furrows with approximately 40 cm width were left uncovered between ridges. Potatoes are normally harvested when the field dries out in late August after the intensified precipitation in most years. However, there were a lot of rainfalls in August and early September in 2010, which postponed the harvest till the end of September.

2.2 Measurement methods

2.2.1 Weather observation

Basic meteorological elements were measured at 2.5 m above ground level with Automatic Weather Stations (WS-GP1, Delta-T Devices Ltd., UK) and a net radiometer (NR-LITE, Campbell Scientific Inc., US) at both of the research sites. Measured variables by weather observation included air temperature (T), wind speed (u), wind direction, relative humidity (RH), precipitation, global radiation (R_g), and net radiation (R_n) in 2010 and 2011. Manual observation was auxiliarily performed to record weather conditions in 2010, including present weather, sky condition, and sky cover.

A modification to the original devices was an additional amplifier (Ina 118, University of Bayreuth) for the net radiometer. Based on its calibration factor of $0.0152 \text{ mV W}^{-1} \text{ m}^2$, the original output signal of the net radiometer ranges approximately from -3 mV to 15 mV if the actual net radiation ranges between -200 and 1000 W m^{-2} as a rough estimation. It covers only a narrow band of the measurement range (from -9999.9 mV to 9999.9 mV) by the control box of the ultrasonic anemometer (see Chapter 2.2.3). Thus, the amplifier was used to magnify the original output signal of the net radiometer 501 times, resulting in an enlarged output ranging approximately from -1500 mV to 7500 mV .

Quality assurance was applied to ensure the reliability of meteorological observations. The status of batteries, installation levels, orientations of sensors, and clocks were checked regularly, which is described in detail as follows:

- Batteries of the weather stations were replaced with new ones if they were lower than 6 V in order to avoid data missing caused by battery failure.
- Installation levels were readjusted if necessary after heavy rainfalls.
- The sensor orientation is the reference to calculate the wind direction, and sometimes even has a critical influence on solar radiation if the radiation sensor is shadowed by the anemometer or rain gauge. Although the orientation was checked with care at the beginning of the field campaign as required by the installation manual, it could be disturbed by frequent strong winds or heavy rains during the summer monsoon. Obvious drift as much as 24° was observed in the field campaign in 2010. Sensor orientations were therefore checked with a compass and recorded regularly in the field. As the geographical north is 8.25° east of magnetic north in this region, the corrections of wind direction observation with both the sensor orientation drift and the magnetic declination were afterwards applied in post-processing procedures.
- The built-in clocks of both the weather stations and data sampling computer for the net radiometer were checked and synchronized on a regular basis. The drifts of them were recorded and afterwards used for the correction of time stamps.

2.2.2 Biomass measurement

Measured biomass variables included leaf area index (LAI), canopy height (h), and densities of fresh and dry biomass in the field. Plant biomass samples were collected manually at both sites approximately every two weeks in 2010 (Table 2.3). Each time 5 to 8 whole plants were randomly selected. Each plant was immediately hand-washed and separated into green leaves, dead parts, stems, roots, etc., and then weighed on a scale to obtain the fresh weights. Leaf area was obtained from the destructively sampled biomass by measuring the area of leaves using a leaf area meter (LI-3000A, LI-COR Inc., USA). LAI was afterwards defined as the one-side leaf area per plant multiplied by the planting density. The samples were later dried at 75°C or 80°C for at least 1 week in an oven, then weighed again to obtain the dry weights. The densities of fresh and dry biomass were determined as the mean fresh and dry weights

multiplied by the planting density, respectively. The canopy height of crops was determined as the mean of the heights of 5 plants randomly sampled out of the largest canopy heights covering 10 % of the area (Foken, 2008b). In 2011, although the biomass measurement was unavailable, the canopy height was measured approximately every 10 days.

Table 2.3: Biomass sampling dates and sample numbers (n).

Rice		Potato	
Date	n	Date	n
2010-06-07	5	2010-06-07	7
2010-06-29	8	2010-06-10	5
2010-07-05	8	2010-06-23	8
2010-07-23	5	2010-07-07	8
2010-08-07	5	2010-07-21	5
2010-08-30	5	2010-08-12	5
2010-09-18	5	2010-08-26	5

2.2.3 Eddy-covariance measurement

Ecosystem-atmosphere fluxes of sensible heat (Q_H), latent heat (Q_E), and NEE as well as the friction velocity (u^*) over the crop canopy were determined by using an eddy-covariance (EC) measurement system. The EC system was equipped with an ultrasonic anemometer (USA-1, METEK GmbH, Germany) measuring the three dimensional wind vector and sonic temperature, and a fast-response open-path infrared analyser (LI-7500, LI-COR Inc., USA) to measure the fluctuations in carbon dioxide and water vapour densities. The ultrasonic anemometer and the gas analyzer were both installed at 2.5-m height above ground level in the potato field and 2.8-m height above the flooded water level in the rice field on a tripod mast, and worked at a sampling frequency of 20 Hz.

As only one EC system was available and two sites were studied in 2010, the EC system had to be moved from one location to the other approximately every two weeks. In 2011 the system worked continuously and exclusively at the rice site.

The EC software package TK2 (the latest version is updated to TK3, Mauder and Foken, 2004; Mauder et al., 2006; Mauder and Foken, 2011), developed by the Department of Micrometeorology, University of Bayreuth, post-processed the high-frequency raw data according to all international agreed procedures. The correction strategy has been recently summarized by

Foken et al. (2012b). Half-hourly aggregated sensible and latent heat fluxes and NEE with quality flags (Foken and Wichura, 1996) were available as results.

For further technical information about the field campaign, see Zhao et al. (2011).

2.3 Data processing

2.3.1 Data quality control

Trustworthy data are necessary for reliable conclusions. However, low-quality data exist in the high-frequency observations as well as in the time series of the 30-min flux values. The following data-quality selection criteria (Lüers et al., 2014) were applied in this study in order to examine time series of fluxes and generate a high-quality database:

1. The software TK2 checks and eliminates spikes of 20-Hz records.
2. TK2 filters direct measurements (e.g. horizontal wind speed, vertical wind speed after rotation, sonic temperature, absolute humidity, carbon dioxide and water vapour concentrations) and subsequently derived variables (e.g. covariances, wind direction, atmospheric stability, and all fluxes) by applying reasonable physical consistency limits.
3. A quality classification of the derived 30-min fluxes is used to eliminate low quality classes. This study used the overall quality classification strategy combining steady-state test (trend conditions) and the integral turbulence characteristics test (to test the development of turbulent conditions) to mark low quality data (Foken and Wichura, 1996; Foken et al., 2004). The overall quality flag for each 30-min flux value has a value of 1–9 calculated by TK2. According to Foken et al. (2004), flux data with classes 1–6 can be used for long-term measurements without limitations, while flux data with classes 7–8 could be used for rough orientation and should be deleted if necessary, and flux data with class 9 should always be rejected. Therefore, this thesis marked the flux data with overall quality flags of 7–9 as low-quality data, and used the flux data with flags of 1–6 for further analysis.

The quality control approach by Foken and Wichura (1996), abbreviated as FW1996, is now a standard method, which has been used during recent years in most of the available EC data processing softwares (Foken et al., 2012b). FW1996 can only be applied if raw high frequency data or 5-minute covariance and standard deviation data are available. Similarly to FW1996,

a friction velocity (u^*) threshold criterion (Goulden et al., 1996) is often used in gap-filling techniques. The scientific background of u^* filtering is to exclude all those data which do not indicate turbulence and where EC assumptions are not fulfilled, thus the EC method cannot be used (Foken et al., 2012a). The u^* filtering tries to guarantee that non-turbulent data is not considered. However, turbulence still exists even for low u^* under steady-state conditions and no intermittent turbulence. These cases are excluded by the u^* filtering. Ruppert et al. (2006) suggest that FW1996 has the advantage over the u^* filtering for a flux data quality assessment, because the rejection of data by these tests is less restrictive, which leads to an increase of the number of valid data that can be used for parameterization, especially in summer nights when ecosystem respiration is active. Most of the past published studies use the u^* filtering within time windows as long as weeks or months, based on long-term measurements focused on forests. These measurements are from periods much longer than the growing seasons of crops (in this study only 4 months). These long time observations generate, in general, enough good-quality data for the statistics and parameterization available. Unfortunately, u^* filtering will exclude too large a fraction of data because the fast-growing periods of rice and potatoes are very short, therefore FW1996 has a significant benefit in this study. As both the steady-state test and the integral turbulence characteristics test were used, u^* filtering was unnecessary in this study.

4. An instrument-based status filter is used to mark those values during certain periods as outliers. This filter includes the information from the weather stations to detect rain periods and the diagnostic value of LI-7500. The open-path EC system is disturbed by rain and fog events and therefore produces an unreliable observation. These bad-weather events can be detected and recorded either by the weather station or by the diagnostic signal from the gas-analyzer. In this study, the diagnostic signals from LI-7500 digital outputs, including the values of automatic gain control (AGC), the status of the chopper motor and the chopper temperature controller, the detector cooler, and the sync between the LI-7500 embedded software and the chopper motor, were used to determine the periods when the gas analyzer was untrustworthy, besides using humidity and precipitation records from the weather stations to determine the rain and fog events. It was found that the rain or fog periods determined by the nearby weather station and the untrustworthy periods determined by the diagnostic signals were all included in the periods when AGC-values were over or below the instrument specific baseline, i.e. 50 in this study. Therefore, all the periods in question could be detected by just a simple check of whether the AGC is unequal to the instrument's baseline.

5. The internal boundary layer and footprint information was used to estimate the contribution by the target surface (see Chapter 3.2). Turbulent flux data were marked as irrelevant records when flux contributions from the target land-use type were less than 70 % and the aerodynamic measurement height was larger than $0.5\sqrt{x}$ (Eigenmann et al., 2011), where x is the fetch.

6. A statistical algorithm for outlier check is performed on the basis of the comparison between each 30-min value and the values before and after. Briefly speaking, a time series of absolute deviations for each direct measurement and for the derived fluxes is calculated, which is afterwards used to run a quantile check to detect major outliers and finally followed by a standard deviation filter as thresholds. The calculations of the absolute deviations, the quantiles, and the standard deviations are adjustable with window sizes and multiplying factor. More details could be found in Lüers et al. (2014).

The 30-min dataset, excluding low quality data, irrelevant records, and outliers by the multiple-step filter, was used as the high-quality database for subsequent gap-filling and parameterization.

2.3.2 Data gap-filling

LAI and canopy height

A simple non-linear model was parameterized using measured LAI (see Chapter 2.2.2) and the days after planting (DAP) following Hashimoto (1990):

$$\text{LAI} = a_1 \text{DAP}^{a_2} \exp(a_3 \text{DAP}). \quad (2.1)$$

With fitted a_1 , a_2 , and a_3 , this function reproduced the LAI values with a coefficient of determination (R^2) of 0.98 and 0.99, slope of 1.00 and 0.97 for potato and rice, respectively. Therefore, this model was used to fill the gaps in LAI measurement to obtain continuous LAI in the croplands.

Data gaps in canopy height were filled by linear interpolation.

Meteorological data

Data gaps in basic meteorological data were occasionally caused by the malfunction of the sensors. These gaps were filled with the observation by weather stations at nearby fields, i.e. a dry field located 1.1 km away from the potato field, and another rice field located 1.6 km away from the rice field (for details see Zhao et al., 2011). The comparison of available data at each two nearby sites showed good linear relationships for the air temperature, humidity and solar radiation with linear slope of 0.97 – 1.05 and R^2 of 0.97 – 0.99 (not shown).

Flux data

To obtain the seasonal budget and pattern of evapotranspiration and NEE, gap-filling strategies were applied on the basis of environmental and meteorological drivers. Data gaps in evapotranspiration were filled with the simulation by Penman-Monteith approach with an optimal parameterization of stomatal resistance (see Chapter 4.4). Data gaps in ecosystem respiration were filled with the simulation by the temperature-dependence function (see Chapter 2.4.5). Data gaps in GPP were filled with the combination of simulated values by the light response function using the optimal time windows and the simulated values by the leaf-light response function (see Chapter 5). Data gaps in NEE were subsequently filled with gap-free data of respiration and GPP.

2.3.3 Canopy energy components

the canopy energy balance equation is written as:

$$-R_n = Q_G + Q_H + Q_E + \Delta Q, \quad (2.2)$$

where R_n is the net radiation; Q_G is the ground heat flux; Q_H is the sensible heat flux; Q_E is the latent heat flux; ΔQ is the stored heat in the canopy. The signs follow the conventional meteorological definitions that the fluxes away from the surface are positive. The energy balance in Eq. 2.2, however, is not closed in most EC experiments. This imbalance can be compensated by an additional term called "residual" (Res). The calculation of Res requires the estimation of R_n , which was observed directly in the field (see Chapter 2.2.1), Q_H and Q_E , which were measured using the EC technique (see Chapter 2.2.3), and Q_G and ΔQ , which are described as follows.

The ground heat flux Q_G can be simply estimated by assuming a constant ratio p_G between Q_G and R_n (Liebethal and Foken, 2007):

$$Q_G = -p_G R_n. \quad (2.3)$$

For the potato field, the estimation of Q_G used $p_G = 0.14$ in the daytime (Liebethal and Foken, 2007) and $p_G = 0.5$ in the night-time (Allen et al., 1998), while the stored heat in the canopy (ΔQ) is normally small and assumed negligible (Oncley et al., 2007).

The unique land characteristics of the rice field requires different considerations about the estimation of Q_G and ΔQ . The heat stored in the standing water in the rice field must be taken into account because of the high heat capacity of water. It was reported that the energy balance closure in a flooded rice field was improved by 5 % when adding ΔQ into the energy balance equation (Hossen et al., 2012). Another study demonstrated that the heat stored in the paddy water can be 5 % of R_n in the daytime (Tsai et al., 2007). Therefore, 5 % of R_n is taken as a rough estimation of ΔQ in the rice field in this thesis. The feature of the standing water in the rice field could subsequently have an influence on the heat transfer on the soil surface, therefore the value of p_G for the rice field, potentially different from that for the potato field, should be applied. This study used 28 % of the available energy, equally 20 % of R_n , reported by Tsai et al. (2007) as an approximate estimation of Q_G for the rice field.

2.3.4 Correction for energy balance closure

Many studies have reported that the energy balance shown in Eq. 2.2 is not closed (i.e. $Res \neq 0$) when Q_H and Q_E are obtained from the measurement by the EC technique (Foken, 2008a). For instance, Foken et al. (2010) noted that the a residual of up to 25 % of the available energy (Q_A , the sum of R_n and Q_G) was found at low-vegetation sites. Twine et al. (2000) assumed that the Bowen ratio (the ratio of sensible to latent heat flux, $Bo = \frac{Q_H}{Q_E}$) is correctly measured by the EC system so that Res can be partitioned into Q_H and Q_E according to Bo as a correction method for energy balance closure (EBC). This correction method, indicated as EBC-Bo, has been widely used. Recent studies, however, demonstrated that the energy balance can be significantly improved with the contribution from secondary circulations which can hardly be measured by the EC system (e.g. Kanda et al., 2004; Foken, 2008a; Foken et al., 2010, 2011). Some studies noted that a large part of Res should be partitioned into Q_H (Mauder and Foken, 2006; Ingwersen et al., 2011) rather than Q_E . As

the scalar similarity between Q_H and Q_E is not valid throughout all scales, Charuchittipan et al. (2014) suggested an alternative EBC correction with the buoyancy flux, indicated as EBC-HB:

$$Q_H^{\text{EBC-HB}} = Q_H^{\text{EC}} + f_{\text{HB}} \text{Res}, \quad (2.4)$$

$$Q_E^{\text{EBC-HB}} = Q_E^{\text{EC}} + (1 - f_{\text{HB}}) \text{Res}, \quad (2.5)$$

with

$$f_{\text{HB}} = \left(1 + \frac{C_1}{Bo^{\text{EBC-HB}}}\right)^{-1} = \frac{Q_H^{\text{EBC-HB}}}{Q_H^{\text{EBC-HB}} + C_1 Q_E^{\text{EBC-HB}}}, \quad (2.6)$$

and

$$C_1 = 0.61 \bar{T} \frac{c_p}{\lambda} \quad (2.7)$$

where c_p is the specific heat of air; λ is the heat of evaporation for water; superscripts indicate the measurement or correction methods. The coefficient 0.61 in Eq. 2.7 originates from converting the virtual temperature T_v into real temperature T by $T_v = T(1 + 0.61q)$ where q is the specific humidity. $Bo^{\text{EBC-HB}}$ should be either calculated iteratively until it converges (Charuchittipan et al., 2014), or by solving Eqs. 2.4 – 2.6 resulting in the analytical expressions:

$$f_{\text{HB}} = 0.5 + \frac{C_2}{\text{Res}}, \quad (2.8)$$

$$Q_H^{\text{EBC-HB}} = Q_H^{\text{EC}} + 0.5 \text{Res} + C_2, \quad (2.9)$$

$$Q_E^{\text{EBC-HB}} = Q_E^{\text{EC}} + 0.5 \text{Res} - C_2, \quad (2.10)$$

where

$$C_2 = \frac{\sqrt{(Q_H^{\text{EC}} + C_1 Q_E^{\text{EC}} - \text{Res} + C_1 \text{Res})^2 + 4(1 - C_1) Q_H^{\text{EC}} \text{Res} - Q_H^{\text{EC}} - C_1 Q_E^{\text{EC}}}}{2(1 - C_1)}. \quad (2.11)$$

This solution is confirmed to agree with the iterative calculation, while another analytical solution to Eqs. 2.4 – 2.6 is therefore rejected. Eqs. 2.8 – 2.11 have the advantage that they can be easily used in a spreadsheet software rather than programming. With the EBC-HB correction, more than half of Res (i.e. C_2 is positive) is partitioned into Q_H when $Bo \gtrsim 0.07$, because buoyancy mainly transports Q_H rather than Q_E near the surface.

2.3.5 Partitioning of evapotranspiration

Ecosystem evapotranspiration (ET) is an equivalent of the latent heat flux often expressed in mm d^{-1} . ET can be partitioned into evaporation (EV) and transpiration (TR) by an empirical equation dependent on LAI and the light extinction coefficient and $k = 0.45$ (Hossen et al., 2012):

$$TR = ET(1 - \exp(-kLAI)). \quad (2.12)$$

$$EV = ET \exp(-kLAI). \quad (2.13)$$

2.4 Models

2.4.1 Penman-Monteith equation

Data gaps exist in data-sets of turbulent heat fluxes measured by the eddy-covariance technique (see Chapter 2.3.1). These gaps can be filled by simulation estimated by the Penman-Monteith (PM) equation (Penman, 1948; Monteith, 1965). The PM model is commonly used to estimate Q_E or evapotranspiration (ET) with the "big-leaf" assumption that the sensible and latent heat comes from the same height and temperature, and the canopy has an adequate fetch. This equation integrates the energy and aerodynamic considerations, written as

$$Q_E^{\text{PM}} = \frac{s_c(-R_n - Q_G) + \frac{\rho c_p(e_s - e_a)}{r_a}}{s_c + \gamma(1 + \frac{r_s}{r_a})}, \quad (2.14)$$

where e_s is the saturated vapour pressure (hPa) described as a function of the temperature according to Clausius-Clapeyron's equation, $e_s = 6.112 \exp \frac{17.62t}{243.12+t}$ over water at -45 to 60 °C (Sonntag, 1990); s_c is the slope of the saturation vapour-pressure curve, $s_c = \frac{4284e_s}{(243.12+t)^2}$; e_a is the partial vapour pressure of the air; ρ is the air density; γ is the psychrometric constant, 0.667 hPa K^{-1} for an air pressure of 1000 hPa and a temperature of 20 °C; r_s is the stomatal

resistance of the entire "big leaf", or simply the canopy resistance; r_a is the aerodynamic resistance. The estimation of the sensible heat flux by the PM method is simply calculated as the difference between the available energy and modelled latent heat flux ($Q_H^{PM} = -Q_A - Q_E^{PM}$).

The estimation of Q_E by Eq. 2.14 requires the parameterization of r_a and r_s . The estimation of r_a which can be performed as (Allen et al., 1998)

$$r_a = \frac{\ln \frac{z-d}{z_{om}} \ln \frac{z-d}{z_{oh}}}{\kappa^2 u}, \quad (2.15)$$

where z is height at which wind speed is measured; d is displacement height, estimated as $\frac{2}{3}$ of the vegetation height (h); κ is Von-Kármán constant, equal to 0.40; and u is horizontal wind speed at sensor height z ; z_{om} is roughness height for momentum, approximated as $p_m h$, where p_m is taken as 0.1; z_{oh} is roughness height for water vapour, approximated as $p_h z_{om}$, where p_h is taken as 0.1.

The parameterization of r_s is one of the most challenging works in the PM method and one of the highlights in this study, which is described in the following chapter.

2.4.2 Parameterization of the stomatal resistance

FAO approach

The stomatal resistance (r_s) is necessary to be parameterized as a primary factor in the evapotranspiration process (Monteith, 1965). The Food and Agriculture Organization (FAO) proposed that r_s can be estimated by a LAI dependent approach (Allen et al., 1998):

$$r_s = \frac{r_{si}}{LAI_{active}}, \quad (2.16)$$

where r_{si} is the stomatal resistance of a single well-illuminated leaf with a value between 70 to 80 s m^{-1} for estimation of hourly or shorter-time-based Q_E for agricultural crops (Allen, 2005), and LAI_{active} is the LAI of the active sunlit leaves, which is generally the upper part of the canopy and can be estimated as $LAI_{active} = 0.5LAI$. This approach for the estimation of r_s is indicated as FAO approach in this study.

FAO approach has been widely applied with the assumption that soil evaporation is negligible and r_s is an integrated resistance of all leaves in parallel. The estimation of r_s could have evident influence on the PM-FAO modelled data and further on the consistency between the PM-FAO model and observation.

KP approach

Many studies mentioned that the assumption of the "big leaf" with constant r_{si} in the FAO approach could be a constraint in the accuracy of the simulation by the PM model (e.g. Rana et al., 1994; Perez et al., 2006). Katerji and Perrier (1983) suggested a semi-empirical model in which r_s can be parameterized by the establishment of a linear relationship between $\frac{r_s}{r_a}$ and $\frac{r^*}{r_a}$, indicated as the KP approach in this study:

$$\frac{r_s}{r_a} = a \frac{r^*}{r_a} + b, \quad (2.17)$$

with

$$r^* = \frac{(s_c + \gamma)\rho c_p(e_s - e_a)}{s_c\gamma(-R_n - Q_G)}, \quad (2.18)$$

where a and b are regression coefficients. To derive a and b by linear regression, r_s is determined experimentally from the half-hourly observations by inverting the PM equation (Eq. 2.14):

$$r_s = \frac{r_a s_c(-R_n - Q_G) + \rho c_p(e_s - e_a) - r_a Q_E(s_c + \gamma)}{\gamma Q_E}. \quad (2.19)$$

The KP approach includes the related meteorological variables including R_n , VPD and r_a into one simple equation. Moreover, the KP approach takes into account the aerodynamic resistance r_a as an influencing factor on r_s , assuming that r_s is a combination of the resistance of all leaves, the resistance of the soil surface, and the resistance between these surfaces and the 'big leaf' where r_a plays a role. It has been reported to be a good estimation of r_s at either the hourly or daily scale for irrigated grass (Lecina et al., 2003; Steduto et al., 2003), prairies (Pauwels and Samson, 2006), mixed forest (Shi et al., 2008), and several crops including alfalfa (Katerji and Perrier, 1983), lettuce (Alves and Pereira, 2000), sweet sorghum (Rana et al., 2001), sunflower (Rana et al., 1997a), grain sorghum (Rana et al., 1997a), soybean (Rana et al., 1997b), clementine orchard (Rana et al., 2005), and tomato (Katerji and Rana, 2006), under Mediterranean climate conditions, but has not been extensively applied. As Katerji et al. (2011) suggested that the KP approach needs to be validated on a variety of crops to

define their suitability, this thesis evaluated the KP approach for an irrigated rice field and a non-irrigated potato field.

2.4.3 Sensitivity test

Sensitivity coefficients

The influence of the meteorological and physiological variables on the PM model can be investigated with the model sensitivity to input and parametric data. The sensitivity analysis was performed by the non-dimensional relative sensitivity coefficient (McCuen, 1974; Beven, 1979):

$$S_i = \lim_{\Delta V_i \rightarrow 0} \left(\frac{\Delta Q_E / Q_E}{\Delta V_i / V_i} \right) = \frac{\partial Q_E}{\partial V_i} \cdot \frac{V_i}{Q_E}, \quad (2.20)$$

which represents the relative change in Q_E resulting from the relative change in the i -th variable V_i . A positive/negative S_i indicates that Q_E increases/decreases with the increase of V_i . A larger absolute value of S_i indicates stronger influence of V_i on Q_E .

Combining Eqs. 2.14 and 2.20, the sensitivity coefficients for available energy (Q_A), vapour pressure deficit (VPD), stomatal resistance (r_s), and aerodynamic resistance (r_a) can be calculated as:

$$S_{Q_A} = \frac{\partial Q_E}{\partial Q_A} \cdot \frac{Q_A}{Q_E} = \left(1 + \frac{\rho c_p \text{VPD}}{s_c Q_A r_a} \right)^{-1}, \quad (2.21)$$

$$S_{\text{VPD}} = \frac{\partial Q_E}{\partial \text{VPD}} \cdot \frac{\text{VPD}}{Q_E} = 1 - S_{Q_A}, \quad (2.22)$$

$$S_{r_s} = \frac{\partial Q_E}{\partial r_s} \cdot \frac{r_s}{Q_E} = - \left(1 + \frac{s_c + \gamma}{\gamma} \cdot \frac{r_a}{r_s} \right)^{-1}, \quad (2.23)$$

$$S_{r_a} = \frac{\partial Q_E}{\partial r_a} \cdot \frac{r_a}{Q_E} = -S_{r_s} - S_{\text{VPD}}. \quad (2.24)$$

GLUE procedure

In order to determine the best parameterization of the PM function, the Generalized Likelihood Uncertainty Estimation (GLUE, Beven and Binley, 1992) procedure was employed in

this study. The GLUE procedure works with many sets of parameters and accepts different sets of parameter values which result in equally good performance of the model. Parameters with random values in a given distribution within specified ranges are tested. The performance of the model is afterwards evaluated by the goodness-of-fit measures (see Chapter 2.4.7).

This study applied the GLUE procedure in the following way: firstly, the tested parameters and the ranges as well as the statistical distributions of their values were pre-determined. For the PM-FAO model, the tested parameters were limited to r_{si} , p_m , and p_h . Their values were limited within the range from 0 to 320 s m^{-1} (Garratt, 1992) for r_{si} , and from 0 to 1 for both p_m and p_h , all in uniform distributions. The tested parameters of the PM-KP model were limited to a and b . The ranges and distributions of their values were determined by 1000 runs of parameterization of Eq. 2.17, each of which randomly sampled 40 records of the daytime high-quality dataset to derive the values of a and b (see Chapter 4.4).

For the next step, random sets of tested parameters were independently produced for 10000 model runs. The values of parameters ranged within the pre-determined range and followed the pre-determined distribution. An individual Nash-Sutcliffe model efficiency coefficient (NSEff, see Chapter 2.4.7) between the model and the EBC-HB corrected latent heat flux was obtained for each run. The optimal parameters for the best model performance could then be found.

2.4.4 Partitioning of NEE

The carbon dioxide flux measured by the eddy-covariance technique indicates the net ecosystem exchange (NEE), which can be partitioned into gross primary productivity (GPP) and respiration (R_{eco}) by :

$$NEE = GPP + R_{eco}. \quad (2.25)$$

The partitioning strategy follows most published work (Falge et al., 2001; Reichstein et al., 2005; Papale et al., 2006; Lasslop et al., 2010). Briefly speaking, the high quality database was separated into daytime data (when $R_g > 20 \text{ W m}^{-2}$) and night-time data (when $R_g \leq 20 \text{ W m}^{-2}$) and cross-checked against sunrise and sunset time derived from the local time and standard sun-geometrical routines. R_{eco} in night-time is equal to the measured NEE assuming no photosynthesis ($GPP = 0$). The night-time R_{eco} was used for the parameterization of the temperature dependence function (see Chapter 2.4.5), and the fitted parameters were used not only to fill the gaps of night-time R_{eco} , but also to extrapolate to daytime R_{eco} , which

resulted from the assumption that the temperature response of R_{eco} in daytime is the same as that in the night-time. Afterwards, the extrapolated daytime R_{eco} was used together with the observed daytime NEE to calculate the daytime GPP by Eq. 2.25.

2.4.5 Temperature-dependence function of ecosystem respiration

The night-time R_{eco} was used for the parameterization of the temperature dependence of R_{eco} in the Lloyd-Taylor function (Lloyd and Taylor, 1994; Falge et al., 2001):

$$R_{\text{eco}} = R_{\text{ref}} e^{E_0 \left(\frac{1}{T_{\text{ref}} - T_0} - \frac{1}{T - T_0} \right)}, \quad (2.26)$$

where R_{ref} ($\mu\text{mol m}^{-2} \text{s}^{-1}$) is the respiration at a reference temperature (T_{ref} , set as 283.15 K), E_0 (K) is the temperature sensitivity, and T_0 (K) is a constant value of 227.13 K as in Lloyd and Taylor (1994). A single value of E_0 was calculated for each site over the entire observation period. R_{ref} was evaluated for a nine-day sliding window. The study by Lasslop et al. (2012) suggested a site-specific choice between air and soil temperature. The soil temperature in the rice field is within a narrow range and the variation in soil temperature is reduced because of the standing water, therefore the air temperature is suggested to be used instead of soil temperature (Saito et al., 2005). It is also used for the potato field due to the unavailable measurement of soil temperature.

2.4.6 Leaf and light response of GPP

The gaps of GPP are usually filled using a conventional non-linear regression approach based on an R_g dependency. As the rectangular hyperbolic function shows the best overall performance among many light response functions used for daytime gap-filling (Falge et al., 2001), the relationship between GPP and R_g is expressed by the Michaelis-Menten function (Michaelis and Menten, 1913)

$$\text{GPP} = \frac{\alpha R_g \beta}{\alpha R_g + \beta}, \quad (2.27)$$

where α ($\mu\text{mol s}^{-1} \text{W}^{-1}$) is the initial slope of the curve, and β ($\mu\text{mol m}^{-2} \text{s}^{-1}$) is the saturated carbon dioxide uptake rate when R_g is close to infinity.

For constant vegetation conditions, VPD was suggested to be the main nonradiative control of carbon response (Moffat et al., 2010). A VPD factor was introduced to account for the

stomatal response to dry air conditions. β , the saturated GPP in the light response function, can be expressed by an exponential function of VPD (Lasslop et al., 2010):

$$\beta = \begin{cases} \beta_0 e^{-k_\beta(\text{VPD}-\text{VPD}_0)} & , \text{VPD} > \text{VPD}_0 \\ \beta_0 & , \text{VPD} \leq \text{VPD}_0 \end{cases} \quad (2.28)$$

where the threshold VPD_0 (hPa) is set to 10 hPa (Lasslop et al., 2010).

For changing vegetation conditions, the development of plant leaves naturally has an influence on the carbon response. Thus, site-specific optimal time windows were tested and used to distinguish the seasonal dependencies of the parameterization of Eq. 2.27. Individual fitted values of α and β were determined for each time window.

The application of the time-window scheme is limited when the period of the missing data is longer than the time-window itself. These cases often occur due to power failure at the locations of field campaigns or during longer rain or fog events in the summer monsoon and subsequent typhoon seasons in Korean Peninsula. Some other gap-filling strategies, e.g. mean diurnal variation and look-up tables, are normally based on monthly or even seasonal time windows as well. Conventionally, these time-window related strategies could fill these large gaps by interpolating the parameters or the fluxes calculated before and after the gaps. Unfortunately, they have difficulties when the period of the missing data is longer than the time-window. For instance, if a gap takes place during the period at the peak of LAI when the potential photosynthesis ability reaches the maximal efficiency, this simple interpolation will underestimate GPP.

Suppose each unit area of leaves which are active in photosynthesis has equal ability of carbon uptake. A leaf-light response function by introducing a LAI factor into Eq. 2.27 is proposed as

$$\frac{\text{GPP}}{\text{LAI}_{\text{act}}} = \frac{\alpha' R_g \beta'}{\alpha' R_g + \beta'}, \quad (2.29)$$

or

$$\text{GPP} = \text{LAI}_{\text{act}} \frac{\alpha' R_g \beta'}{\alpha' R_g + \beta'}, \quad (2.30)$$

where LAI_{act} is the mean LAI which is active in photosynthesis, approximately taken as measured LAI in this study. The parameters α' and β' can be defined as specific light use efficiency and specific saturated GPP. α' and β' are constant and do not change with the

vegetation development. Therefore, the whole dataset (R_g , GPP, LAI_{act}) within the growing season can be used to parameterize Eq. 2.30. Consequently, large gaps in GPP can be filled with the derived parameters α' and β' , because the non-linear development of LAI is already included.

The leaf-light response function (Eq. 2.30) is a combination of both leaf and light responses of GPP. The light response function (Eq. 2.27) is a special case of Eq. 2.30 when the vegetation condition is constant. For a given solar radiation, the multiplier $\frac{\alpha' R_g \beta'}{\alpha' R_g + \beta'}$ should be constant, indicated as a slope a_{LAI} , therefore a leaf response function should be

$$GPP = a_{LAI} LAI. \quad (2.31)$$

2.4.7 Evaluation of simulations

The performance of the models in this study was evaluated by the comparison between field observation and model simulation. The coefficient of determination (R^2) was used as the measure of total variance which the model accounted for, calculated as the square of the correlation coefficient (R) between the prediction (P_i) and the observation (O_i):

$$R^2 = \left(\frac{\sum_{i=1}^n (O_i - \bar{O})(P_i - \bar{P})}{\sqrt{\sum_{i=1}^n (O_i - \bar{O})^2} \sqrt{\sum_{i=1}^n (P_i - \bar{P})^2}} \right)^2, \quad (2.32)$$

where \bar{P} and \bar{O} are the averages of predicted and observed values.

Additionally, mean absolute error (MAE), root mean square error (RMSE), and normalized root mean square error (NRMSE) were calculated to indicate the magnitude and distribution of the individual errors. They are calculated as:

$$MAE = \frac{1}{N} \sum_{i=1}^N (P_i - O_i), \quad (2.33)$$

$$RMSE = \sqrt{\frac{1}{N} \sum_{i=1}^N (P_i - O_i)^2}, \quad (2.34)$$

$$\text{NRMSE} = 100 \frac{\text{RMSE}}{O_{\max} - O_{\min}}. \quad (2.35)$$

The overall performances of these simulations are evaluated by ranking either the Nash-Sutcliffe model efficiency coefficient (NSEff, Nash and Sutcliffe, 1970) or the index of agreement (I , Willmott, 1981):

$$\text{NSEff} = 1 - \frac{\sum_{i=1}^n (O_i - P_i)^2}{\sum_{i=1}^n (O_i - \bar{O})^2}, \quad (2.36)$$

$$I = 1 - \frac{\sum_{i=1}^n (P_i - O_i)^2}{\sum_{i=1}^n (|P_i - O_i| + |P_i + O_i|)^2}. \quad (2.37)$$

NSEff varies between minus infinity to 1, and I varies between 0 to 1, both with larger values indicating better performance of the simulation. A value of NSEff = 1 or I = 1 indicates a perfect agreement between observation and simulation. NSEff = 0 means the model is as good as the mean observation, while I = 0 means a complete disagreement. Both indices have an advantage over the commonly used R^2 because NSEff and I are sensitive to both the mean and variances of the observation and simulation (Legates and McCabe Jr, 1999). The best simulation is the one which has NSEff or I closest to unity and with the lowest RMSE.

Taylor diagrams (Taylor, 2001) were used to plot standard deviation (SD), correlation coefficient (R), and NRMSE in one figure in order to test the sensitivity of different models. In a Taylor diagram, each single point specifies the performance of one scheme, with the radial distance as SD, the polar angle as R , and distance to observation point as NRMSE. A farther distance between two simulations indicates a higher sensitivity.

3 Meteorological and surface parameters

3.1 Weather conditions

The meteorological characteristics during the growing seasons in 2010 and 2011 are shown in Fig. 3.1. As both sites were located only 1.5 km away from each other without big obstacles in between, the daily meteorological conditions were quite similar. Therefore, only those at the rice field are shown.

The annual mean air temperature in 2010 was 8.5 °C. Mean temperatures in March and April were 1.9 and 3.0 K colder than the last 11-year mean (see Chapter 2.1.1), resulting in a delay

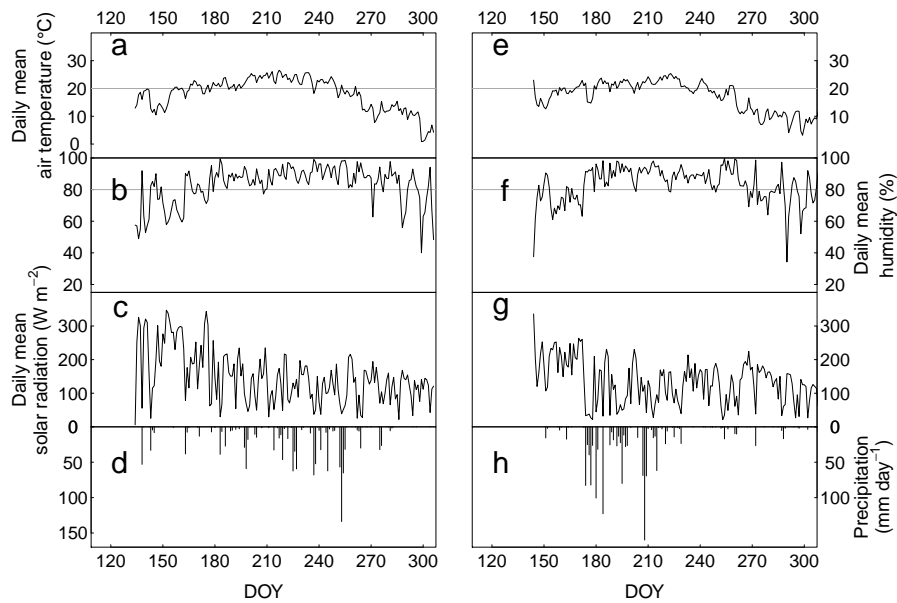


Figure 3.1: Meteorological observations during the crop growing seasons in 2010 (left panel) and 2011 (right panel) in the rice field. Observed variables are daily mean air temperature (a and e), humidity (b and f), solar radiation (c and g), and precipitation (d and h).

of half or one month in crops planting/transplanting. Daily mean temperature varied from 8 °C to 27 °C during the growing seasons (from late May to September) in 2010. The warmest month was August with a monthly mean of 22 °C. The daily mean relative humidity was often high, above 80 % on most days from June to August, resulting in many fog events. The relative humidity above the rice field was usually up to 4 % higher than above the potato field (not shown). The annual precipitation was 1586 mm in 2010, close to the annual mean of 1577 mm over the last 11 years. 75 % of the annual precipitation fell in the crop growing season in June – September. However, the precipitation in June (70 mm) and July (222 mm) was only half of the 11-year monthly mean, while the precipitation in September (427 mm) was more than twice the 11-year monthly mean, indicating a time shift of the summer monsoon. Typhoon Kompasu (International Designation: 1007) hit the research region in the early morning and exited in the afternoon on September 2nd in 2010, which brought strong wind with a maximum of 12.5 m s⁻¹ and precipitation of 62 mm d⁻¹ to the research sites.

The annual mean air temperature in 2011 was 8.1 °C. Mean temperatures in March and April were 1.8 and 2.7 K lower than the last 12-year mean. Daily mean temperature ranged from 11 °C to 25 °C during the growing seasons. The precipitation was intensified with 1849 mm, 77 % of which fell in the crop growing season in June – September. In contrast to 2010, the monthly precipitation in June (406 mm) and July (761 mm) in 2011 was much more than the 12-year mean (149 mm in June and 431 mm in July), while in August and September it was less than half of the 12-year mean.

The research region has the longest daytime when the sun reaches its greatest height and brings the strongest incoming solar radiation into the outer surface of the atmosphere in the northern hemisphere in summer. However, a significant depression in solar radiation was observed with a monthly mean of 241 W m⁻² in June and 162 W m⁻² in July in 2010, close to the 11-year mean. This depression was prolonged to August and September with monthly mean solar radiation 20 % less than the 11-year mean. The solar radiation in July in 2011 was 130 W m⁻², which was even less than that in August when the daytime was shorter.

The intensive rainfall during the summer monsoon had great influence on the completeness of the flux dataset. The month-to-month variation of the data completeness indicated that approximately 20 % of data were missing in May, June, and October (if excluding the periods when observations were unavailable caused by the power failure or the vacation of the instruments), while the data gaps doubled in July, August, and September. Large gaps (continuously several days) of the EC measurement were found during the monsoon rain events. The major cause of the gaps in the high quality database was the unreliable measurement by

the open-path gas analyzer under poor instrument status in bad weather, resulting in most (60 %) of all the gaps in both years, especially in September 2010 and July 2011 when the precipitation was the most intensive. Minor causes of gaps were the low quality defined by the steady-state test and the integral turbulence characteristics test (9 % of all the gaps), outliers defined by the statistical test (8 %), and other conditions (22 %) including wind direction with inadequate fetch.

3.2 Internal boundary layer and footprint

Agro-ecosystems are often located on complex terrains with a variety of characteristics such as climate gradient, different soil properties, patches of land use type, and so on. Thus, the internal boundary layer and footprint model are useful tools to evaluate the influence of complex topography on flux measurement. The internal boundary layer effect, presenting the influence of the neighbouring surface characteristics on the target area, was estimated with the height of the new equilibrium layer (Jegede and Foken, 1999; Mauder et al., 2006) and the transition area (Savelyev and Taylor, 2005). The aerodynamic measurement height (defined as the geometric measurement height minus the zero-plane displacement which is estimated as $2/3$ of the canopy height) must be below the height of the new equilibrium layer, roughly determined as $0.3\sqrt{x}$ where x is the fetch, to ensure that the measurement should represent the target land-use type. When the aerodynamic height is above $0.5\sqrt{x}$, the measurement is related to the neighbouring surface rather than the target surface. The measurement taking place in the layer between $0.3\sqrt{x}$ and $0.5\sqrt{x}$, assumed as a transition area, is acceptable for further data analysis for the target analysis (Eigenmann et al., 2011).

The footprint analysis was performed using a Lagrangian stochastic forward model to estimate two-dimensional contributions of source areas (Rannik et al., 2000; Göckede et al., 2004). As computations take the model much time, source weight functions for half-hourly measurement were picked from pre-calculated tables following a procedure used in Göckede et al. (2004, 2006, 2008). If the flux contribution from the target surface (rice and potato in this thesis) is larger than 70 %, then the corresponding half-hourly turbulent flux value is accepted for further analysis.

The flux contribution from the target land-use type for different wind direction sectors and stability classes is shown in Table 3.1 following Mauder et al. (2006) and Eigenmann et al. (2011). The target rice field contributed most (68 % to 93 %) of the related area in various

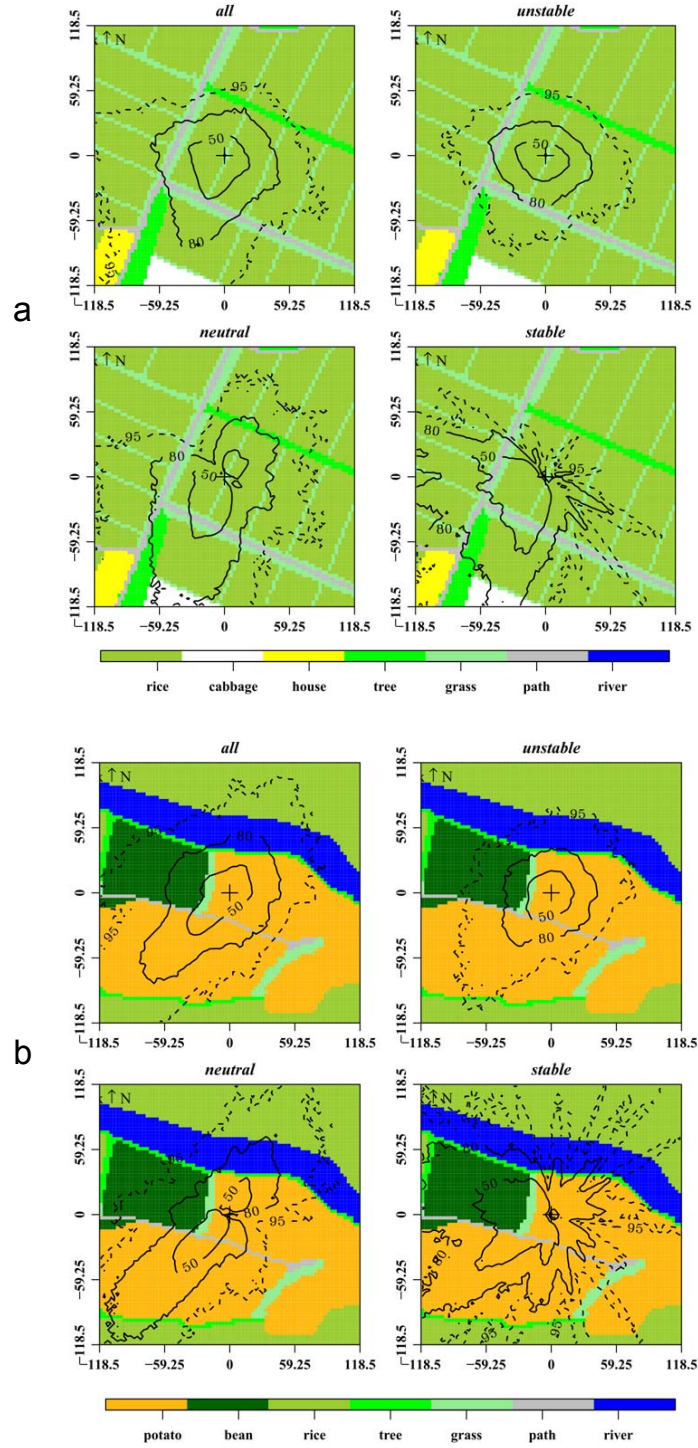


Figure 3.2: Footprint analysis for the rice site (a) and the potato site (b) during the crop growing season in 2010. The figure for the rice site in 2011 is not shown because it is similar to that in 2010.

stratification conditions in both 2010 and 2011 due to the large homogeneous surface of rice paddies (Table 3.1). With the internal boundary layer evaluation criterion by Eigenmann et al. (2011) and a sensor height of 2.8 m in this study, the sensor was well below the height of the transition area formed by adjacent change of surface characteristics in the rice field. Unavoidably, the nearby trees at the edge of the plot on the northeast and southwest, the grass verges between plots, and the surrounding paths were the main obstacles having influence

Table 3.1: Flux contribution from the target land use type (rice or potato) in wind direction and stability classes calculated from real observed data. Unstable condition means the stability parameter $\zeta < -0.0625$, stable means $\zeta > 0.0625$, neutral means $-0.0625 < \zeta < 0.0625$. x is the fetch. The measuring height was 2.5 m in the potato field and 2.8 m in the rice field. Numbers larger than 70 % are highlighted in bold type. N/A indicates no observation available under corresponding conditions.

Wind sector:	30 °	60 °	90 °	120 °	150 °	180 °	210 °	240 °	270 °	300 °	330 °	360 °
Internal boundary layer evaluation in the potato field:												
x (m)	42	66	102	75	76	70	82	26	18	20	31	40
$0.5\sqrt{x}$ (m)	3.2	4.1	5.0	4.3	4.4	4.2	4.5	2.5	2.1	2.2	2.8	3.2
Flux contributions, in %, from the target land-use type of potato:												
all	79	91	98	99	96	92	92	83	54	51	72	81
unstable	86	95	99	100	98	96	94	86	69	67	81	87
neutral	75	84	91	91	89	86	90	82	42	33	56	71
stable	28	69	88	N/A	90	74	77	75	15	10	32	N/A
Internal boundary layer evaluation in the rice field:												
x (m)	48	60	41	38	47	43	39	48	40	37	44	52
$0.5\sqrt{x}$ (m)	3.5	3.9	3.2	3.1	3.4	3.3	3.1	3.5	3.2	3.0	3.3	3.6
Flux contributions, in %, from the target land-use type of rice in 2010:												
all	68	85	87	86	83	71	75	86	90	89	92	88
unstable	68	83	86	85	83	73	80	93	93	91	92	89
neutral	69	88	92	92	86	69	74	82	86	85	89	86
stable	N/A	N/A	N/A	88	80	71	57	68	80	80	81	N/A
Flux contributions, in %, from the target land-use type of rice in 2011:												
all	71	91	93	93	89	73	73	85	86	84	88	90
unstable	69	91	93	92	90	74	77	91	88	85	89	91
neutral	72	91	93	93	85	73	71	79	82	80	82	86
stable	N/A	N/A	92	90	76	67	66	73	79	80	N/A	N/A

on the observation sensors, especially under stable and neutral conditions in the rice field (Fig. 3.2a), which resulted in a rejection of 6 % of the observations as interrupting information.

At the potato site, both the footprint analysis (Fig. 3.2b) and internal boundary layer evaluation (Table 3.1) show that most of the related area (51 % to 99 %) was contributed by the target potato field. The eddy-covariance sensor was influenced by the adjacent bean field on the northwest with a new equilibrium layer of 2.1 m and the river on the north, which were the main disturbances by the surface heterogeneity. Nevertheless, the wind-roses show that the prevalent wind direction was southwest. Only 3 % to 4 % of the wind with low wind speed came from the direction of the neighbouring bean field, and 7 % came from the direction of the river (Zhao et al., 2011). Therefore the influence of main adjacent obstacles was decreased. As a result, 5 % of the measurements were rejected as irrelevant data.

3.3 Biomass development

The growing period of crops is roughly composed of four stages, i.e. initial, development, mid-season, and late season (Allen et al., 1998). The biomass development of rice and potato in Haeon 2010 and 2011 is shown in Fig. 3.3 as well as in the panorama illustrations in Fig. 3.4 and video clips at <http://goo.gl/DPBjIn>. In the rice field, the plants had a height of 0.17 m at the beginning of the initial stage with a LAI of less than $0.03 \text{ m}^2 \text{ m}^{-2}$ and the above-ground biomass of $77 \times 10^3 \text{ kg ha}^{-1}$ in early June. The green parts including the leaves and stems grew rapidly in the development stage, when a maximum increasing rate of LAI reached $0.24 \text{ m}^2 \text{ m}^{-2}$ per day in late July. This resulted in a substantial increase of the above-ground biomass up to $8.2 \times 10^6 \text{ kg ha}^{-1}$. The plant height and LAI of rice reached a maximum of 0.88 m and $5.8 \text{ m}^2 \text{ m}^{-2}$, respectively, in August. From the beginning of the mid-season, the grains emerged and grew fast with the decrease of green leaves until the late-season.

The curve of rice plant height in 2011 was similar to that in 2010 but with a time lag because the transplanting date in 2011 was four calendar days earlier than in 2010. As the leaf area measurement was unavailable in 2011, it was assumed that the development of LAI in 2011 had the same pattern as 2010 on the basis of days after transplanting. Therefore, the continuous LAI in 2011 was estimated by Eq. 2.1 using the parameters fitted by the measurements in 2010.

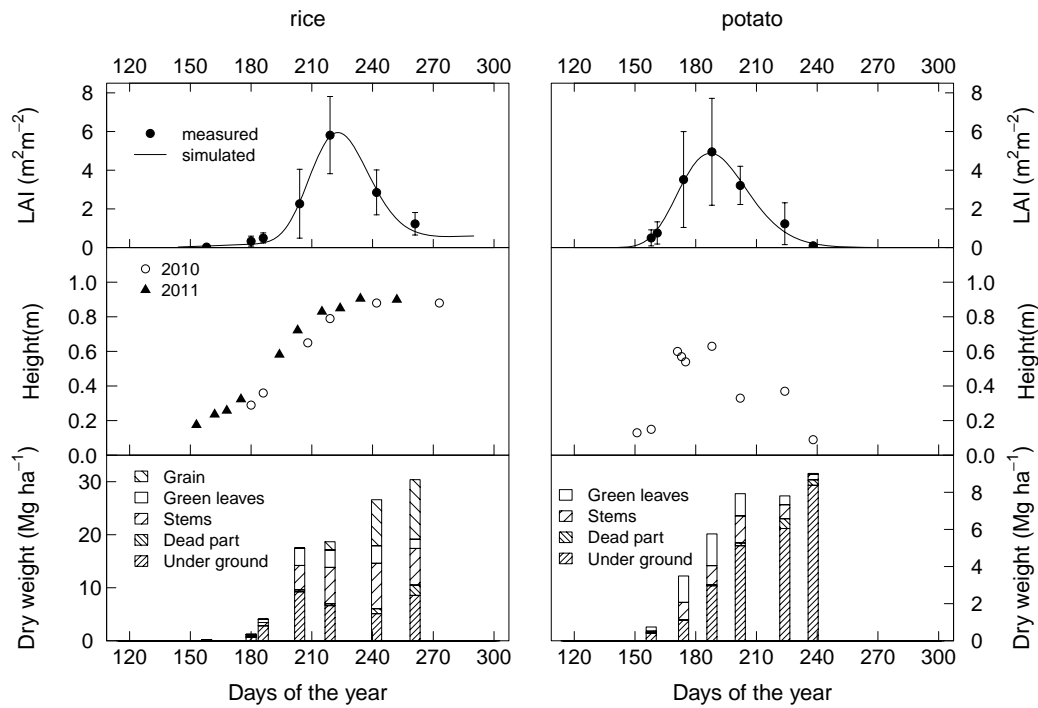


Figure 3.3: Biomass development of rice (left) and potato (right). Note that the grain was weighted without threshing. The graphs are based on the observation in 2010 except the plant height in the rice field in both 2010 and 2011.

The potato plants grew from under the ground when the soil temperature met the need for growth in the initial stage. Afterwards, the potato started a rapid growth in the development stage, with the height from 0.13 m growing to 0.6 m, and the LAI from $0.5 \text{ m}^2 \text{ m}^{-2}$ to $4 \text{ m}^2 \text{ m}^{-2}$ within just one month. The maximum growing rate of LAI reached $0.21 \text{ m}^2 \text{ m}^{-2}$ per day during this stage in June. In the following mid- and late-seasons, the new tubers grew while green leaves declined. At the end of the growing season, almost all green leaves disappeared. The harvest of the potatoes typically took place in late August or early September only if the field was dry enough. In 2010, however, the intensive rainfall in August led to too wet and heavy soils until the end of September. Therefore, the late potato season in 2010 was longer than in normal years.

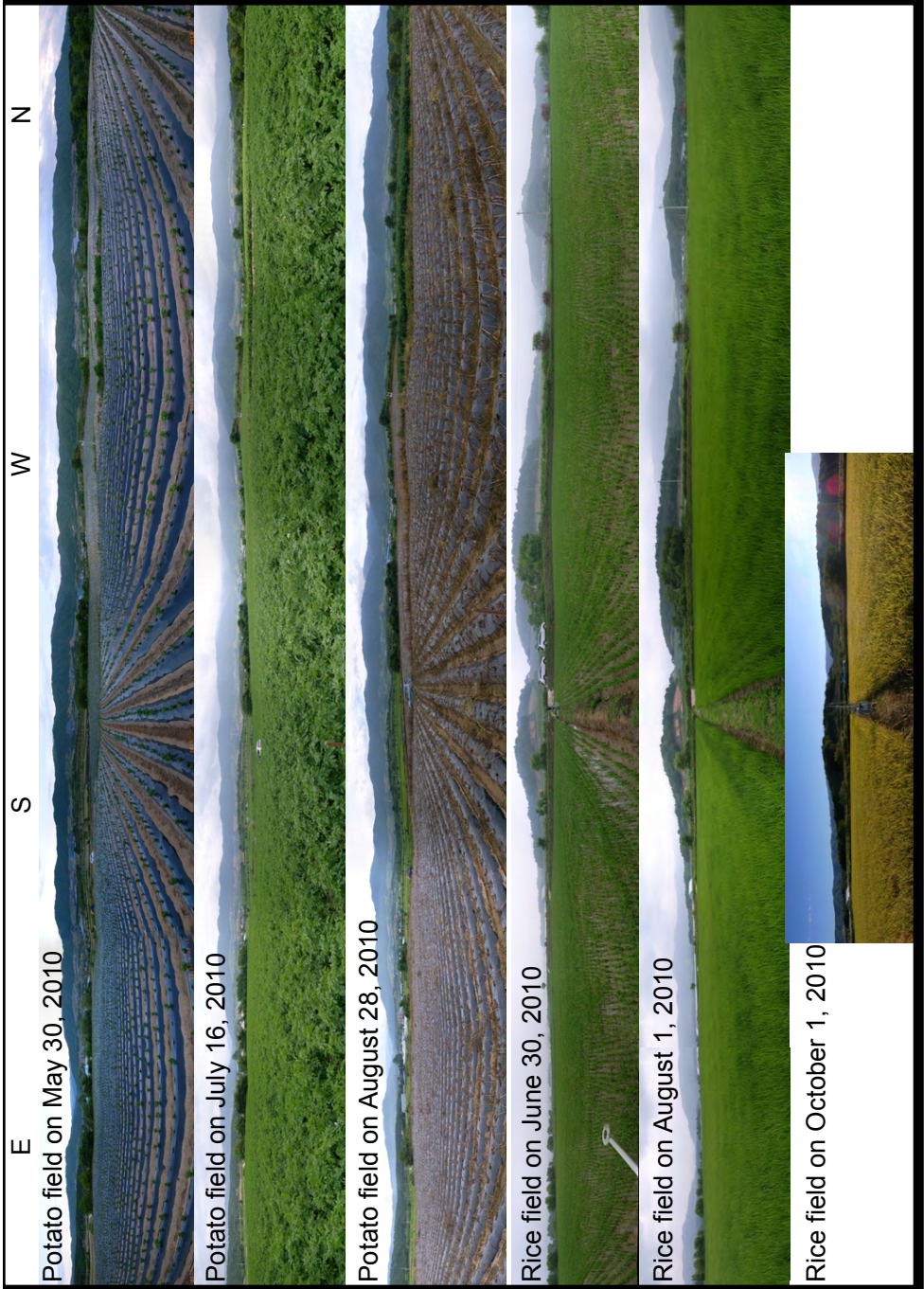


Figure 3.4: Panoramas of the rice field and potato field. Photographs by Peng Zhao.

4 Ecosystem evapotranspiration and energy components

4.1 Energy balance

The non-closure of the energy balance could result in the underestimation of heat fluxes between the surface and the atmosphere and further have influence on the evaluation of evapotranspiration models. Therefore, it is necessary to investigate the energy balance in order to improve the estimation of actual sensible and latent heat fluxes. The relative closure of the energy balance for each site in the whole observation period in this study is defined as the linear regression slope of daytime turbulent heat flux measured by eddy-covariance ($Q_H^{EC} + Q_E^{EC}$) against the available energy ($-Q_A$). Generally, the relative closure on average was 88 % ($R^2 = 0.87, n = 855$) for the rice field in 2010 and 85 % ($R^2 = 0.91, n = 1702$) in 2011, and 74 % ($R^2 = 0.91, n = 1066$) for the potato field, which agrees with studies in different agricultural sites (Mauder and Foken, 2006; Foken, 2008a). The lack of energy balance closure by eddy-covariance measurements has been reported by many investigators in a variety of surface conditions and has been demonstrated to be caused by large scale eddies or secondary circulations and advective flux components resulting from landscape heterogeneity (e.g. Mauder et al., 2007; Foken, 2008; Stoy et al., 2013). These secondary circulations move slowly, which cannot be observed by eddy-covariance with normally 30-min averaging time. Consequently, their contributions to the sensible and latent heat fluxes are missing.

This study used two methods to check the contribution of energy in large time scales. The first is Reynolds decomposition, which decomposes a variable into mean and fluctuation parts. A triple decomposition for the block ensemble average of vertical flux was proposed by Finnigan et al. (2003) and recently investigated and explained by Charuchittipan et al. (2014). This decomposition partitions the block ensemble average of flux into the mean term, the block-to-block variation term, and the turbulent term. As the mean term can be set to zero by planar fit rotation for the long term coordinate, the block-to-block variation term represents the large

scale eddies (called mesoscale motion) which are not detected by the 30-min eddy-covariance measurement. The second method is wavelet analysis following Mauder et al. (2007) and Charuchittipan et al. (2014). Wavelet analysis is a common useful tool for analyzing localized variations of power within a time series by decomposing the time series into time and frequency space simultaneously. The knowledge of both the amplitude of any periodic signals and the variation of this amplitude can be obtained.

The sensible and latent heat fluxes, contributed by large scale eddies during DOY 251 to DOY 273 in 2010 for the rice field and during DOY 152 to DOY 175 for the potato field, are shown in Fig. 4.1. Mesoscale heat fluxes were observed at both sites. At the rice field, large positive mesoscale latent heat fluxes (\tilde{Q}_E) were often found in the afternoon, while negative \tilde{Q}_E were often found at night-time or in the early morning. A relatively small negative \tilde{Q}_H was found in the afternoon or at night-time. Above the potato field, \tilde{Q}_H was often positive in the afternoon, while \tilde{Q}_E was often negative.

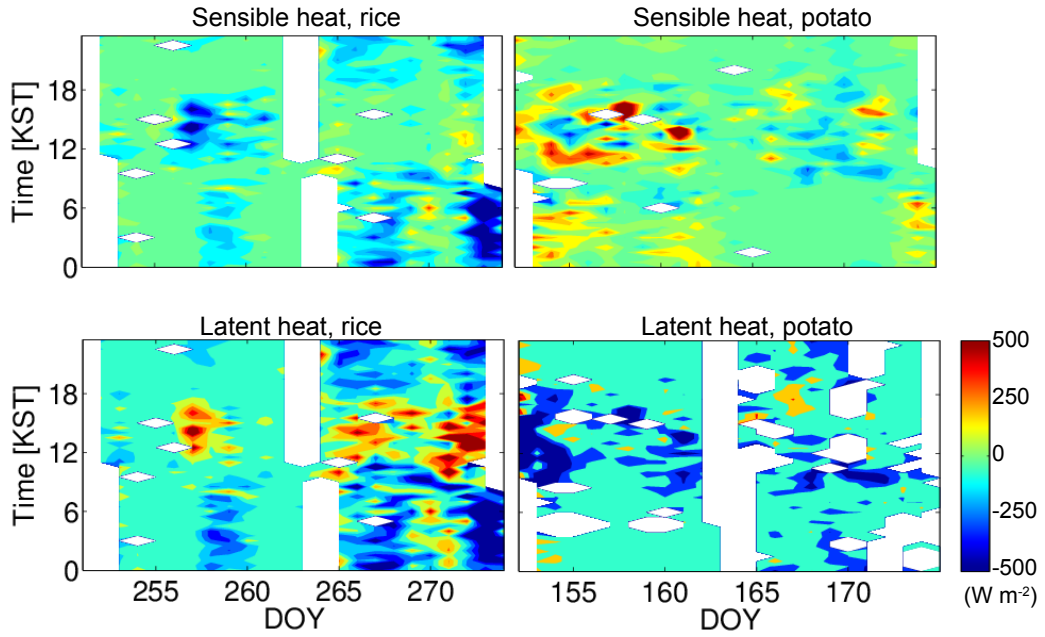


Figure 4.1: Hovmöller diagrams of observed mesoscale fluxes of sensible heat and latent heat in the rice field and in the potato field in 2010.

The periods from DOY 257 to 261 in 2010 for the rice field, and the periods from DOY 158 to 162 in 2010 for the potato field were selected as representatives to show the wavelet diagrams (Fig. 4.2). Daily cycles, covering time scales ranging from seconds to less than half an hour, were found in both sensible and latent heat fluxes at both sites. The contribution of these

small scale turbulent exchange could be sufficiently detected by the single EC complex. Large scales of the turbulence spectrum with their wavelengths of around four hours, however, were also found, which would be missed by the EC calculation based on a typical averaging period of 30 minutes. Such large scale circulation was caused by the upward movement of relatively warm and moist air near the ground surface, which was exchanged with relatively cool and dry air from above, resulting in a contribution mainly to sensible heat. This contribution was positive in the potato field, while in the rice field it was negative, which agrees with the mesoscale fluxes shown in Fig. 4.1.

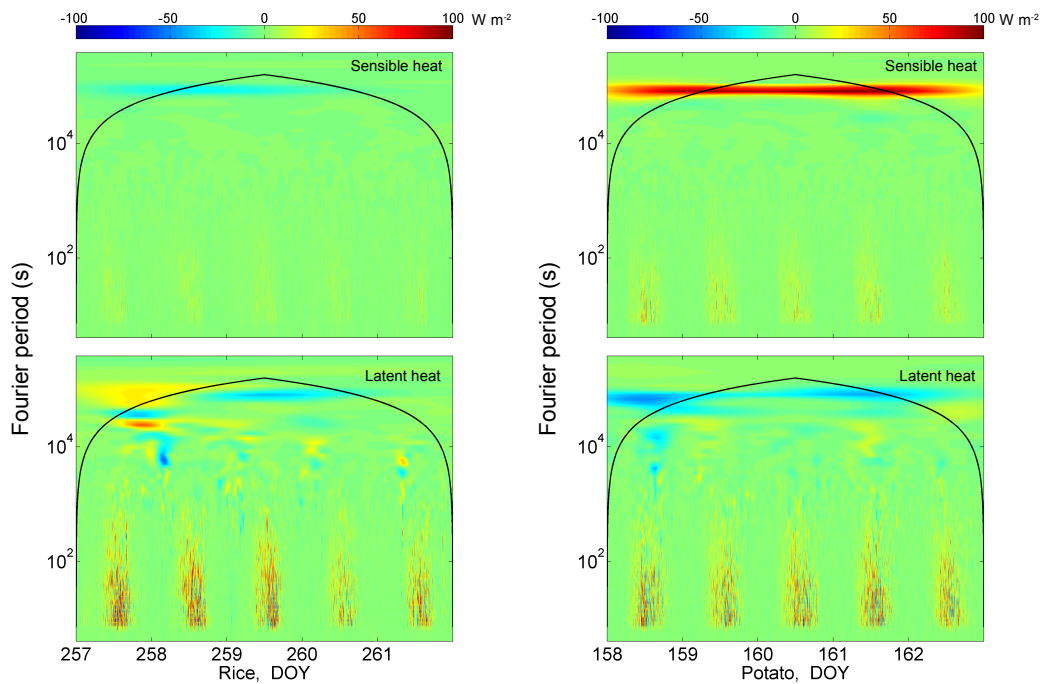


Figure 4.2: Wavelet cross-scalogram of sensible (upper panels) and latent (lower panels) heat fluxes at the rice (left) and potato (right) sites. The colour bar denotes the value in W m^{-2} and the black line is the cone of influence.

Both the mesoscale flux and wavelet analysis show the contribution of the secondary circulations to the heat fluxes. The scalar similarity between the sensible flux and the latent heat flux does not hold in all scales, and the secondary circulations near the surface mainly transport sensible heat. Therefore, the sensible heat missed by the 30-minute eddy-covariance measurement could be underestimated if the energy balance closure is corrected by the Bowen ratio method (EBC-Bo, see Chapter 2.3.4), but could be better compensated by the buoyancy flux ratio method (EBC-HB) suggested by Charuchittipan et al. (2014) that the residual should

be partitioned according to the buoyancy flux ratio rather than the Bowen ratio. Therefore, EBC-HB was used to correct the energy balance closure in this study. For the rice field, EBC-HB increased the latent heat flux (Q_E) on average by 3 %, and sensible heat flux (Q_H) by 50 %, while EBC-Bo increased Q_E and Q_H by 17 %. In contrast, EBC-HB for the potato field increased Q_E by 4 % and Q_H by 115 %, while EBC-Bo increased Q_E and Q_H by 20 %, as the Bowen ratio is relatively higher than in the rice field (see Chapter 4.3). The EBC corrected heat fluxes will be used to evaluate and improve the performance of the evapotranspiration models.

4.2 Diurnal variation

The diurnal variations of surface energy components are shown in Fig. 4.3. The night-time turbulent fluxes of energy were close to zero due to the low energy availability in the absence of

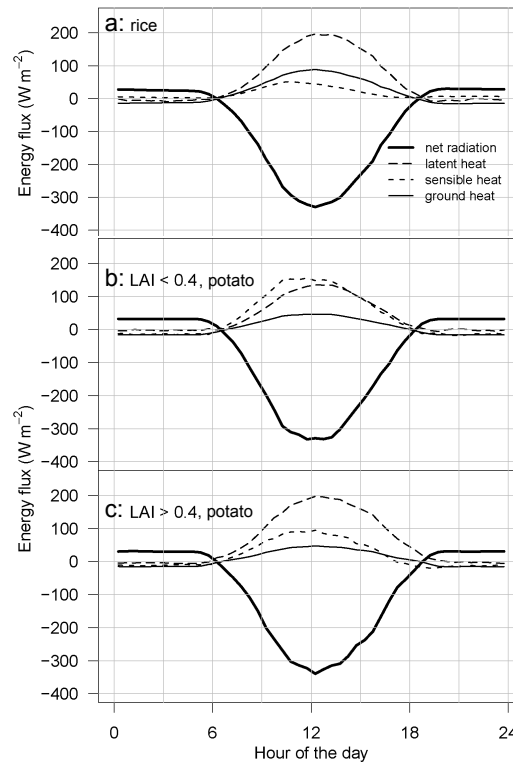


Figure 4.3: Mean diurnal courses of net radiation, ground heat flux, sensible and latent heat fluxes. Data are averaged over the whole growing season in the rice field (a), and over the season when $\text{LAI} < 0.4 \text{ m}^2 \text{ m}^{-2}$ (b) and when $\text{LAI} > 0.4 \text{ m}^2 \text{ m}^{-2}$ (c) in the potato field.

solar radiation and the stable stratification of the night-time boundary layer. In the daytime, the increase of all the components started in the morning at about 6:30, reached the peak at midday at about 12:00, and decreased until 19:00, resulting in a bell shape for both sites. Solar radiation is the primary determinant of the half-hourly latent heat flux, as the linear regression (not shown) indicates that the solar radiation can explain 88 % of the variation in the latent heat flux in the rice field ($n = 1466, p < 0.01$) and 84 % in the potato field ($n = 1786, p < 0.01$).

An evident difference in the pattern of the energy partitioning was found between the rice field and the potato field. The latent heat flux was the major part (approximately 60 % of the net radiation) and the sensible heat flux was the minor part throughout the growing season no matter how the vegetation developed in the rice field. In the potato field, the dominant energy component was also the latent heat flux when the vegetation was well developed ($LAI > 0.4 \text{ m}^2 \text{ m}^{-2}$). However, the latent heat flux was smaller than the sensible heat flux when the surface vegetation in the potato field was not well developed at the early and late growing stages.

4.3 Seasonal variation

The seasonal courses of dominant energy budget components in 2010 are shown in Fig. 4.4. The seasonal courses show that latent heat flux was the dominant energy component throughout the growing season in the rice field. Sensible and ground heat fluxes contributed a small portion of the seasonal energy budget. The seasonal pattern of latent heat flux generally followed that of net radiation. As the depressions of latent heat fluxes coincided with the rainfall events, the relatively high day-to-day variability in net radiation and latent heat flux indicates the high influence of cloud cover observed during the summer monsoon. The partitioning of available energy in the rice field shows that the portion of available energy directed to latent heat flux was approximately 87 % ($Bo = 0.28$) in the growing season in the rice field in 2010. Such small Bowen ratios are normally found in flooded fields in Asia, e.g. in Philippines (Alberto et al., 2009), in Taiwan (Tsai et al., 2007), and in Bangladesh (Hossen et al., 2012), indicating large energy partitioning to latent heat.

In the potato field, the seasonal pattern of energy partitioning was dependent on the surface vegetation conditions. Latent heat flux was larger than the sensible heat flux during most of the study period in the potato field, except that the latent heat flux was close to the sensible

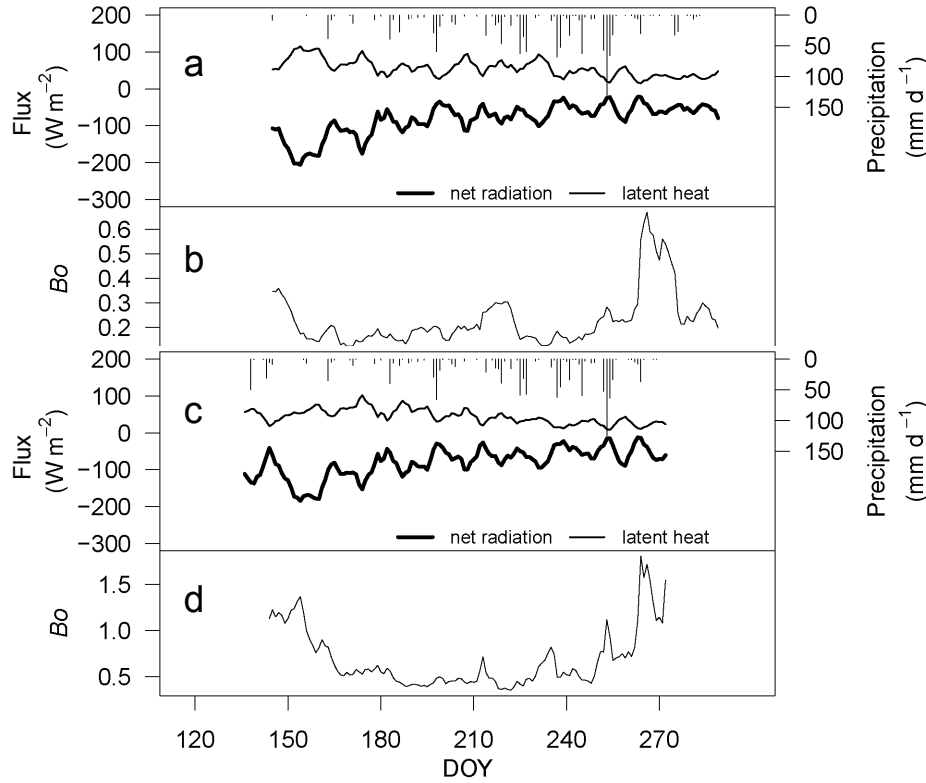


Figure 4.4: Seasonal variation of daily net radiation, latent heat flux, precipitation, and Bowen ratio in the rice field (a, b) and in the potato field (c, d) in 2010.

heat flux at the early and late growing stages, as described in Chapter 4.2. The mean of Bowen ratio for the potato field was 0.51. Bowen ratio decreased to the minimum in the potato field when green leaves were fully developed, indicating that the portion of available energy used for ET increased with the green-leaf density. A difference in the energy partitioning between the potato growing months was found. The portion of the available energy directed to latent heat flux was 60 % ($Bo = 0.67$) before and after the summer monsoon, and was enlarged to 72 % ($Bo = 0.39$) in July when LAI and air temperature were both high along with intensive precipitation.

Generally speaking, the latent heat flux played a major role in the turbulent heat fluxes for both sites. As discussed in Chapter 4.1, the latent heat flux could either be underestimated if no EBC correction is applied, or be overestimated if EBC correction is applied with EBC-Bo method, especially for the rice field. Thus, the EBC-HB correction method has the advantage to provide more reliable turbulent heat flux data for further analysis.

The seasonal courses of ET and its components in the rice field are shown in Fig. 4.5a. Daily ET in the rice field ranged from 0.9 mm d^{-1} on intensive rainy days to 4 mm d^{-1} on clear summer days. The average of ET was 2 mm d^{-1} , which was smaller than the values reported by Hossen et al. (2012) for a rice field in South Asia and those values reported by Tabbal et al. (2002) for rice fields in subtropical regions. The total ET was 283 mm in the rice field with the measurement of 71 mm and gap-filling of 212 mm during the growing seasons.

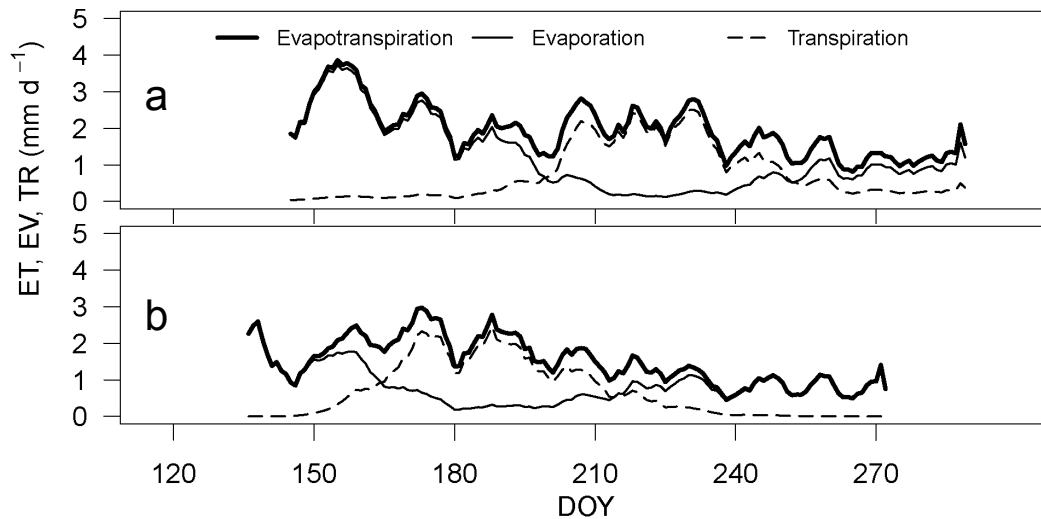


Figure 4.5: Seasonal variation of daily evapotranspiration (ET), evaporation (EV), and transpiration (TR) in the rice field (a) and the potato field (b) in 2010.

Based on Eqs. 2.12 and 2.13, whether evaporation or transpiration plays a dominant role depends on whether LAI is smaller than $1.5 \text{ m}^2 \text{ m}^{-2}$ (obtained by solving Eqs. 2.12 and 2.13 with the condition $\text{TR} = \text{EV}$) or not. Therefore, the dominant component of ET was evaporation at the early growing stage before DOY 186 in the rice field. Afterwards when LAI grew over $1.5 \text{ m}^2 \text{ m}^{-2}$, transpiration exceeded evaporation, increased with the vegetation development, and became the major component. After DOY 252 when LAI declined below $1.5 \text{ m}^2 \text{ m}^{-2}$, the dominant role was again evaporation.

The partitioning of ET results in an estimation of seasonal evaporation and transpiration shown in Table 4.1. In the rice field, evaporation contributed 84% of ET when $\text{LAI} < 1.5 \text{ m}^2 \text{ m}^{-2}$, and only 20% when $\text{LAI} > 1.5 \text{ m}^2 \text{ m}^{-2}$. In total, the dominant part of ET was evaporation, which was 60% of the entire evapotranspiration during the whole growing period in the rice field. Therefore, the factors affecting evaporation are more important than those

affecting transpiration for the improvement of ET model performance for the rice field (See Chapter 4.4).

Table 4.1: Partitioning of evapotranspiration. ET: evapotranspiration. EV: evaporation. TR: transpiration

Sites	Periods	ET (mm)	EV (mm)	TR (mm)
Rice	2010	283	175	108
Rice	2010 when LAI < 1.5 m ² m ⁻²	175	152	23
Rice	2010 when LAI > 1.5 m ² m ⁻²	108	23	85
Potato	2010	206	113	93
Potato	2010 when LAI < 1.5 m ² m ⁻²	107	91	16
Potato	2010 when LAI > 1.5 m ² m ⁻²	99	22	77

The seasonal course of ET and its components in the potato field are shown in Fig. 4.5b. Daily ET in the potato field was 1.5 mm on average, ranging from 0.5 mm on intensive rainy days to 3 mm on clear summer days. The total ET was 206 mm in the potato field, smaller than in the rice field, with the measurement of 86 mm and gap-filling of 120 mm during the growing seasons, which was a small fraction of the total seasonal precipitation (1196 mm). Comparing the total ET in the potato field in this study with other studies, it is significantly lower than non-mulching potato fields (Parent and Anctil, 2012), mainly because mulching serves as a barrier between the soil and the atmosphere, which decreases the soil evaporation (Kar and Kumar, 2007). Evaporation from plastic or straw mulching for other crop species was also reported lower than non-mulching croplands. For instance, ET above completely mulched soil was 25 % to 29 % lower than that without mulching in a maize field by the study of Doss et al. (1970), or 17 % lower by the study of Zhou et al. (2009). Even partly mulching could reduce the ET by 11 % (Zhou et al., 2009). A study by Hou et al. (2010) showed that the reduction by mulching in a tomato field was 10 % to 12 %. The proportion of soil evaporation to ET without mulching was 26 % (Kang et al., 2003) or 30 % (Liu et al., 2002), which could be reduced to 10 % with mulching (Ding et al., 2013).

Total seasonal evaporation in the potato field was nearly identical to transpiration. Although evaporation contributed 85 % of the ET when LAI was below 1.5 m² m⁻², during other periods it only contributed 22 %. Seasonal trends of evaporation and transpiration shows that the dominant component of ET was evaporation at the early growing stage before DOY 164. Afterwards, transpiration exceeded evaporation and increased with the vegetation development. After DOY 215, the dominant role was again evaporation. As a whole, transpiration plays

a comparable role to evaporation in ET. Therefore, the factors affecting evaporation are as important as those affecting transpiration for the improvement of ET model performance for the potato field (See Chapter 4.4).

4.4 Penman-Monteith model and stomatal resistance

The Penman-Monteith (PM) function (Monteith, 1965) is a widely applied calculation for ecosystem evapotranspiration. As one of the major difficulties in application of the PM method, the determination of the stomatal resistance (r_s) has drawn a lot of attention (Cleugh et al., 2007; Wang and Dickinson, 2012). Among numeric models for simulating r_s , FAO and KP models (see Chapter 2.4.2) have the advantage of simplicity and good performance. Previous chapters (Chapter 4.1 – 4.3) provide reliable EBC corrected turbulent heat fluxes, and demonstrate that influencing factors on evaporation and transpiration should be treated in different ways between the rice field and the potato field. This chapter will firstly demonstrate the necessity and importance to accurately estimate r_s , and then test Hypothesis 1 of this thesis (Chapter 1.3) to reveal whether the PM-KP method may perform better than the PM-FAO model for the estimation of ET for croplands.

4.4.1 Sensitivity coefficients

The relative influence of available energy (Q_A), vapour pressure deficit (VPD), aerodynamic resistance (r_a), and stomatal resistance (r_s) on simulated latent heat fluxes by the PM model was investigated by the sensitivity coefficients (Eqs. 2.20 – 2.24). These coefficients were firstly calculated on a half-hourly base. The data in the daytime through the growing season were then taken into account to derive the mean values for diurnal and seasonal patterns (Fig. 4.6).

In the case of the rice field, both the sensitivity coefficients for available energy (S_{Q_A}) and for VPD (S_{VPD}) are positive. The available energy uniformly plays a primary role in the variation of ET simulation. It determines 50 % – 80 % of the ET variation throughout most of the day. As the sum of S_{Q_A} and S_{VPD} is one (Eq. 2.22), these two coefficients show opposite diurnal patterns. S_{VPD} ranges between 20 % and 40 % in most hours, and has values even larger than S_{Q_A} in the early morning and later afternoon. The sensitivity coefficient for aerodynamic resistance (S_{r_a}) is almost constantly small with a range between –17 % and

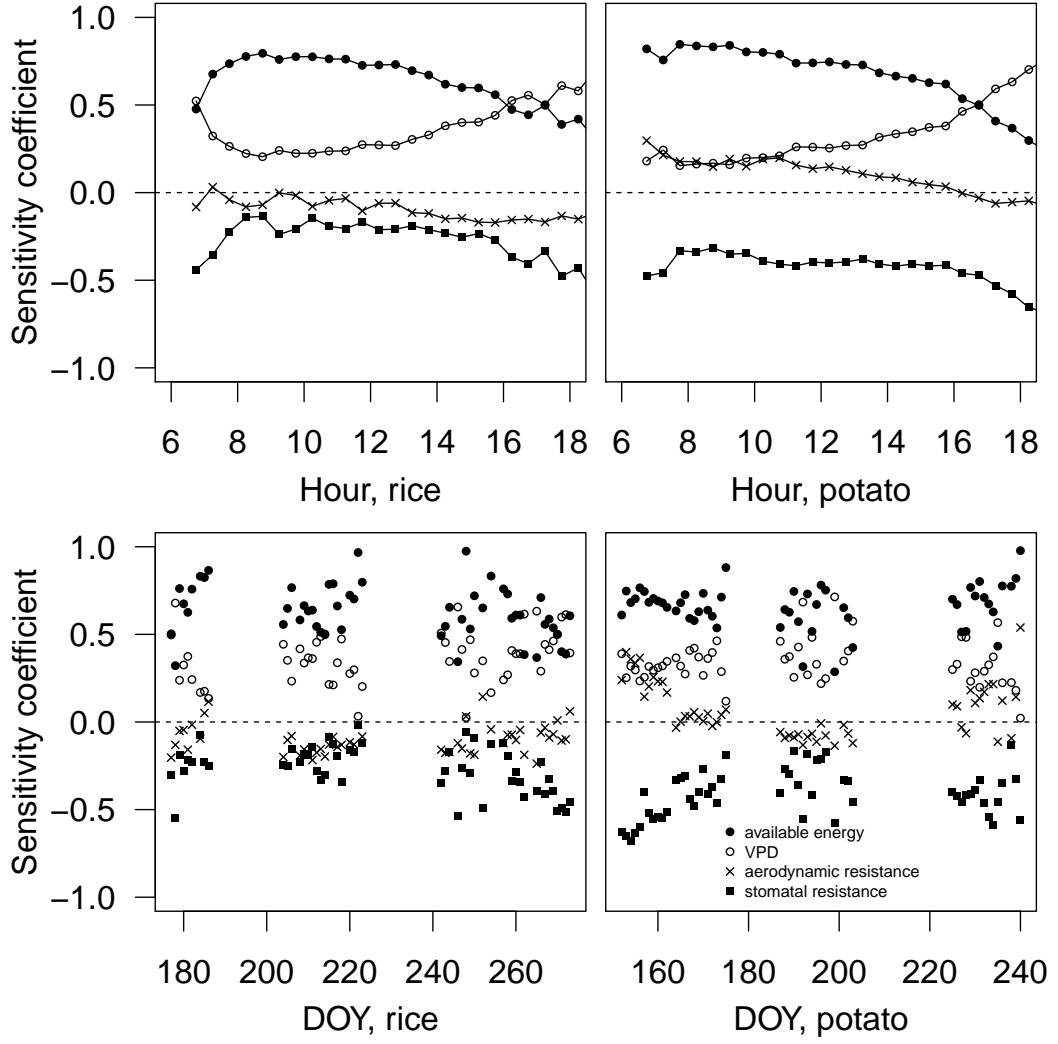


Figure 4.6: Diurnal (upper panel) and seasonal (lower panel) patterns of Penman-Monteith model sensitivity coefficients for available energy (closed circle), vapour pressure deficit (VPD, open circle), aerodynamic resistance (cross), and stomatal resistance (closed square) for the rice field and the potato field in 2010.

3 %, most of which are negative. The sensitivity coefficient for stomatal resistance (S_{r_s}) is constantly negative ranging between -14% and -48% with the highest absolute values in the early morning and late afternoon. On average, Q_A , VPD, r_a , and r_s determine 61 %, 39 %, 9 %, and 30 % of ET variation, respectively. The increase of Q_A , VPD, and the decrease of r_s result in the increase of ET, while r_a has a minor influence on ET. The seasonal patterns of the sensitivity coefficients show generally consistent results with the diurnal mean. Furthermore,

the sensitivity coefficients do not show significant seasonal variation, probably because the permanent standing water in the rice field acted as a major source of ET and had no significant change.

In the case of the potato field, the available energy also plays the primary role in ET. It determines 54 % – 84 % of ET variation throughout most of the day. S_{VPD} has a range between 15 % – 78 % with the maximum occurring in the late afternoon. S_{r_a} is positive in most hours of the day, with relatively large values around 20 % in the morning, and decreases to around zero in the afternoon. S_{r_s} is constantly negative and determines 32 % – 68 % of ET variation. On average, Q_A , VPD, r_a , and r_s determine 65 %, 35 %, 10 %, and 44 % of ET variation, respectively. The sensitivity coefficients show significant seasonal variations. The monthly mean of S_{VPD} in July is 41 %, which is larger than those in June (32 %) and August (30 %). However, S_{r_s} shows the opposite trend, with the minimum monthly mean of 33 % in July, smaller than those in June (46 %) and August (42 %). S_{r_a} has small negative values with absolute mean value of 8 % in July, while positive values with mean values of 14 % in June and 11 % in August. As the surface vegetation changes rapidly with the fully development in August in the potato field (see Chapter 3.3), the seasonal variation in the sensitivity coefficients could possibly result from the dependence of ET on the surface vegetation.

The comparison of the sensitivity coefficients between the two fields indicates the common result that r_s , besides Q_A and VPD, plays a very important role in ET estimation by the PM model. It even has more influence on ET than VPD for the potato field. As Q_A and VPD can be accurately obtained from the field observation with modern devices, the estimation of r_s is a key problem for the PM model.

4.4.2 PM-FAO model

The sensitivity of the PM-FAO model performance was tested by the GLUE method (see Chapter 2.4.3). Besides the variables (available energy, air temperature, vapour pressure deficit) describing the thermodynamic state of the atmosphere which can be obtained from observation, stomatal resistance (r_s) and aerodynamic resistance (r_a) have to be parameterized. Therefore, this study applied the GLUE method to the sensitivity test on the single leaf stomatal resistance (r_{si}) and the coefficients p_h and p_m (Fig. 4.7), which are used to estimate r_s (Eq. 2.16) and r_a (Eq. 2.15) for the potato site. The maximum as well as the minimum of the model efficiency coefficient is obviously changed with the randomly-modified value of r_{si} . The maximum model efficiency coefficient, for instance, shows a peak value of 0.81 at

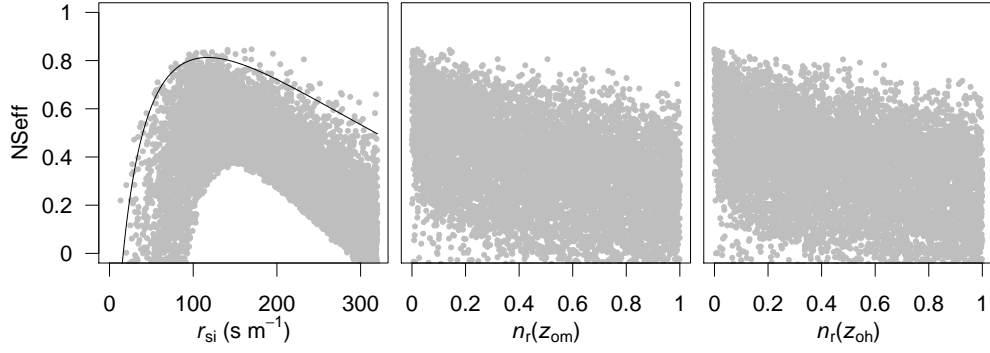


Figure 4.7: Sensitivity graphs for PM-FAO modelled Q_E to modifications in r_{si} , p_m , and p_h in the potato field. The solid line highlights no modification to p_m , and p_h .

$r_{si}=117 \text{ s m}^{-1}$. Either an increase or decrease of r_{si} results in a sharp decrease of the model efficiency coefficient to 0.6 at $r_{si}=320 \text{ s m}^{-1}$ or to below 0 at $r_{si}<20 \text{ s m}^{-1}$. Better than the literature values of r_{si} between 70 and 80 s m^{-1} proposed by Allen (2005) which shows the maximum model efficiency coefficient ranging from 0.72 to 0.77, $r_{si}=117 \text{ s m}^{-1}$ could be used as an optimal estimation. In contrast, the model efficiency is not quite sensitive to p_m or p_h . The maximum model efficiency coefficient decreases slightly from 0.81 to 0.70 when p_m or p_h increases from 0 to 1. The estimation for the aerodynamic resistance (r_a) usually uses a typical value of 0.1 for p_m and p_h , which is an acceptable estimation for the performance of the PM-FAO model and is used in the subsequent analysis in this study.

The PM-FAO model using $r_{si} = 75 \text{ s m}^{-1}$ (the medium of the proposed value by Allen et al., 2005) performs well, with model efficiency coefficient $NSeff = 0.75$ and regression slope ($Q_E^{\text{PM-FAO}}$ against $Q_E^{\text{EBC-HB}}$) of 1.06 ($n = 1061$). By using $r_{si} = 117 \text{ s m}^{-1}$, the model performance is slightly improved with model efficiency coefficient $NSeff = 0.81$ and smaller regression slope of 0.94. The decline of the slope is due to the larger value of r_{si} , resulting in an increase of the denominator of the PM function and consequently the decrease of the simulated Q_E .

In order to check the details of the PM-FAO model performance, the evaluation of the model was classified into subgroups according to grouped values of air temperature, wind speed, relative humidity, LAI, plant height and DOY with specified intervals (Fig. 4.8). For instance, the model efficiency at the temperature of 10 °C was calculated as model efficiency coefficient between $Q_E^{\text{PM-FAO}}$ and $Q_E^{\text{EBC-HB}}$ within the temperature range of 7.5 to 12.5 °C. The model efficiency is consistently good across the whole range of temperatures with a model efficiency

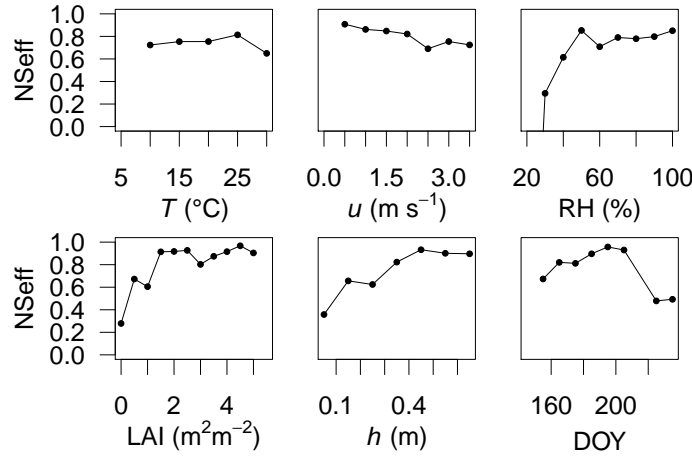


Figure 4.8: Performance of PM-FAO model in relation to the air temperature (T), wind speed (u), relative humidity (RH), leaf area index (LAI), plant height (h), and DOY, in the potato field.

coefficient around 0.7. At low wind speed, the model efficiency is high (around 0.9), but drops slightly to below 0.8 when wind speed is over 2.5 m s^{-1} .

In contrast, the model performance shows greater variety with humidity. The model efficiency is very low when the air is dry, possibly because of the regulation of leaf water potential by stomata. Oren et al. (1999) found that $\frac{1}{r_s}$ decreases linearly with $\log(\text{VPD})$ for plant species and concluded that stomatal sensitivity is proportional to the magnitude of $\frac{1}{r_s}$ at low VPD ($\leq 10 \text{ hPa}$), which was later demonstrated to be consistent with the linear model presented by Katul et al. (2009). In other words, plants tend to close their stomata so that plants lose less water when VPD is high. This regulation could result in a deviation of r_s from the estimation by Eq. 2.16, and consequently the poor efficiency of the PM-FAO model in the case of the dry air.

Good performance is achieved at high humidity ($> 50 \%$), large LAI ($> 1.5 \text{ m}^2 \text{ m}^{-2}$), and tall plant height ($h > 0.3 \text{ m}$) with a model efficiency coefficient around or over 0.8. Actually, these humid and fully developed vegetation conditions took place simultaneously from mid June to July (DOY 170 to 210), resulting in good performance of the PM-FAO model for the potato field in the summer monsoon.

The pattern of the sensitivity test for the rice field is similar (therefore not shown), with the only remarkable difference that the optimal r_{si} of 38 s m^{-1} is much smaller than the typical range of r_{si} . The model performance is significantly improved if using $r_{si} = 38 \text{ s m}^{-1}$, resulting

in a model efficiency coefficient $N_{\text{Seff}}=0.91$ and regression slope of 0.96 ($n = 847$), which is better than the model performance using the literature value of $r_{\text{si}} = 75 \text{ s m}^{-1}$ with a model efficiency coefficient $N_{\text{Seff}} = 0.80$ and regression slope of 0.80. The values of the slope lower than unity indicate that the PM-FAO approach has a tendency to underestimate Q_E for the rice field in this study, especially in the case of high values of Q_E . The sensible heat flux is consequently overestimated on the basis of the energy balance closure concept.

The performance of the PM-FAO model for the rice field was also evaluated in subgroups of air temperature, wind speed, relative humidity, LAI, plant height and DOY (Fig. 4.9). The model efficiency is consistently good across the range of LAI and plant height, with the minimum model efficiency coefficient of 0.8 at small LAI. Poor model performance at low temperature ($< 10^\circ\text{C}$) is because low temperature was only observed in the early morning at the early or late growing stage of rice, which coincided with the occurrence of small LAI and small Q_E . Best model performance could be seen at low wind speed. The increase of wind speed ($> 1.5 \text{ m s}^{-1}$) slightly decreased the model efficiency. The explanation is that Q_E is expected to be enhanced under windy conditions on sunny days in summer, but this effect is insufficiently represented by the PM-FAO model with the dependence of r_s only on LAI (Perez et al., 2006), especially over a surface which is a mixture of vegetation and flooded water such as the rice field, because the open standing water, as an evident source of evaporation, is unrelated to stomata. Unlike the low model efficiency when the air is dry in the potato field, the model efficiency shows independence on the relative humidity, because the major role of

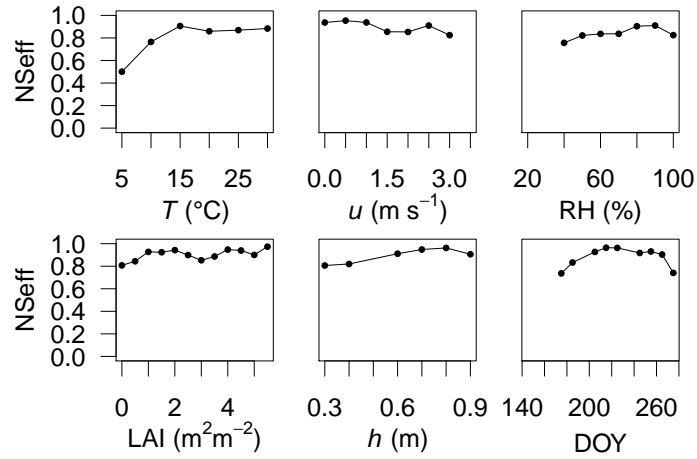


Figure 4.9: Performance of PM-FAO model in relation to the air temperature (T), wind speed (u), relative humidity (RH), leaf area index (LAI), plant height (h), and DOY, in the rice field, 2010.

evapotranspiration in the rice field is played by the open water, therefore the regulation of stomata to VPD could not be detected in this analysis.

To sum up this section, the PM-FAO model performance is sensitive to the estimation of r_s rather than r_a for both croplands. In case of the potato field, the conventional PM-FAO calculation with the literature value is still recommended for a fully developed vegetation surface, while a site-specifically calibrated value of r_{si} is optional. For less developed vegetation surface, an improvement of the model is needed. In case of the rice field, the conventional PM-FAO calculation with the literature value is insufficient. The improvement of the model performance could be realized either by a site-specifically calibrated value of r_{si} or by the PM-KP model which will be discussed in the following chapter.

4.4.3 PM-KP model

In order to solve the previously shown problems in the PM-FAO model, which does not take into consideration the dependence of r_s on meteorological variables, the synthesized influence of the meteorological parameters on r_s is studied using the KP model. It was calibrated for the rice field and the potato field individually. This calibration yields the KP coefficients a and b for each species from the linear regression between $\frac{r_s}{r_a}$ and $\frac{r_s^*}{r_a}$ (Eq. 2.17). As it has been demonstrated that 20 values of hourly data were sufficient for a reliable calibration (Katerji and Rana, 2006; Katerji et al., 2011), this thesis randomly sampled 40 half-hourly records out of the daytime high quality data (totally 594 records from the potato site and 361 from the rice site) for calibration. Such calibration procedure was repeated for 1000 runs so as to yield the statistical distributions of a and b (Fig. 4.10).

In the case of the potato field, a normal distribution was discovered in both the slope a with 0.63 ± 0.21 (mean \pm standard error), and the intercept b with 1.47 ± 0.42 , indicating a relatively wide peak. In the case of the rice field, a showed a normal distribution with 0.52 ± 0.08 , and b with -0.06 ± 0.14 , indicating a relatively narrow peak. Although the mean of a and b are comparable with published values (Table 4.2), the variations of them have not been reported. The range of both coefficients for the rice site was approximately one third of those for the potato field, indicating that the error resulting from the random sampling of the data is smaller and therefore the calibration is more stable for the rice field than for the potato field. Thus, one random sample with a limited number of observation records in the whole crop growing seasons could be sufficient to parameterize a and b for the rice field, but could yield a large deviation in a and b for the potato field.

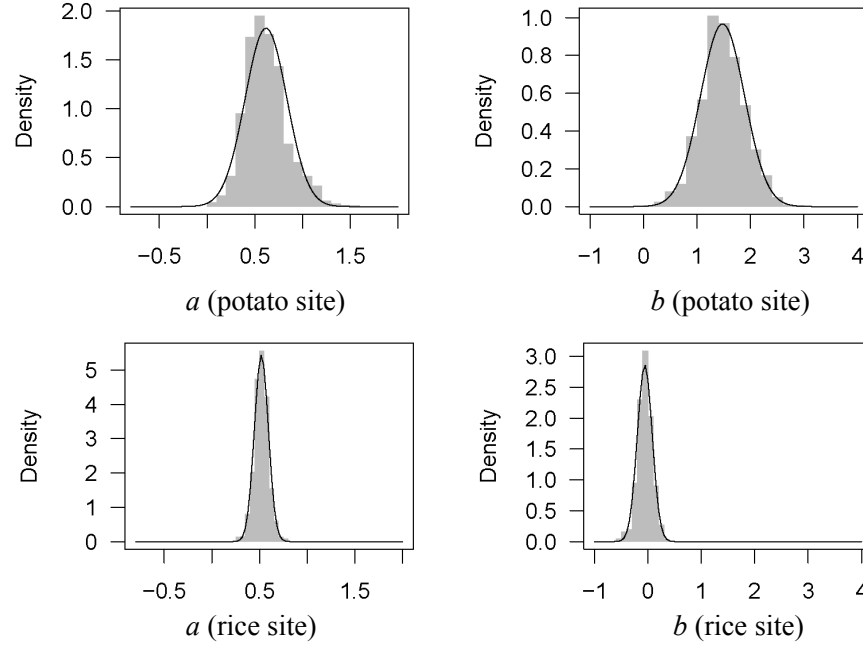


Figure 4.10: Statistical distribution of the regression coefficients a and b of the KP equation (Eq. 2.17).

Table 4.2: Calibration coefficients of KP model.

Species	LAI	a	b	References
Soya bean	0.8 – 4	0.95	1.55	Katerji and Rana (2006)
Sweet sorghum	1 – 6.4	0.85	1.00	Katerji and Rana (2006)
Grain sorghum	3.8 – 4.2	0.54	0.61	Katerji and Rana (2006)
Tomato	0.5 – 3.8	0.54	2.4	Katerji and Rana (2006)
Grass	2 – 2.5	0.16	0.00	Katerji et al. (2011)
Rice	0 – 5.8	0.52 ± 0.08	-0.06 ± 0.14	this study
Potato	0 – 4	0.63 ± 0.21	1.47 ± 0.42	this study

Fig. 4.11 shows the sensitivity of the PM-KP model performance to the values of a and b (both randomly in normal distribution) by the GLUE method. The maximum model efficiency coefficient for the potato field ranges from 0.62 to 0.76 across the distribution of a and b , while the minimum model efficiency coefficient increases with the increase of a and b until it reaches the peak with model efficiency coefficient $N_{\text{Seff}} = 0.6$ before decreases. In contrast, both the maximum and minimum of the model efficiency coefficient for the rice field are relatively stable, indicating less model sensitivity to the value of KP coefficients, because of the narrow variation range of a and b .

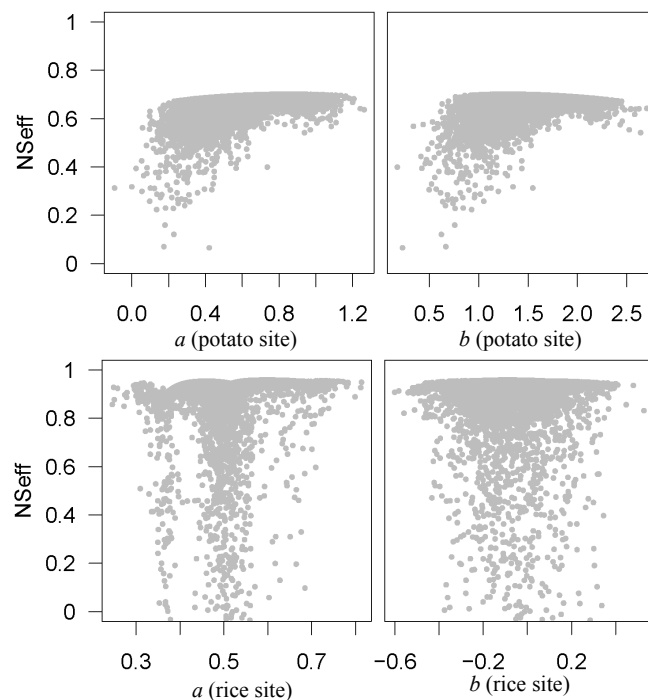


Figure 4.11: Sensitivity graphs for PM-KP modelled Q_E to modifications in KP coefficients a and b .

The best parameterization could therefore be derived on the basis of the highest model efficiency. The best parameters for the potato field are $a = 0.76$ and $b = 1.86$, resulting in the a model efficiency coefficient $N_{\text{Seff}} = 0.76$ and regression slope of 0.85 ($n = 1061$) in the linear regression between the simulation and observation ($Q_E^{\text{PM-KP}}$ against $Q_E^{\text{EBC-HB}}$). Compared with the performance of the PM-FAO model, the PM-KP model performs worse and Q_E is underestimated if the model is applied in the whole growing season of potato. However, if the evaluation of the model is classified into subgroups according to grouped values of LAI, plant height, and DOY, the performance of the PM-KP model at small LAI ($< 1.5 \text{ m}^2\text{m}^{-2}$)

and short plant ($h < 0.3$ m) in August (Fig. 4.12) is better than that of the PM-FAO model (Fig. 4.8).

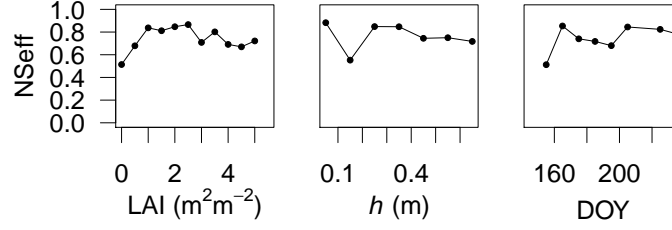


Figure 4.12: Performance of PM-KP model in relation to leaf area index (LAI), plant height (h), and DOY, in the potato field.

In contrast, the optimal values of the KP coefficients for the rice field, i.e. $a = 0.6$ and $b = -0.09$, yield a model efficiency coefficient of 0.96 and the regression slope ($Q_E^{\text{PM-KP}}$ against $Q_E^{\text{EBC-HB}}$) of 0.97 ($n = 847$), which is better than the PM-FAO model. In other words, the PM-KP model is more efficient than the PM-FAO model for the rice field. The limitation of PM-FAO model for the rice field is possibly because Eq. 2.16 yields too large values of r_s when LAI is very small, whereas the flooded rice field for small LAI is almost an open water surface and the actual r_s is close to zero, thus r_s is underestimated by the FAO model. The KP model has the advantage because it is consistent with the fact that Q_E is dominantly controlled by the meteorological factors rather than LAI in well-irrigated crops (Perez et al., 2006).

To sum up this section, the PM-KP model performs better than the PM-FAO model for ET estimation for the rice field and for poorly developed potato field. Therefore, this study used the PM-KP approach to fill the data gaps of evapotranspiration for the rice field in the whole growing season. In case of the data gaps in ET for the potato field, the PM-KP model is used for the season when $\text{LAI} < 1.5 \text{ m}^2\text{m}^{-2}$, while the PM-FAO model is used for the season when $\text{LAI} > 1.5 \text{ m}^2\text{m}^{-2}$.

5 Carbon dioxide exchange

The estimation of net ecosystem exchange of carbon dioxide (NEE) is very important to estimate the agro-ecosystem carbon balance. This chapter will firstly present the differences in seasonal contributions of respiration and photosynthetic assimilation to NEE between the rice field and the potato field, and then investigate the influencing factors to respiration and photosynthetic assimilation in croplands. As results, Hypothesis 2 of this thesis (Chapter 1.3) about the improvement of the light response function will be tested.

5.1 Time courses

The time courses of the net flux of carbon dioxide (NEE) were composed of the high-quality data by the eddy-covariance measurement and the data by gap-filling. The gap-filled data shared 60 % of the NEE dataset for the potato field, 75 % and 65 % for the rice field in 2010 and in 2011, respectively. The diurnal and seasonal patterns of NEE and its components (GPP and R_{eco}) in the rice field are shown in Fig. 5.1a and b. NEE was around zero at the beginning of the growing season because of small values of CO_2 uptake and release by newly-transplanted rice plants. The pattern of GPP began to show clear diurnal variation around DOY 163 while R_{eco} was still rather small, resulting in a diurnal variation of NEE and the rice field acted obviously as a net CO_2 sink. Half-hourly NEE during the development stage (DOY 144 to 215) fluctuated from -25 to $6 \mu mol m^{-2} s^{-1}$. From around DOY 180, GPP increased rapidly along with the fast development of rice plants, and reached the peak around DOY 225 in 2010 and DOY 220 in 2011, which played a decisive role on NEE reaching a maximum with a mid-day net uptake of approximately $-37 \mu mol m^{-2} s^{-1}$, at the same time that LAI reached its peak. Meanwhile, R_{eco} increased gradually and reached the maximum around DOY 196 and 217 in 2010 and DOY 205 in 2011. Afterwards, R_{eco} exhibited a few large values, and decreased close to zero until harvest. At the late-season stage (DOY 260 to 290), NEE in the rice field decreased to the same level as in the early initial stage.

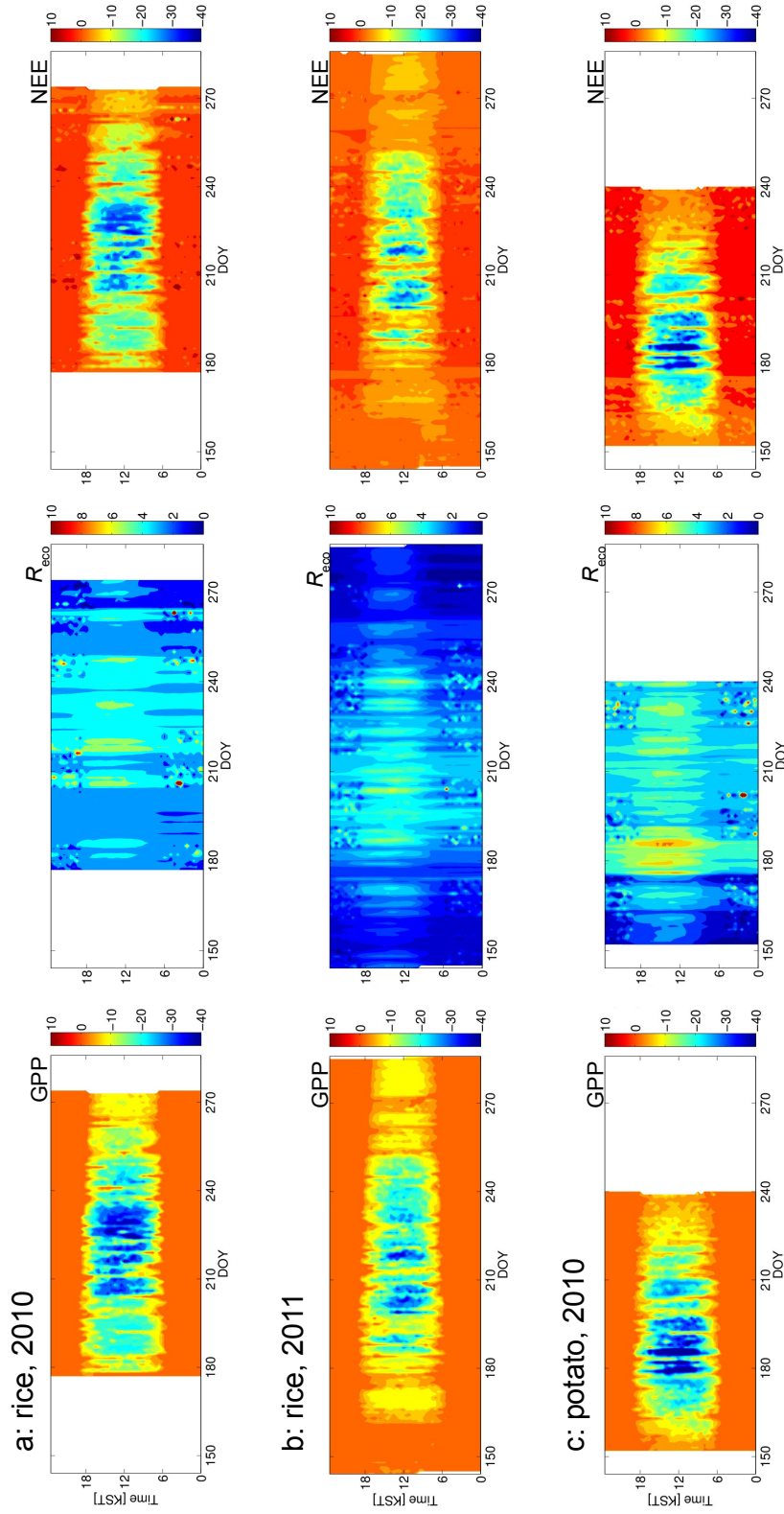


Figure 5.1: Hovmöller diagrams of GPP (left panel), R_{eco} (middle panel), and NEE (right panel) in the growing season in the rice field in 2010 (a) and in 2011 (b), and in the potato field in 2010 (c). Data values are presented in $\mu\text{mol CO}_2 \text{ m}^{-2} \text{ s}^{-1}$.

The difference in CO₂ flux between 2010 and 2011 in the rice field was (1) that the seasonal maximum of GPP and NEE in 2011 appeared about 5 days earlier than in 2010, because of the difference in transplanting dates (see Table 2.1), and (2) that the CO₂ net uptake in 2011 was lower than that in 2010, because of the more intensive precipitation which reduced solar radiation in 2011 (see Chapter 2.2.1). Consequently, the seasonal sum of carbon budget components in the rice field in 2010 were -681 g C m^{-2} of GPP, 363 g C m^{-2} of R_{eco} , and -318 g C m^{-2} of NEE, higher than those values in 2011, i.e. -602 g C m^{-2} of GPP, 341 g C m^{-2} of R_{eco} , and -260 g C m^{-2} of NEE.

In the potato field, the general seasonal pattern of carbon dioxide fluxes (Fig. 5.1c) also followed the development of LAI. NEE was close to zero at the initial stage (before DOY 155), resulted from low values of both GPP (due to the ground surface mainly composed of bare soil) and R_{eco} (due to low temperature in spring). Afterwards, when the vegetation started to grow dramatically at the development stage (from DOY 156 to 181), GPP increased sharply and reached the maximum around DOY 180, as well as NEE reached a peak with a mid-day net uptake of $-45 \mu \text{ mol m}^{-2} \text{ s}^{-1}$. Several large values (around $-40 \mu \text{ mol m}^{-2} \text{ s}^{-1}$) of GPP and NEE were found at the subsequent mid-season stage due to high LAI and sunny weather. After that, NEE decreased rapidly along with the decline of green leaves (see Chapter 3.3) until the late-season stage (after DOY 216). Daily NEE turned positive at the end of the observation period, indicating a net source of carbon dioxide because of the declining photosynthesis rate of potato in the stage when green leaves almost died out and enhanced R_{eco} from the under-ground biomass. Normally, farmers harvest potatoes when the fields are dry enough for agricultural machinery in August or beginning of September, but in 2010 rainfalls made the fields wet, and farmers had to wait until the fields were dry enough to harvest potatoes at the end of September or beginning of October. It could be expected that the potato field remained a slight source of carbon dioxide during the waiting time until harvest. The seasonal sums of carbon budget components in the potato field were -598 g C m^{-2} for GPP, 339 g C m^{-2} for R_{eco} , and -259 g C m^{-2} for NEE.

Depression of GPP in the seasonal course was found at both sites. Several intermittent low values of GPP occurred on cloudy days when solar radiation was declined (see Fig. 3.1). For example, the maximum solar radiation was only $200 - 300 \text{ W m}^{-2}$ under cloudy weather on DOY 183 – 184 and DOY 199 – 200 in 2010, resulting in much depressed GPP dropping to half of the value on the neighbouring sunny days. These events had great influence on GPP because they took place when LAI in the potato field reached the peak. At the same time, their influence on GPP in the rice field was unremarkable, because the photosynthesis

assimilation ability in the rice field was low due to small LAI. Similarly, the solar radiation depression in August had a more remarkable influence on GPP in the rice field than in the potato field. In 2011, more cloudy conditions (especially in June and July) took place due to more intensified precipitation, which totally reduced the seasonal mean solar radiation by 10 % and consequently decreased GPP by 12 % compared with 2010.

5.2 Respiration

The dependence of ecosystem respiration on temperature and the respiration at the reference temperature (R_{ref}) is described in the Lloyd-Taylor function (Eq. 2.26, Chapter 2.4.5). Although the warm conditions in summer were suggested to be an enhancement factor for R_{eco} and consequently for the mid-depression of NEE (Kwon et al., 2010), the role of R_{ref} on the NEE depression has not been studied. In consideration of the rapid development of the cropland vegetation, this thesis studied the influence of seasonal change of crops on the R_{ref} . A nine-day sliding time window was used for the parameterization of Eq. 2.26 and a time series of the ecosystem respiration at 10 °C (R_{ref}) was obtained (Fig. 5.2a). Because of the assumption that R_{ref} per unit above-ground biomass should be constant through the flooded periods (Saito et al., 2005), it was expected to be seen that R_{ref} should increase with the growing trend of the above-ground biomass in the rice field. Surprisingly, R_{ref} in the rice field showed an interesting bimodal seasonal pattern with two peaks around DOY 201 and DOY 232 while the above-ground biomass grew almost throughout the growing season. R_{ref} increased with the increase of above-ground biomass and reached the first peak approximately one month before the above-ground biomass reached the maximum.

The standing water throughout the growing season of rice works as a barrier for the carbon dioxide exchange between the under-water soil and atmosphere because the diffusion rate of carbon dioxide in water is only 0.1 % of that in the air (Lide, 2004). Miyata et al. (2000) found that standing water in the rice field reduces carbon dioxide efflux between the soil and the atmosphere by two orders of magnitude, so the contribution of soil respiration and underground biomass could be ignored and it could be assumed that the above-ground biomass makes up the entire source of carbon dioxide flux from the system after flooding (Campbell et al., 2001; Saito et al., 2005). In this study, the standing water had a depth of 1 - 10 cm (Table 2.2) throughout the whole growing season of rice owing to the pre-monsoonal irrigation and intensive monsoonal precipitation. Thus, the respiration of above-ground biomass was regarded as the only dominant contributor to R_{eco} . The respiration of above-ground biomass

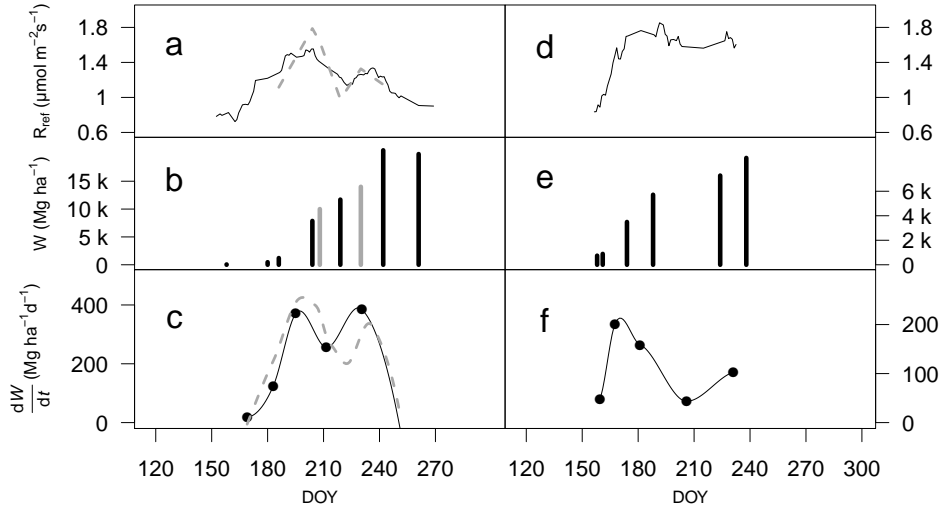


Figure 5.2: Seasonal course of R_{ref} (top), dry weight (middle), and growth rate of above-ground biomass (bottom) in the rice field in 2011 (left) and in the potato field in 2010 (right). The black lines or bars are observations. The grey line in the top-left sub-figure is the simulation by Eq. 5.1. The grey bars in the middle-left sub-figure are artificially inserted data. The grey line in the bottom-left sub-figure is the modified curve (see Chapter 5.2).

comprises two components: the construction respiration and the maintenance respiration, referring to carbon dioxide evolution from the processes of generating energy for the synthesis of dry matter, and for the cell maintenance, respectively (Ryan, 1990). Thus, the total respiration of a plant can be expressed as the sum of the contributions from the biomass and its growing rate:

$$R_{\text{plant}} = a_W \frac{dW}{dt} + b_W W \quad (5.1)$$

where W is the dry weight of biomass per unit area, $\frac{dW}{dt}$ is the growing rate of W , a_W and b_W are partitioning coefficients (Landsberg, 1986). The growing rate of W (Fig. 5.2c) also shows a two-peak mode similar to the pattern of R_{ref} (Fig. 5.2a), indicating the contribution by $\frac{dW}{dt}$ besides W . The time lags of the peaks between R_{ref} and $\frac{dW}{dt}$ could be caused by the lack of sampling times which possibly missed some development stages of the plants. This potential possibility was tested by artificially inserting two values into the seasonal course of W (Fig. 5.2b), which shifted the curve of the biomass growing rate into the grey line in Fig. 5.2c with the peaks coinciding with the peaks of R_{ref} . Moreover, multiple linear regression was applied to Eq. 5.1, and the dimensionless coefficient a_W was simulated as 4.5×10^{-5} , and b_W as $4.0 \times 10^{-13} \text{ s}^{-1}$ with $R^2=0.96$. The modelled curve was plotted in Fig. 5.2a and shows good agreement with the R_{ref} .

The seasonal pattern of R_{ref} in the potato field (Fig. 5.2d) is more complicated than in the rice field owing to the contribution of soil respiration, which can account for up to 75 % of R_{eco} (Law et al., 2002). Although the estimation of soil respiration is unavailable in this study, the influence of $\frac{dW}{dt}$ on R_{ref} in the potato field still can be seen during the early stage of the growing season when R_{ref} increases simultaneously. This demonstrated the contribution to R_{ref} by both the above-ground biomass and its growing rate.

The enhancement in R_{eco} has been suggested to be one of the dominant causes of the observed mid-season depression in NEE (Kwon et al., 2010). R_{eco} has been normally reported to be enhanced by high temperature. For instance, a multi-year study of a larch plantation in Japan by Hirano et al. (2003) and Hirata et al. (2007) indicated that the reduced NEE in August was attributed to the increase of R_{eco} under warmer soil temperature. Kwon et al. (2009) also indicated that R_{eco} follows the seasonal trends of temperature in a deciduous forest site and a cropland site in South Korea. This study suggests that the amount and the rapid growth rate of biomass could be other causes of the enhancement in R_{eco} in croplands.

5.3 Photosynthetic assimilation

5.3.1 Light impact and time window approach

Light response functions are often applied to the estimation of daytime GPP because light is the key external driver of photosynthesis assimilation. The time window (TW) approach, segmenting the whole season into several periods, is usually applied with the assumption that the surface condition is almost constant within each period. However, the vegetation develops rapidly in croplands, which may need the time window as narrow as possible. The selection of the time window width has not been reported yet. Therefore, the variability of carbon dioxide uptake controlled by surface vegetation was studied in this thesis by the time window approach, which classifies observations into time intervals and parameterize Eq. 2.27 to distinguish different seasonal responses within different periods.

This study tested different widths of the time window. The high quality database was sorted into 16-day, 8-day, 4-day, or 2-day TWs. Individual fittings of the parameters (α and β) in Eq. 2.27 were determined for each time interval. The performances of simulations with these parameters for daytime GPP are shown in Fig. 5.3 and Table 5.1. The TW scheme apparently improves the agreement between the simulation and the observation, with high

index of agreement (I) up to 0.98. If the width of TW increases above a certain length (more than 16 days in this study), the performance decreases significantly.

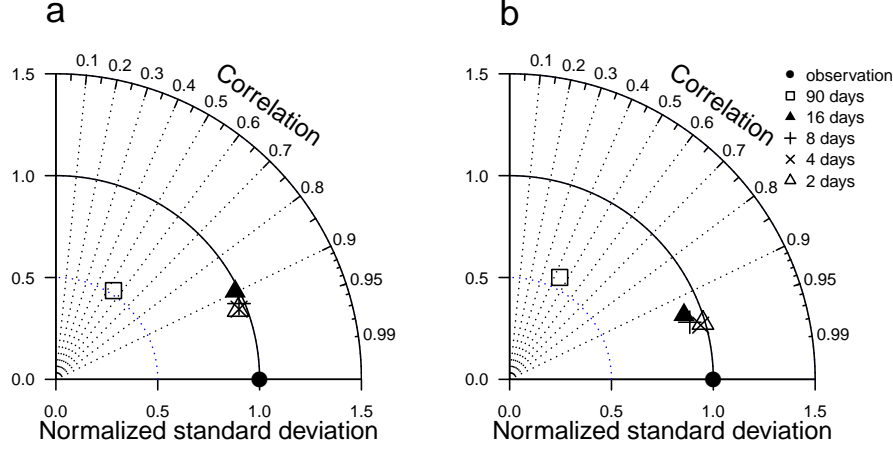


Figure 5.3: Taylor diagrams for the performances of simulations for GPP applying the time-window scheme at the potato field (a) and the rice field (b). The polar radial distance is the normalized standard deviation (NSD). The polar angle is the correlation coefficient (R). The points denote the mean observation (●), the simulations with time windows of 90 days (□), 16 days (▲), 8 days (+), 4 days (×), and 2 days (△).

For the potato field, the mean average error is $2.2 \mu\text{mol m}^{-2} \text{s}^{-1}$ for 8-day TW, and $1.9 \mu\text{mol m}^{-2} \text{s}^{-1}$ for both 4-day TW and 2-day TW, indicating that 4-day TW is as good as 2-day TW and better than 8-day TW. For the rice field, 8-day, 4-day and 2-day TW perform similarly, with identical mean average errors of $1.6 \mu\text{mol m}^{-2} \text{s}^{-1}$. The 2-day TW performs even a little worse than the 4-day TW at the rice field probably due to the insufficient data coverage. Therefore, the time window for the best performance of the Michaelis-Menten model is 4-day for the potato field and 8-day for the rice field.

In order to better understand the determinants of the parameterization of the light response function, the seasonal patterns of the parameters α and β in Eq. 2.27 were obtained using the optimal time windows. At the beginning of the growing season, both α and β were very small because of the weak ability of photosynthesis by initial green leaves. They reached to a peak when LAI increased to the maximum. Afterwards, α and β decreased sharply when the green leaves were disappearing. The same seasonal patterns of α and β as LAI were found (not shown) and their linear relationships with LAI were shown for both sites (Fig. 5.4) with R^2 ranging between 0.90 to 0.95. This indicates that LAI could be used as a predictor for the parameterization of α and β .

Table 5.1: Comparison between the simulation and observation of NEE, including MAE, RMSE, I , and R . TB means temperature binning methods. TW means time window. LL means the leaf-light response method.

Scheme	Potato				Rice			
	MAE	RMSE	I	R	MAE	RMSE	I	R
TB 28 K	4.8	6.2	0.66	0.55	6.0	7.5	0.61	0.44
TB 14 K	4.8	6.2	0.66	0.55	4.9	6.4	0.75	0.63
TB 8 K	4.8	6.2	0.70	0.55	4.0	5.3	0.85	0.77
TB 4 K	4.7	6.1	0.72	0.58	3.7	5.0	0.87	0.80
TB 2 K	4.5	6.1	0.72	0.57	3.8	5.0	0.87	0.79
TW 90 days	4.8	6.2	0.66	0.55	6.0	7.5	0.61	0.44
TW 16 days	2.6	3.3	0.95	0.90	1.9	2.9	0.97	0.94
TW 8 days	2.2	2.9	0.96	0.93	1.6	2.5	0.97	0.95
TW 4 days	1.9	2.6	0.97	0.93	1.6	2.2	0.98	0.96
TW 2 days	1.9	2.6	0.97	0.94	1.6	2.3	0.98	0.96
LL	3.0	4.3	0.93	0.88	5.2	6.6	0.88	0.85

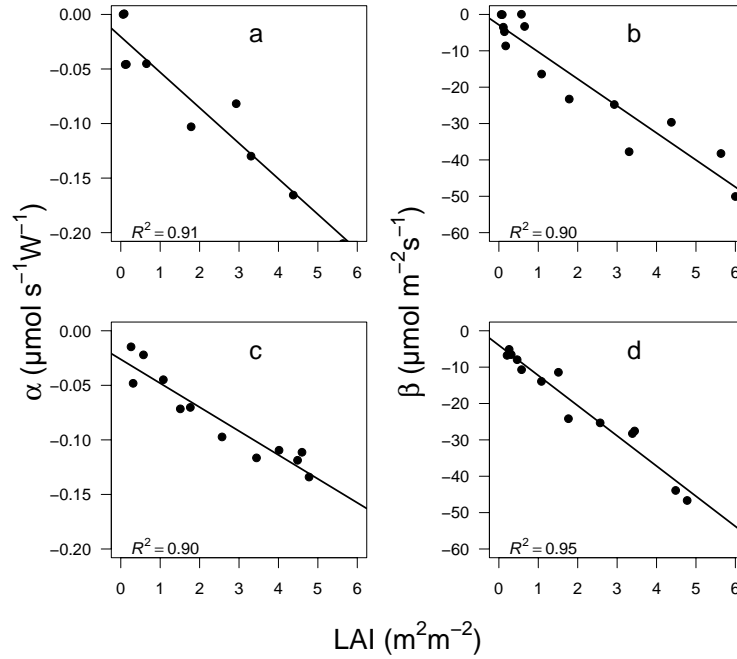


Figure 5.4: Relationship of the coefficients α and β in Eq. 2.27 against LAI in the rice field (a and b) and in the potato field (c and d).

Although the time window approach has been widely used in literature on the basis of the seasonal changes in leaf area, soil moisture and photosynthetic capacity, a study on the decision of time window width has not been reported. The width of time window is empirical and varying from one month to a full year for forest sites (Falge et al., 2001; Stoy et al., 2006; Moffat et al., 2007). For grassland, the use of a 5-day window to capture the rapid change of the surfaces was reported (Ammann et al., 2007). A short time window of 4 to 15 days is normally used to account for seasonal parameter variability (Lasslop et al., 2010). This study demonstrated that the decision of the window width is necessary to improve the model performance and could be optimized by using the statistics.

5.3.2 New leaf-light response function

Generally, the widths of time windows for gap-filling depend on both (1) how rapidly the vegetation develops, and (2) how large the gaps are, because the time-window approaches cannot fill gaps larger than the selected time window (Falge et al., 2001; Stoy et al., 2006), which could be problematic for those sites often influenced by power failure or bad weather. Moreover, the time window approaches lead to the requirement of continual updating and adjusting of the regression scheme (Baldocchi, 2003). In order to solve these problems, this thesis introduces the LAI influence on GPP and proposes the leaf-light response function (Eq. 2.30), suggesting that GPP is a function of both solar radiation and LAI. Therefore, the leaf-light response function was validated in three steps: firstly, for any constant value of LAI, the light response function (Eq. 2.27) must hold. Secondly, for any constant value of solar radiation, the LAI response function (Eq. 2.31) must hold. Finally, the whole dataset must follow the leaf-light response function (Eq. 2.30).

The first step was performed in the following way: observations with several constant values of LAI (1, 2, 4 m^2m^{-2} with a tolerance window of $\pm 0.1^2\text{m}^{-2}$) were picked out of the high quality database. For each group with a constant LAI, the non-linear-regression was applied to parameterize the light-response function Eq. 2.27. The model for each constant LAI value had small standard error (SE) of 0.009 to 0.017 $\mu\text{mol s}^{-1}\text{W}^{-1}$ for α , and 2 to 12 $\mu\text{mol m}^{-2}\text{s}^{-1}$ for β , which demonstrated that the light response functions hold for a constant LAI. Moreover, the absolute value of α increased from 0.041 to 0.101 $\mu\text{mol s}^{-1}\text{W}^{-1}$ and β from 16 to 57 $\mu\text{mol m}^{-2}\text{s}^{-1}$ with the increase of LAI from 1 to 4 m^2m^{-2} , which indicated that the values of both α and β were influenced by LAI value (Table. 5.2).

Table 5.2: Modelled parameters of the light response function in LAI ($\text{m}^2 \text{m}^{-2}$) intervals.

LAI ($\text{m}^2 \text{m}^{-2}$)	α ($\mu\text{mol s}^{-1} \text{W}^{-1}$)	β ($\mu\text{mol m}^{-2} \text{s}^{-1}$)	SE of α ($\mu\text{mol s}^{-1} \text{W}^{-1}$)	SE of β ($\mu\text{mol m}^{-2} \text{s}^{-1}$)
1	-0.041	-16	0.009	2
2	-0.064	-30	0.009	4
4	-0.101	-57	0.017	12

The second step was performed in a similar way: observations with several constant values of solar radiation (100, 200, 400, 600 W m^{-2} with a tolerance window of $\pm 20 \text{W m}^{-2}$) were picked out of the high quality database. For each group with a constant solar radiation, the linear regression between GPP and LAI was applied (Eq. 2.31, Table 5.3). GPP showed good correlation (R^2 ranging between 0.87 to 0.95, standard error of the slope a_{LAI} ranging between 0.09 to 0.30 $\mu\text{mol m}^{-2} \text{s}^{-1}$) with LAI for a given value of solar radiation, which demonstrated that the LAI response functions (Eq. 2.31) hold. Furthermore, the absolute value of the linear slope between GPP and LAI increases from 2.08 to 6.52 $\mu\text{mol m}^{-2} \text{s}^{-1}$ with the increase of solar radiation from 100 to 600 W m^{-2} , indicating the influence of solar radiation on a_{LAI} .

Table 5.3: Modelled parameters of the LAI response function in solar radiation intervals.

R_g (W m^{-2})	a_{LAI} ($\mu\text{mol m}^{-2} \text{s}^{-1}$)	SE of a_{LAI} ($\mu\text{mol m}^{-2} \text{s}^{-1}$)	R^2
100	-2.08	0.09	0.88
200	-3.68	0.20	0.87
400	-5.65	0.21	0.95
600	-6.52	0.30	0.94

The mixed influence of both LAI and solar radiation could already be seen in the first and second steps, which resulted naturally in the third step. The non-linear regression of the leaf-light response function (Eq. 2.30) was applied to the whole high quality dataset. The modelled values of α' are $-0.039 \mu\text{mol s}^{-1} \text{W}^{-1}$ for potato and $-0.024 \mu\text{mol s}^{-1} \text{W}^{-1}$ for rice, while the values of β' are $-15.6 \mu\text{mol m}^{-2} \text{s}^{-1}$ for potato and $-11.5 \mu\text{mol m}^{-2} \text{s}^{-1}$ for rice. α' is 63 % larger, and β' is 36 % larger in the potato field than in the rice field, indicating that potato has a more robust ability of carbon assimilation than rice on the basis of unit LAI. The leaf-light response of GPP can be seen in Fig. 5.5. For a given LAI, Eq. 2.30 becomes the conventional light response function (Eq. 2.27). For a given solar radiation, Eq. 2.30 becomes the LAI response function (Eq. 2.31). Combining both the light response function (Eq. 2.27)

and the leaf-light response function (Eq. 2.30) yields the relationship between α and α' as $\alpha = \alpha' \text{LAI}$, and between β and β' as $\beta = \beta' \text{LAI}$, which can explain the linear relationship of α and β against LAI shown in Fig. 5.4.

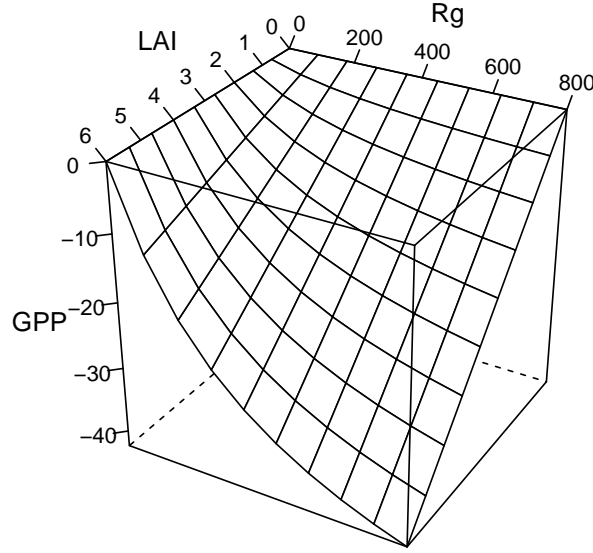


Figure 5.5: Leaf-light response of GPP in the potato field according to Eq. 2.30. GPP is given in $\mu\text{mol CO}_2 \text{ m}^{-2} \text{ s}^{-1}$, LAI in $\text{m}^2 \text{ m}^{-2}$, and R_g in W m^{-2} .

A good agreement between the simulated GPP by the leaf-light response function and the derived GPP from the observed NEE and simulated respiration was found. The linear regression showed R^2 of 0.85, slope of 1.00 ± 0.01 , and intercept of $1.38 \pm 0.18 \mu\text{mol m}^{-2} \text{ s}^{-1}$ in the potato field (Fig. 5.6), and R^2 of 0.72, slope of 1.02 ± 0.02 , and intercept of $3.44 \pm 0.33 \mu\text{mol m}^{-2} \text{ s}^{-1}$ in the rice field (not shown). The index of agreement also confirmed the reliability of the simulation with 0.93 for the potato field and 0.88 for the rice field. This good performance of the leaf-light response function indicates that it could be used to parameterize the light response of crops as an alternative method to the time-window scheme to capture the seasonal change of the vegetation and surface conditions.

The leaf-light response function could use the whole data base for parameterization of Eq. 2.30 without any grouping, therefore it has the potential advantage to fill large data-gaps. An average of 35 % of flux observations are reported in the literature as missing or rejected (Falge et al., 2001). Data gaps are due to system breakdown, calibration, and maintenance, or caused by farming or human activities, or by unfavourable atmosphere conditions when the assumptions required by the EC technique are not fulfilled (Foken and Wichura, 1996). As the

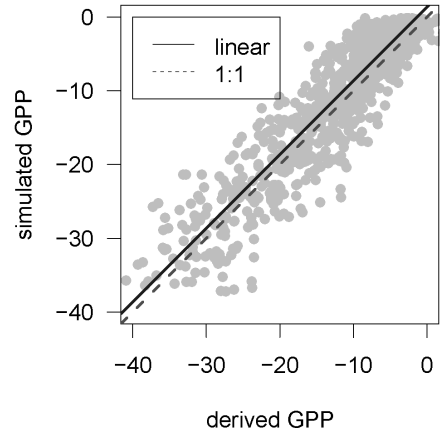


Figure 5.6: Comparison between derived GPP (from observed NEE and simulated R_{eco}) and simulated GPP (by the leaf-light response function) in $\mu\text{mol m}^{-2} \text{s}^{-1}$ in the potato field in 2010.

conventional gap-filling methods suffer from a lack of data in each data class, if the width of time windows or temperature classes (mean diurnal variance method and non-linear regression method) or the width of the cells (look-up table method) does not match the statistical data distribution. The dilemma exists in the requirement for a time-window to be short enough to exclude the errors contained in the nonlinear dependence of environmental variables (Falge et al., 2001) and to be long enough to contain sufficient data for calculating a meaningful statistic needed to apply the mean diurnal variance method, the look-up table method, or the non-linear regression method. Due to this thesis, this problem can now be avoided by using the new leaf-light response function (Eq. 2.30). Therefore, using half-month as a threshold, small gaps (smaller than the threshold) of GPP data were filled with the simulated values by the light response function with the possible optimal time windows, while large gaps (larger than the threshold) of GPP data were filled the simulated values by the leaf-light response function. This strategy was inherited by the gap-filling for NEE data in this thesis.

The performance of simulation by the leaf-light response function strongly depends on the estimation of the LAI itself. Incorrect values are a source of discrepancy between simulated and observed GPP. The errors could result from:

1. The sampling. In this study, every measured LAI value was estimated from several randomly sampled plants in both field sites. Since individual plants develop differently from each other, the limited number of samples could result in an error through the calculation of a representative mean. In order to reduce this error, this study limited

the sampling area within the footprint-area of the EC measurement, and collected as many (at least five) samples as possible.

2. The interpolation. LAI normally remains constant at a potato field when the crop is fully developed (González-Sanpedro et al., 2008). The limitations of the field campaign provide a sparse LAI data-set with only one measurement at the peak during the mid-season stage (Fig. 3.3). Thus, a simple linear interpolation to fill the time-steps between the distinct LAI measurements could miss some development stage of the plants and underestimate the real LAI before and after the peak value. In order to avoid this problem, this thesis applied the non-linear interpolation by Eq. 2.1, which has been demonstrated to have good performance in literature (Hashimoto, 1990; Ding et al., 2013).
3. The effective LAI. During the mid seasons when LAI is large, the overlapping of green leaves results in less effective photosynthesis than during the early and late seasons, which makes the estimated mid-season LAI larger than the effective LAI (so called foliar clumping effect).

5.3.3 Sky condition impact

The database was separated into the diffuse radiation (DR) group and the mixed radiation (MR) group to study the photosynthesis ability of plants under diffuse radiation and direct radiation. The DR group consisted of those observations when the sun was totally obscured by clouds, resulting in that the short-wave radiation was composed of only diffuse radiation (i.e. the solar radiation scattered by atmospheric gases, aerosols, and/or clouds). As contrasted, the MR group consisted of those observations when the sun was not totally shadowed by clouds, resulting in that the canopy received short-wave radiation mixed with direct and diffuse radiation. Thus, the DR condition occurred on overcast or partly-cloudy days, while the MR condition occurred on partly-cloudy days and clear sky days. The separation of these two groups follows the criteria by Law et al. (2002). In a practical way, the records which follow a smooth curve of diurnal solar radiation are marked as clear sky condition, while the rest are marked as cloudy sky condition. The separation is cross-checked by the manual weather observation and the web-cam pictures as a confirmation, showing that they agree with each other very well.

The leaf-light response function was used to estimate the specific light use efficiency (α') and specific saturated GPP (β') for both DR and MR conditions. The potato field had $\alpha' = -0.039 \mu\text{mol s}^{-1} \text{W}^{-1}$ and $\beta' = -15.2 \mu\text{mol m}^{-2} \text{s}^{-1}$ under MR condition, while similar values under DR condition with $\alpha' = -0.040 \mu\text{mol s}^{-1} \text{W}^{-1}$ and $\beta' = -15.5 \mu\text{mol m}^{-2} \text{s}^{-1}$. The leaf-light response showed almost the same under both conditions, indicating the undistinguishable response of potato to direct and diffuse radiations. The rice field had $\alpha' = -0.022 \mu\text{mol s}^{-1} \text{W}^{-1}$ and $\beta' = -9.1 \mu\text{mol m}^{-2} \text{s}^{-1}$ under MR condition, while larger values were observed under DR condition with $\alpha' = -0.029 \mu\text{mol s}^{-1} \text{W}^{-1}$ and $\beta' = -11.9 \mu\text{mol m}^{-2} \text{s}^{-1}$. It showed that α' and β' under DR condition were approximately 30 % larger than under MR condition, which indicated that the light use efficiency with diffuse radiation was higher than with direct radiation in the rice field. It was demonstrated that the productivity of vegetation is evidently affected by clouds and other atmospheric particles because of its sensitivity to diffuse radiation (Roderick et al., 2001) and the high ability of diffuse radiation to penetrate to lower depths of the canopy (Goulden et al., 1997; Law et al., 2002). Therefore, the difference in the diffuse radiation effect between the rice and potato fields is probably because the rice plants grow upward vertically, resulting in an easier penetration of diffuse radiation than in the potato plants which spread more horizontally and intercept the penetration of diffuse radiation. As a result, only the stronger effect of diffuse radiation in the rice field could be distinguished by the leaf-light function.

Although higher light use efficiency for photosynthesis under diffuse radiation condition has been demonstrated for forests by recent studies, related studies on croplands are rare. Law et al. (2002) showed more net carbon dioxide uptake under cloudy conditions than under clear sky conditions in boreal aspen and coniferous forests. Gu et al. (2003) indicated that the enhancement in diffuse radiation caused by volcanic aerosols in the air increased the noontime photosynthesis by up to 23% in a deciduous forest. Such effect owing to aerosol loading was also found in a broadleaf deciduous forest, a mixed forest, and agricultural areas by Niyogi et al. (2004). A study on artificial neural networks indicates that the light use efficiency with diffuse radiation was three times larger than direct radiation (Moffat et al., 2010). Mercado et al. (2009) used a global model and showed that the diffuse radiation increased the land carbon sink by approximately 25 % in the global dimming period, i.e. a period when a decrease in global radiation at the Earth's surface was observed after 1950s. Similar studies on croplands is rare, probably because the vegetation status of crops changes very fast, resulting in the difficulty to distinguish the effect of diffuse radiation from the effect of LAI. For example, Chameides et al. (1999) used a crop response model and reported the decrease in crop yields caused by the decrease in solar radiation, while they indicated

that ignoring the diffuse radiation leads to uncertainty in the estimation of solar radiation's influence on crop yields. Thus, the study on this topic becomes more accessible if using the leaf-light response function (Eq. 2.30) proposed in this thesis.

The intensive precipitation during the summer monsoon season brings about low levels of solar radiation. During field campaigns in this study, the clear, overcast, and partly cloudy days covered 7 %, 45 %, and 48 %, respectively, of the observation days during the growing seasons in 2010 as influenced by the summer monsoon. The surfaces received both the direct and diffuse radiation when the sky was clear, and almost only diffuse radiation when the sky was overcast. The situation was complicated when the sky was partly covered by clouds. On partly cloudy days, the canopy received mostly diffuse radiation when the sun was sometimes totally obscured by clouds. The canopy received a mixture of diffuse and direct radiation when solar beams went through gaps between individual clouds and reached sunlit leaves. Under this condition, the canopy not only received as much direct radiation as on clear days, but also received more diffuse radiation scattered by the clouds in the vicinity as well, which was called cloud gap effect (Gu et al., 1999). A larger proportion of diffuse radiation on many partly cloudy and overcast days could possibly be a compensation to the depression of GPP especially in the rice field.

5.3.4 Temperature impact

The temperature dependence of carbon dioxide assimilation was investigated by the parameterization of Eq. 2.27 with a temperature binning scheme, i.e. binning observations into 14 K, 8 K, 4 K, or 2 K temperature classes. Individual fittings of α and β were determined for each temperature class. The performances of temperature-binning approaches are shown in Fig. 5.7. All the temperature-binning approaches (class widths between 28 K and 2 K) for the potato field had a poor performance, with low index of agreement $I < 0.72$ and low model efficiency coefficient $N_{\text{Seff}} < 0.32$. The consequently reduced class width only slightly improved the explained variance for NEE for the potato field, which proves a poor sensitivity of the potatoes to temperature. But for the rice field, I increased from 0.61 to 0.85 and the model efficiency coefficient N_{Seff} from 0.16 to 0.58 when decreasing the width of the temperature bins from 28 K to 8 K, which indicates a higher temperature sensitivity of the rice.

Different opinions exist on the temperature dependence of carbon dioxide assimilation. The assimilation of carbon dioxide has an optimal temperature, below or above which the photosynthesis ability will decrease (Saxe et al., 2002). Nevertheless, it is found that air temperature

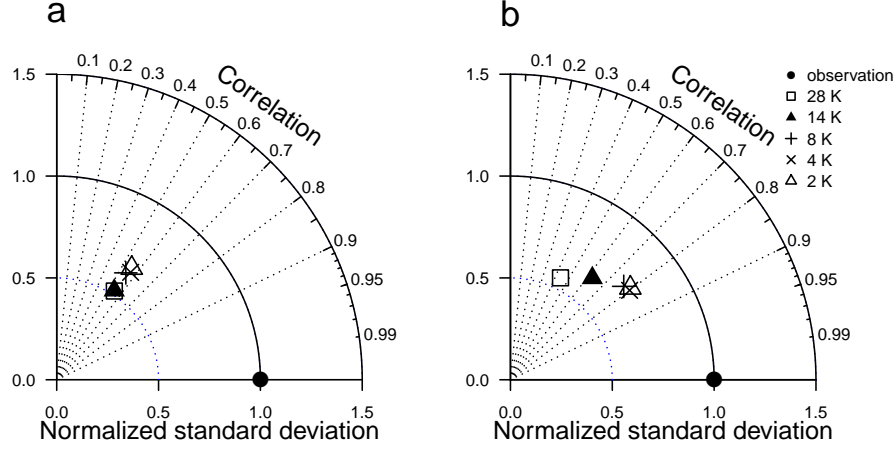


Figure 5.7: Taylor diagrams for the performances of simulations for GPP applying the temperature binning scheme at the potato field (a) and the rice field (b). The polar radial distance is the normalized standard deviation (NSD). The polar angle is the correlation coefficient (R). The points denote the mean observation (●) and the simulations with temperature classes of 28 K (□), 14 K (▲), 8 K (+), 4 K (×), and 2 K (△).

has weak influence on photosynthesis during summer in forests (Bassow and Bazzaz, 1998). The application of a temperature-binning scheme has been less common than the time window scheme in the recent years, but the reason has not been explained in the literature. For both sites in this study, the classes of 8 K, 4 K and 2 K have a similar performance, indicating that it is unnecessary to bin the data into temperature classes smaller than 8 K. This range is larger than the 4 K temperature classes used by Falge et al. (2001) for a variety of sites including croplands and the 2 K temperature classes used by Ruppert et al. (2006) for a forest site. They also reported that additional time windows do not significantly improve the temperature binning method, because the existing long-time seasonal temperature response of the long-living and slow-growing coniferous forest is already covered by the time-independent allocation of the values into the temperature bins. But this cannot work for short-living and fast-growing crops, thus the temperature-binning scheme and time-window scheme perform differently, which is now shown in Table 5.1 in this study. Either the leaf-light response function or the time-window scheme, even with the 16-day time-window approach, result in a much better agreement than the smallest temperature binning (2 K) approach. This implies that — if the seasonal or daily weather conditions are in a normal climate range — the long-time seasonal and short time diurnal temperature response of the crops play a minor role compared to the fast changing development stages (carbon dioxide-accumulation ability expressed, for example, by the LAI) of the crop plant. Furthermore, the temperature binning approach was

applied to the leaf-light response function. No improvement was found for the simulation of GPP (not shown). Thus, this thesis demonstrates that the temperature dependency can be ignored if the plant development is well considered for croplands.

The temporal distribution within temperature classes (Fig. 5.8) could explain why a smaller temperature binning could improve the simulation for both sites in spite of the minor temperature dependency. Some temperature values were observed only during some special periods. For instance, the temperature class of 2 °C to 10 °C at the potato field fell exactly into the time interval of DOY 144 to 160, which made the overall simulation of the 8 K temperature binning approach better than the simulation of larger temperature classifications. Since the temperature class of 18 °C to 26 °C was distributed over almost the whole growing season, the temperature binning scheme mixed these time windows together and failed to perform a good simulation.

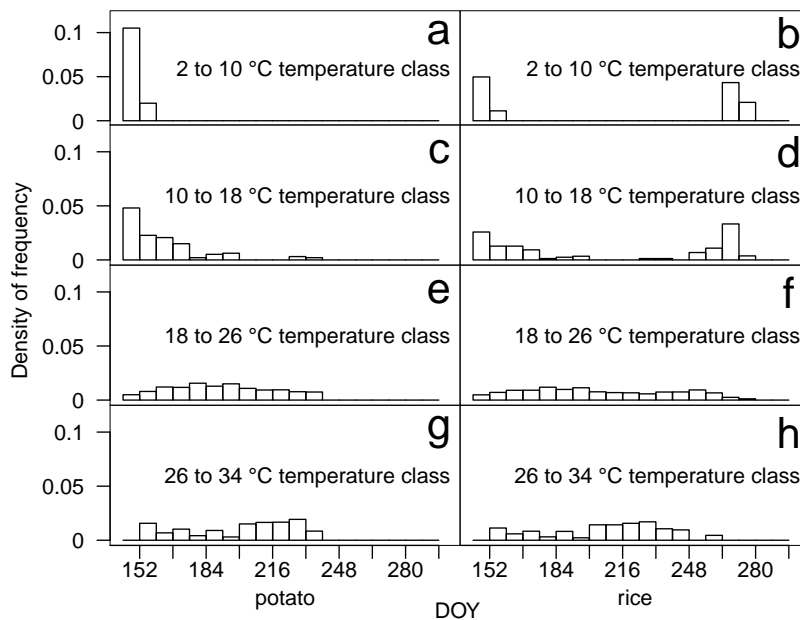


Figure 5.8: Temporal distribution of temperature measurements within temperature classes at the potato field (a, c, e, g) and the rice field (b, d, f, h).

Generally speaking, temperature binning contains some, but not all, relevant information of seasonal response for NEE gap-filling for croplands, which is insufficient for the regression of the light response function. The air temperature has both a diurnal and a seasonal cycle within a year. As the diurnal cycle of temperature is partly a function of solar radiation, which is included in the light response function, and the seasonal cycle of temperature is contained

in the time-window scheme or the leaf-light response, it is suggested that temperature binning could be ignored if the plant development is well simulated.

5.3.5 Humidity impact

Vapour pressure deficit (VPD) was suggested to be introduced into the Michaelis-Menten function to account for the dependence of GPP on air humidity (Lasslop et al., 2010), but in humid areas this influence might play a minor role. In this study, the combination of Eq. 2.27 and Eq. 2.28 with the time-window scheme was used to test the VPD effect on both sites. The mean diurnal cycles of solar radiation, VPD, GPP derived from observed NEE and simulated respiration (indicated as "derived GPP"), and GPP simulated by Eq. 2.27 and Eq. 2.28 in the potato field in June 2010 are shown in Fig. 5.9. The solar radiation had a symmetric pattern with the peak at mid-day, while VPD increased until reaching the maximum in the afternoon. Without the consideration of VPD response, the symmetric diurnal pattern of the simulated GPP followed the pattern of solar radiation. The derived GPP, however, showed an asymmetric pattern with the maximum before mid-day. With the consideration of VPD response shown in Eq. 2.28, the simulated GPP agreed much better with the observation, especially in the afternoon, because higher temperature and higher VPD leads to a higher evaporation rate and then to a stomatal closure (Lasslop et al., 2010).

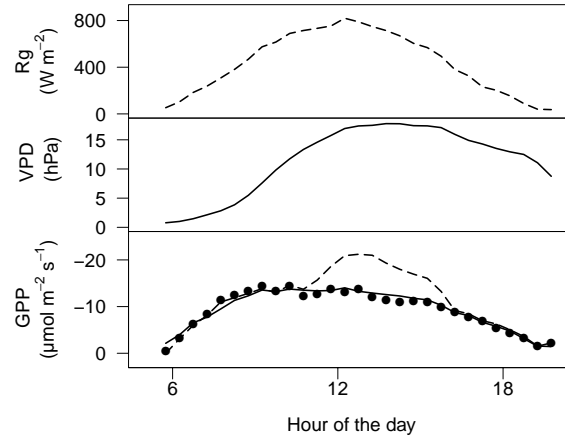


Figure 5.9: Mean diurnal cycles of solar radiation (top), VPD (middle), derived GPP (bottom, dots) and simulated GPP by the time-window scheme without VPD (bottom, dashed line) and with VPD-factor (bottom, solid line) for the potato field during the early growing season.

The asymmetric diurnal pattern of GPP is only found in June 2010 in the potato field when VPD was below the threshold VPD_0 (see Eq. 2.28). With the permanently flooded water in the rice field, and the intensive precipitation and high humidity in the summer monsoon in both fields, the observed VPD is below the plant physiological threshold (Fig. 5.10). As most of the growing seasons are overlapped with the summer monsoon, the influence of VPD could be generally ignored in both sites.

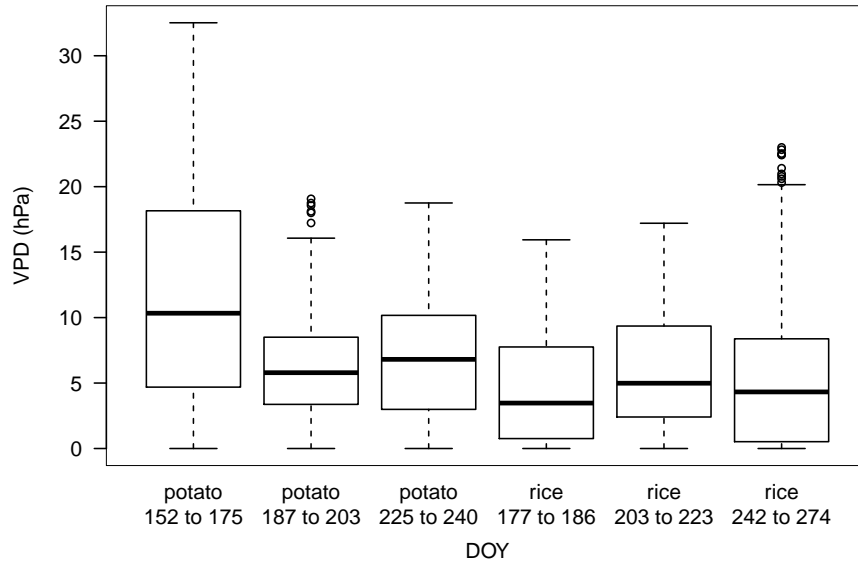


Figure 5.10: Boxplot of VPD during each measurement period at the potato field and the rice field. The boxplot is composed of the median (solid line), the lower quartile and upper quartile (i.e. the 25th and 75th percentile, box), the lowest datum still within 1.5 times of interquartile range (IQR) of the lower quartile, and the highest datum still within 1.5 IQR of the upper quartile (markers).

6 Conclusions

This thesis is focused on the agroecosystem-atmosphere exchange of energy and matter in East Asia. Through two years of field campaigns at two typical croplands on the Korea Peninsula and careful data analysis, this study provides a comprehensive insight into the controlling environmental and biological factors of the exchange of water vapour and carbon dioxide in irrigated and non-irrigated crops. With these results the scientific hypotheses raised in Chapter 1.2 could be successfully addressed as conclusions.

Conclusion to Hypothesis 1

Half-hourly turbulent heat fluxes without proper energy balance correction could introduce uncertainty in the evaluation of evapotranspiration models. The newly proposed energy balance closure correction (EBC-HB) method suggested by Charuchittipan et al. (2014), which partitions most of the residual energy into sensible heat (see Chapter 4.1), is used as an improved approach to correct the ET observation by eddy-covariance. This thesis uses EBC-HB corrected ET to evaluate PM-FAO and PM-KP models for the first time, which could provide a more reliable evaluation of these models.

In the case of the PM model for ET estimation, the stomatal resistance plays a very important role for both flooded and non-irrigated croplands. This thesis demonstrates that the conventional PM-FAO approach, which estimates the stomatal resistance as a function of LAI, is sensitive to the assumed value of single leaf stomatal resistance (r_{si}). Although the PM-FAO model works well for both croplands with the literature value of r_{si} (Allen, 2005), the model performance could be improved with site-specifically calibrated values of r_{si} . The optimal r_{si} in the rice field is much smaller than that in the potato field due to the free evaporation from the standing water.

The study on the PM-KP model shows for the first time the normal distributions of the KP coefficients. Furthermore, these distributions indicate that the calibration of the KP model for the rice field is more stable than for the potato field due to random sampling

error. The optimal parameterization could be obtained from the GLUE procedure, indicating a better performance of the PM-KP model than the PM-FAO model for the conditions when evaporation plays a major role (i.e. in the flooded rice field and for small LAI conditions in the potato field).

In conclusion to Hypothesis 1, the PM-KP method could be a better alternative than the PM-FAO model for estimating ET over croplands where evaporation acts as the major share of ET. Hypothesis 1 is therefore partly accepted. Comparing the PM-FAO model and the PM-KP model (Table 6.1), this thesis suggests the strategy for the application of these two models as follows: PM-FAO is a good choice for transpiration-dominated croplands if leaf area index data are available, while PM-KP is a good choice for evaporation-dominated croplands or an acceptable alternative if leaf area index data are unavailable.

Table 6.1: Application of the PM-FAO model and the PM-KP model for croplands.

	PM-FAO	PM-KP
input variables	air temperature, available energy, vapour pressure deficit, wind speed, canopy height, leaf area index	air temperature, available energy, vapour pressure deficit, wind speed, canopy height
parameterized variables	stomatal resistance of single leaf	KP coefficients a and b
model performance for croplands	good for transpiration- dominated ecosystem; better if stomatal resistance of single leaf is site-specifically calibrated	good for evaporation- dominated ecosystem

Conclusion to Hypothesis 2

As a good semi-empirical method, the Michaelis-Menten light-response function has been widely used for data gap-filling of GPP and NEE. It has difficulty in tracking the impact by the surface vegetation change especially for rapidly growing crops. A solution to this problem is the conventional time-window approach, which segments the whole growing season into time intervals and parameterizes Michaelis-Menten functions individually within each interval. This thesis investigated the strategy to determine the proper width of the time window. The coefficients of the Michaelis-Menten function (Eq. 2.27) showed linear relationship with LAI,

indicating the parameterization of the Michaelis-Menten function is important to track the rapid vegetation growth in croplands, and the time window must be sufficiently narrow to ensure that the vegetation condition and the coefficients of the light response function are nearly constant within this time window. This study for the first time demonstrates that the optimal width of the time window is site-specific. The optimization of the time window could be obtained by statistical comparison between different time windows or the Taylor diagrams (Chapter 2.4.7). The best time window for the potato field is smaller than that for the rice field, probably because the carbon assimilation ability of potato is more robust than rice on the basis of unit LAI (Chapter 5.3.2), resulting in a larger divergence in the coefficients of the light response function within an identical time interval. This may explain why a large time window of one month often performs well for forest observations, where LAI changes slowly.

Beside LAI, weather conditions are tested as influencing factors on the carbon dioxide flux. The detailed study on GPP indicates that (1) the influence of air temperature on GPP could be ignored if the influence of LAI development is sufficiently included, that (2) VPD plays a significant role on GPP in the dry, pre-monsoon growing stage of non-irrigated crops and a minor role under Asian monsoon weather conditions.

The parameterization of the light response function, however, suffers from the dilemma that the time-window has to be narrow enough to fulfil the assumption of constant vegetation on one hand, and has to be long enough to contain sufficient data on the other hand. Neither of them could be met when large data gaps occur. The leaf-light response model (Eq. 2.30) proposed in this study, which introduces a LAI multiplier into the light response function, has a successful performance as an innovative but simple approach to simulate GPP for croplands. Because the leaf-light response function uses LAI as input data instead of segmenting the dataset into small time windows, it has an advantage to those datasets which need gap-filling procedures for large gaps.

In conclusion to Hypothesis 2, the Michaelis-Menten approach for estimation of GPP in rapid-developing croplands could be improved by including the influence of surface vegetation conditions, while the site-specific optimization of the time window approach and the leaf-light response function proposed by this thesis are efficient methods.

Conclusion to Hypothesis 3

Land use change on the ecosystem-atmosphere exchange in croplands could have evident impacts on the surface energy and matter budget. This thesis carried out field observations

at two different croplands in the same region and under the control of the same climate system, which reveals and quantifies the differences between irrigated and non-irrigated croplands and their agroecosystem-atmosphere exchange regimes of heat, water vapour, and carbon dioxide (Table 6.2). The seasonal mean sensible heat in the potato field was 2.4 times as large as that in the rice field, while the latent heat in the rice field was 1.4 times as large as that in the potato field. Throughout the whole growing season of the irrigated rice, the latent heat flux was the major component to compensate the available energy, and the partitioning of available energy into sensible and latent heat was independent of the growing stages of the rice plants. However, in the potato field the available energy was consumed by the latent heat and the sensible heat flux in equal parts in the early and late growing seasons. In the potato field, the latent heat flux was the major part of the heat exchange only when green leaves were fully developed, and the Bowen ratio was larger than in the rice field, which indicated a more obvious dependency on the surface vegetation development.

Table 6.2: Seasonal budgets of energy, water and carbon dioxide exchange of irrigated crop (i.e. rice, May 24 to October 17, 2010) and non-irrigated crop (i.e. potato, April 26 to September 30, 2010).

		irrigated crop	non-irrigated crop
energy budget	sensible heat	8 W m^{-2}	19 W m^{-2}
	latent heat	62 W m^{-2}	45 W m^{-2}
H_2O flux	evapotranspiration	283 mm	206 mm
	evaporation	175 mm	113 mm
	transpiration	108 mm	93 mm
CO_2 flux	GPP	-681 gC m^{-2}	-598 gC m^{-2}
	R_{eco}	363 gC m^{-2}	339 gC m^{-2}
	NEE	-318 gC m^{-2}	-259 gC m^{-2}

Different irrigation management between the flooded rice field and non-irrigated potato field resulted in approximately 30 % less water evapotranspired in the potato field than in the rice field on seasonal average. The difference in evapotranspiration between these two fields was 77 mm, mostly attributed to less evaporation in the potato field than in the rice field. As evaporation in the rice field shared a larger part (62 %) of evapotranspiration than in the potato field, it could be expected that the shift of land use from flooded cropland into non-irrigated cropland would significantly save water under the scenario of water scarcity in agriculture.

The seasonal budget of CO_2 exchange demonstrated the difference in GPP, R_{eco} , and NEE between the rice field and potato field. The seasonal sum of the CO_2 flux showed in the

potato field 12 % less GPP, 7 % less R_{eco} , and consequently 20% less NEE than in the rice field, which resulted from the different features, such as length of growing season and ability of photosynthetic assimilation, of these two species. The seasonal patterns of NEE showed that the rice field acted as a sink of CO_2 through the whole season, while the potato field turned from a sink to a slight source at the late growing stage when the above-ground green biomass disappeared. Therefore, the potato field acted as a weaker CO_2 sink than the rice field in the growing season.

In conclusion to Hypothesis 3, the agroecosystem-atmosphere exchange of heat, water and carbon dioxide is significantly different between irrigated and non-irrigated croplands. A conversion between the irrigation management and crop species can have evident impact on the energy, water and carbon balance of a whole agriculture landscape.

A special case is the so-called mid-season depression, i.e. a declined NEE in East Asian summer monsoon. This typical year-by-year reduction of NEE is primarily caused by monsoon specific synoptic weather patterns characterized by cloudy sky conditions and by decreased solar radiation during intensive precipitation events. The new finding in this thesis is that the mid-season depression is associated with integrated environmental and biological conditions. The depressed GPP under reduced solar radiation, combined with an enhanced R_{eco} and relatively high temperatures in summer, leads to a general mid-season depression in NEE. However, enhanced diffuse radiation under cloudy conditions as well as higher photosynthesis ability with diffuse radiation acts as a compensation of GPP depression. In addition, the study on R_{eco} shows that the seasonal pattern of R_{eco} is a combination of an enhancement effect caused by air temperature and an additional effect caused by a seasonal change of both the amount and the growing rate of above-ground biomass in the rice field. In the future the summer monsoon is predicted to be extended and rainfall to be increased in Korea (Yun et al., 2008). Therefore, it could be expected that the mid-season depression would generally be enhanced, resulting in a decrease in seasonal GPP of croplands, while the importance of VPD influence on GPP could be even more weakened, and the positive effect of diffuse radiation on GPP would be dependent if the period of cloudy condition would extend or not.

The rapid development of surface vegetation in both the rice and potato fields were shown in the seasonal change of the LAI. To detect and explain the driving factors of these differences between irrigated and non-irrigated croplands, it is crucial to investigate and track the rapid plant development within short growing seasons for estimation of NEE and ET. Therefore, it is highly recommended that LAI and biomass should be included (1) as additional data for the EC measurement, and (2) in the gap-filling strategy for large gaps and related models for

fast growing vegetation surface such as croplands. Although routine measurement of LAI is not available for many sites, it could be acquired by the analysis of remote sensing or other meteorological proxies. Satellite measurements provide routine observation of the surface vegetation, which is correlated with LAI (Nemani and Running, 1989), with a resolution as high as 1.1 km. Currently the spatial resolution of satellite imaging is too coarse to detect the small scattered mosaic of croplands, but in some intensive managed agricultural regions with large homogeneous croplands, especially rice paddies in Asia remote sensing is already applicable. Meteorological records, such as precipitation and temperature, have been suggested to serve as indicators to estimate LAI for the central Great Plains, USA (Wang et al., 2003). However, the case is more complicated considering croplands because the LAI is strongly determined by the farmers' decision about crop species and planting or harvesting time.

Generally, this thesis concludes that the conversion between irrigated and non-irrigated crops can have significant impact on the energy and matter exchange between agro-ecosystem and atmosphere. It manages to distinguish the influencing biological and environmental factors, including crop species, LAI, biomass, direct and diffuse solar radiation, precipitation, temperature, and VPD, on the ecosystem-atmosphere exchange of energy, water vapour and carbon dioxide in East-Asian croplands. The influence of these factors should be considered to be incorporated into climatic and hydrological models. The new ideas for estimation of GPP, R_{eco} and ET over rapidly growing vegetation could provide useful approaches in the gap-filling strategy in order to improve the completeness of datasets and the reliability of seasonal estimation of energy and matter budgets.

Bibliography

- Alberto, M. C. R., Wassmann, R., Hirano, T., Miyata, A., Kumar, A., Padre, A., and Amante, M. (2009). CO₂/heat fluxes in rice fields: Comparative assessment of flooded and non-flooded fields in the Philippines. *Agricultural and Forest Meteorology*, 149: 1737–1750.
- Alberto, M. C. R., Wassmann, R., Hirano, T., Miyata, A., Hatano, R., Kumar, A., Padre, A., and Amante, M. (2011). Comparisons of energy balance and evapotranspiration between flooded and aerobic rice fields in the Philippines. *Agricultural Water Management*, 98: 1417–1430.
- Allen, R. (2005). Penman-Monteith equation. In Hillel, D., editor, *Encyclopedia of Soils in the Environment*. Elsevier, Oxford, 180–188.
- Allen, R., Pereira, L., Raes, D., and Smith, M. (1998). *Crop evapotranspiration: Guidelines for computing crop water requirements*. FAO Irrigation and drainage Paper 56. FAO, Rome, 300 pp.
- Allen, R., Walter, I., Elliott, R., Howell, T., Itenfisu, D., Jensen, M., and Snyder, R. (2005). *The ASCE Standardized Reference Evapotranspiration Equation*. American Society of Civil Engineers, 59 pp.
- Alves, I. and Pereira, L. S. (2000). Modelling surface resistance from climatic variables? *Agricultural Water Management*, 42: 371–385.
- Ammann, C., Flechard, C., Leifeld, J., Neftel, A., and Fuhrer, J. (2007). The carbon budget of newly established temperate grassland depends on management intensity. *Agriculture, Ecosystems and Environment*, 121: 5–20.
- Baldocchi, D. (2003). Assessing the eddy covariance technique for evaluating carbon dioxide exchange rates of ecosystems: past, present and future. *Global Change Biology*, 9: 479–492.
- Baldocchi, D., Falge, E., Gu, L., Olson, R., Hollinger, D., Running, S., Anthoni, P., Bernhofer, C., Davis, K., Evans, R., Fuentes, J., Goldstein, A., Katul, G., Law, B., Lee, X., Malhi, Y.,

- Meyers, T., Munger, W., Oechel, W., Paw, K. T., Pilegaard, K., Schmid, H. P., Valentini, R., Verma, S., Vesala, T., Wilson, K., and Wofsy, S. (2001). FLUXNET: a new tool to study the temporal and spatial variability of ecosystem-scale carbon dioxide, water vapor, and energy flux densities. *Bulletin of the American Meteorological Society*, 82: 2415–2434.
- Bassow, S. and Bazzaz, F. (1998). How environmental conditions affect canopy leaf-level photosynthesis in four deciduous tree species. *Ecology*, 79: 2660–2675.
- Beven, K. (1979). A sensitivity analysis of the Penman-Monteith actual evapotranspiration estimates. *Journal of Hydrology*, 44: 169–190.
- Beven, K. and Binley, A. (1992). The future of distributed models: model calibration and uncertainty prediction. *Hydrological Processes*, 6: 279–298.
- Béziat, P., Ceschia, E., and Dedieu, G. (2009). Carbon balance of a three crop succession over two cropland sites in South West France. *Agricultural and Forest Meteorology*, 149: 1628–1645.
- Cabangon, R., Tuong, T., Tiak, E., and bin Abdullah, N. (2002). Increasing water productivity in rice cultivation: impact of large-scale adoption of direct seeding in the Muda irrigation system. In *Direct Seeding in Asian Rice Systems: Strategic Research Issues and Opportunities*. Proceedings of an International Workshop on Direct Seeding in Asia, Bangkok, Thailand, 25–28 January 2000, 299–313.
- Campbell, C., Heilman, J., McInnes, K., Wilson, L., Medley, J., Wu, G., and Cobos, D. (2001). Diel and seasonal variation in CO₂ flux of irrigated rice. *Agricultural and Forest Meteorology*, 108: 15–27.
- Cassman, K. G., Dobermann, A., and Walters, D. T. (2002). Agroecosystems, nitrogen-use efficiency, and nitrogen management. *AMBIO*, 31: 132–140.
- Chameides, W. L., Yu, H., Liu, S. C., Bergin, M., Zhou, X., Mearns, L., Wang, G., Kiang, C. S., Saylor, R. D., Luo, C., Huang, Y., Steiner, A., and Giorgi, F. (1999). Case study of the effects of atmospheric aerosols and regional haze on agriculture: An opportunity to enhance crop yields in China through emission controls? *Proceedings of the National Academy of Sciences*, 96: 13626–13633.
- Chang, C.-P. (2004). *East Asian Monsoon*, volume 2. World Scientific Publishing Company Incorporated, 572 pp.

- Charuchittipan, D., Babel, W., Mauder, M., Beyich, F., Leps, J.-P., and Foken, T. (2014). Extension of the averaging time of the eddy-covariance measurement and its effect on the energy balance closure. *Boundary-Layer Meteorology*, accepted.
- Ciais, P., Wattenbach, M., Vuichard, N., Smith, P., Piao, S. L., Don, A., Luyssaert, S., Janssens, I. A., Bondeau, A., Dechow, R., Leip, A., Smith, P., Beer, C., Van Der Werf, G. R., Gervois, S., Van Oost, K., Tomelleri, E., Freibauer, A., Schulze, E. D., and Team, C. S. (2010). The European carbon balance. Part 2: croplands. *Global Change Biology*, 16: 1409–1428.
- Cleugh, H. A., Leuning, R., Mu, Q., and Running, S. W. (2007). Regional evaporation estimates from flux tower and MODIS satellite data. *Remote Sensing of Environment*, 106: 285–304.
- Desai, A., Bolstad, P., Cook, B., Davis, K., and Carey, E. (2005). Comparing net ecosystem exchange of carbon dioxide between an old-growth and mature forest in the upper Midwest, USA. *Agricultural and Forest Meteorology*, 128: 33–55.
- Ding, R., Kang, S., Li, F., Zhang, Y., and Tong, L. (2013). Evapotranspiration measurement and estimation using modified Priestley-Taylor model in an irrigated maize field with mulching. *Agricultural and Forest Meteorology*, 168: 140–148.
- Doss, B., King, C., and Patterson, R. (1970). Yield components and water use by silage corn with irrigation, plastic mulch, nitrogen fertilization, and plant spacing. *Agronomy Journal*, 62: 541–543.
- Eigenmann, R., Kalthoff, N., Foken, T., Dorninger, M., Kohler, M., Legain, D., Pigeon, G., Piguet, B., Schüttemeyer, D., and Traulle, O. (2011). Surface energy balance and turbulence network during the convective and orographically-induced precipitation study (COPS). *Quarterly Journal of the Royal Meteorological Society*, 137: 57–69.
- Fabeiro, C., Martín de Santa Olalla, F., and De Juan, J. (2001). Yield and size of deficit irrigated potatoes. *Agricultural Water Management*, 48: 255–266.
- Falge, E., Baldocchi, D., Olson, R., Anthoni, P., Aubinet, M., Bernhofer, C., Burba, G., Ceulemans, R., Clement, R., Dolman, H., Granier, A., Gross, P., Grünwald, T., Hollinger, D., Jensen, N.-O., Katul, G., Keronen, P., Kowalski, A., Lai, C. T., Law, B. E., Meyers, T., Moncrieff, J., Moors, E., Munger, J., Pilegaard, K., Üllar Rannik, Rebmann, C., Suyker, A., Tenhunen, J., Tu, K., Verma, S., Vesala, T., Wilson, K., and Wofsy, S. (2001). Gap

- filling strategies for defensible annual sums of net ecosystem exchange. *Agricultural and Forest Meteorology*, 107: 43–69.
- Finnigan, J., Clement, R., Malhi, Y., Leuning, R., and Cleugh, H. (2003). A re-evaluation of long-term flux measurement techniques. Part I: averaging and coordinate rotation. *Boundary-Layer Meteorology*, 107: 1–48.
- Foken, T. (2008a). The energy balance closure problem: An overview. *Ecological Applications*, 18: 1351–1367.
- Foken, T. (2008b). *Micrometeorology*. Springer, Berlin, Heidelberg, 308 pp.
- Foken, T. and Wichura, B. (1996). Tools for quality assessment of surface-based flux measurements. *Agricultural and Forest Meteorology*, 78: 83–105.
- Foken, T., Göckede, M., Mauder, M., Mahrt, L., Amiro, B., and Munger, W. (2004). Post-field data quality control. In Lee, X., Massman, W., and Law, B., editors, *Handbook of Micrometeorology*, volume 29 of *Atmospheric and Oceanographic Sciences Library*. Springer, Netherlands, 181–208.
- Foken, T., Mauder, M., Liebethal, C., Wimmer, F., Beyrich, F., Leps, J., Raasch, S., DeBruin, H., Meijninger, W., and Bange, J. (2010). Energy balance closure for the LITFASS-2003 experiment. *Theoretical and Applied Climatology*, 101: 149–160.
- Foken, T., Aubinet, M., Finnigan, J. J., Leclerc, M. Y., Mauder, M., and Paw U, K. T. (2011). Results of a panel discussion about the energy balance closure correction for trace gases. *Bulletin of the American Meteorological Society*, 92: ES13–ES18.
- Foken, T., Aubinet, M., and Leuning, R. (2012a). The eddy covariance method. In Aubinet, M., Vesala, T., and Papale, D., editors, *Eddy Covariance: A Practical Guide to Measurement and Data Analysis*. Springer, Dordrecht, 1–19.
- Foken, T., Leuning, R., Oncley, S., Mauder, M., and Aubinet, M. (2012b). Corrections and data quality control. In Aubinet, M., Vesala, T., and Papale, D., editors, *Eddy Covariance*, Springer Atmospheric Sciences. Springer, Dordrecht, 85–131.
- Foley, J. A., DeFries, R., Asner, G. P., Barford, C., Bonan, G., Carpenter, S. R., Chapin, F. S., Coe, M. T., Daily, G. C., Gibbs, H. K., Helkowski, J. H., Holloway, T., Howard, E. A., Kucharik, C. J., Monfreda, C., Patz, J. A., Prentice, I. C., Ramankutty, N., and Snyder, P. K. (2005). Global consequences of land use. *Science*, 309: 570–574.

- Garratt, J. (1992). The atmospheric boundary layer. Cambridge University Press, Cambridge, 316 pp.
- Göckede, M., Rebmann, C., and Foken, T. (2004). A combination of quality assessment tools for eddy covariance measurements with footprint modelling for the characterisation of complex sites. *Agricultural and Forest Meteorology*, 127: 175–188.
- Göckede, M., Markkanen, T., Hasager, C., and Foken, T. (2006). Update of a footprint-based approach for the characterisation of complex measurement sites. *Boundary-Layer Meteorology*, 118: 635–655.
- González-Sanpedro, M., Le Toan, T., Moreno, J., Kergoat, L., and Rubio, E. (2008). Seasonal variations of leaf area index of agricultural fields retrieved from Landsat data. *Remote Sensing of Environment*, 112: 810–824.
- Goulden, M., Munger, J., FAN, S., Daube, B., and Wofsy, S. (1996). Measurements of carbon sequestration by long-term eddy covariance: Methods and a critical evaluation of accuracy. *Global Change Biology*, 2: 169–182.
- Goulden, M. L., Daube, B. C., Fan, S.-M., Sutton, D. J., Bazzaz, A., Munger, J. W., and Wofsy, S. C. (1997). Physiological responses of a black spruce forest to weather. *Journal of Geophysical Research*, 102: 28987–28996.
- Greco, S. and Baldocchi, D. (1996). Seasonal variations of CO₂ and water vapour exchange rates over a temperate deciduous forest. *Global Change Biology*, 2: 183–197.
- Gu, L., Fuentes, J. D., Shugart, H. H., Staebler, R. M., and Black, T. A. (1999). Responses of net ecosystem exchanges of carbon dioxide to changes in cloudiness: Results from two North American deciduous forests. *Journal of Geophysical Research*, 104: 31421–31434.
- Gu, L., Baldocchi, D. D., Wofsy, S. C., Munger, J. W., Michalsky, J. J., Urbanski, S. P., and Boden, T. A. (2003). Response of a deciduous forest to the Mount Pinatubo eruption: Enhanced photosynthesis. *Science*, 299: 2035–2038.
- Ha, K.-J., Heo, K.-Y., Lee, S.-S., Yun, K.-S., and Jhun, J.-G. (2012). Variability in the East Asian monsoon: a review. *Meteorological Applications*, 19: 200–215.
- Hashimoto, R. (1990). Analysis of the morphology and structure of crowns in a young sugi (*Cryptomeria japonica*) stand. *Tree Physiology*, 6: 119–134.

- Hirano, T., Hirata, R., Fujinuma, Y., Saigusa, N., Yamamoto, S., Harazono, Y., Takada, M., Inukai, K., and Inoue, G. (2003). CO₂ and water vapor exchange of a larch forest in northern Japan. *Tellus B*, 55: 244–257.
- Hirata, R., Hirano, T., Saigusa, N., Fujinuma, Y., Inukai, K., Kitamori, Y., Takahashi, Y., and Yamamoto, S. (2007). Seasonal and interannual variations in carbon dioxide exchange of a temperate larch forest. *Agricultural and Forest Meteorology*, 147: 110–124.
- Hollinger, D. Y., Aber, J., Dail, B., Davidson, E. A., Goltz, S. M., Hughes, H., Leclerc, M. Y., Lee, J. T., Richardson, A. D., Rodrigues, C., Scott, N., Achuatavarier, D., and Walsh, J. (2004). Spatial and temporal variability in forest-atmosphere CO₂ exchange. *Global Change Biology*, 10: 1689–1706.
- Hossen, M. S., Baten, M. A., Khatun, R., and Miyata, A. (2007). Establishment of a flux study site in Bangladesh with its preliminary observation result. *AsiaFlux Newsletter*, 3.
- Hossen, M. S., Mano, M., Miyata, A., Baten, M., and Hiyama, T. (2012). Surface energy partitioning and evapotranspiration over a double-cropping paddy field in Bangladesh. *Hydrological Processes*, 26: 1311–1320.
- Hou, X. Y., Wang, F. X., Han, J. J., Kang, S. Z., and Feng, S. Y. (2010). Duration of plastic mulch for potato growth under drip irrigation in an arid region of Northwest China. *Agricultural and Forest Meteorology*, 150: 115–121.
- Ingwersen, J., Steffens, K., Högy, P., Warrach-Sagi, K., Zhunusbayeva, D., Poltoradnev, M., Gäbler, R., Wizemann, H.-D., Fangmeier, A., Wulfmeyer, V., and Streck, T. (2011). Comparison of Noah simulations with eddy covariance and soil water measurements at a winter wheat stand. *Agricultural and Forest Meteorology*, 151: 345–355.
- IPCC (2013). *Climate Change 2013: The Physical Science Basis. Working Group I Contribution to the Fifth Assessment Report of the Intergovernmental Panel on Climate Change*. Cambridge University Press, Cambridge, 1535 pp.
- IRRI (2009). *Rice production and processing*. <http://www.irri.org>.
- Janssens, I. A., Freibauer, A., Ciais, P., Smith, P., Nabuurs, G.-J., Folberth, G., Schlamadinger, B., Hutjes, R. W. A., Ceulemans, R., Schulze, E.-D., Valentini, R., and Dolman, A. J. (2003). Europe’s terrestrial biosphere absorbs 7 to 12% of European anthropogenic CO₂ emissions. *Science*, 300: 1538–1542.

- Jegede, O. O. and Foken, T. (1999). A study of the internal boundary layer due to a roughness change in neutral conditions observed during the LINEX field campaigns. *Theoretical and Applied Climatology*, 62: 31–41.
- Jo, K., Lee, H., Park, J., and Owen, J. (2010). Effects of monsoon rainfalls on surface water quality in a mountainous watershed under mixed land use. *Korean Journal of Agricultural and Forest Meteorology*, 12: 197–206.
- Kanda, M., Inagaki, A., Letzel, M. O., Raasch, S., and Watanabe, T. (2004). LES study of the energy imbalance problem with eddy covariance fluxes. *Boundary-Layer Meteorology*, 110: 381–404.
- Kang, S., Gu, B., Du, T., and Zhang, J. (2003). Crop coefficient and ratio of transpiration to evapotranspiration of winter wheat and maize in a semi-humid region. *Agricultural Water Management*, 59: 239–254.
- Kang, S., Su, X., Tong, L., Zhang, J., and Zhang, L. (2008). A warning from an ancient oasis: intensive human activities are leading to potential ecological and social catastrophe. *The International Journal of Sustainable Development and World Ecology*, 15: 440–447.
- Kar, G. and Kumar, A. (2007). Effects of irrigation and straw mulch on water use and tuber yield of potato in eastern India. *Agricultural Water Management*, 94: 109–116.
- Katerji, N. and Perrier, A. (1983). Modélisation de l'évapotranspiration réelle et d'une parcelle de luzerne: rôle d'un coefficient cultural. *Agronomie*, 3: 513–521.
- Katerji, N. and Rana, G. (2006). Modelling evapotranspiration of six irrigated crops under Mediterranean climate conditions. *Agricultural and Forest Meteorology*, 138: 142–155.
- Katerji, N., Rana, G., and Fahed, S. (2011). Parameterizing canopy resistance using mechanistic and semi-empirical estimates of hourly evapotranspiration: critical evaluation for irrigated crops in the Mediterranean. *Hydrological Processes*, 25: 117–129.
- Katul, G., Palmroth, S., and Oren, R. (2009). Leaf stomatal responses to vapour pressure deficit under current and CO₂-enriched atmosphere explained by the economics of gas exchange. *Plant, Cell and Environment*, 32: 968–979.
- Kucharik, C. and Twine, T. (2007). Residue, respiration, and residuals: Evaluation of a dynamic agroecosystem model using eddy flux measurements and biometric data. *Agricultural and Forest Meteorology*, 146: 134–158.

- Kutsch, W., Aubinet, M., Buchmann, N., Smith, P., Osborne, B., Eugster, W., Wattenbach, M., Schrumpf, M., Schulze, E., Tomelleri, E., Ceschia, E., Bernhofer, C., Béziat, P., Carrara, A., Tommasi, P. D., Grünwald, T., Jones, M., Magliulo, V., Marloie, O., Moureaux, C., Olioso, A., Sanz, M., Saunders, M., Sørensen, H., and Ziegler, W. (2010). The net biome production of full crop rotations in Europe. *Agriculture, Ecosystems and Environment*, 139: 336–345.
- Kwon, H., Park, T., Hong, J., Lim, J., and Kim, J. (2009). Seasonality of net ecosystem carbon exchange in two major plant functional types in Korea. *Asia-Pacific Journal of Atmospheric Sciences*, 45: 149–163.
- Kwon, H., Kim, J., Hong, J., and Lim, J. (2010). Influence of the Asian monsoon on net ecosystem carbon exchange in two major ecosystems in Korea. *Biogeosciences*, 7: 1493–1504.
- Landsberg, J. (1986). *Physiological Ecology of Forest Production*. Academic Press, Sydney, Australia, 198 pp.
- Lasslop, G., Reichstein, M., Papale, D., Richardson, A., Arneeth, A., Barr, A., Stoy, P., and Wohlfahrt, G. (2010). Separation of net ecosystem exchange into assimilation and respiration using a light response curve approach: critical issues and global evaluation. *Global Change Biology*, 16: 187–208.
- Lasslop, G., Migliavacca, M., Bohrer, G., Reichstein, M., Bahn, M., Ibrom, A., Jacobs, C., Kolari, P., Papale, D., Vesala, T., Wohlfahrt, G., and Cescatti, A. (2012). On the choice of the driving temperature for eddy-covariance carbon dioxide flux partitioning. *Biogeosciences Discussions*, 9: 9829–9873.
- Law, B., Falge, E., Gu, L., Baldocchi, D., Bakwin, P., Berbigier, P., Davis, K., Dolman, A., Falk, M., Fuentes, J., Goldstein, A., Granier, A., Grelle, A., Hollinger, D., Janssens, I., Jarvis, P., Jensen, N., Katul, G., Mahli, Y., Matteucci, G., Meyers, T., Monson, R., Munger, W., Oechel, W., Olson, R., Pilegaard, K., U, K. P., Thorgeirsson, H., Valentini, R., Verma, S., Vesala, T., Wilson, K., and Wofsy, S. (2002). Environmental controls over carbon dioxide and water vapor exchange of terrestrial vegetation. *Agricultural and Forest Meteorology*, 113: 97–120.
- Lecina, S., Martinez-Cob, A., Pérez, P., Villalobos, F., and Baselga, J. (2003). Fixed versus variable bulk canopy resistance for reference evapotranspiration estimation using the Penman-Monteith equation under semiarid conditions. *Agricultural Water Management*, 60: 181–198.

- Lee, S., Vinayachandran, P., Ha, K., and Jhun, J. (2010). Shift of peak in summer monsoon rainfall over Korea and its association with El Niño-Southern Oscillation. *Journal of Geophysical Research*, 115: D02111.
- Legates, D. and McCabe Jr, G. (1999). Evaluating the use of "goodness-of-fit" measures in hydrologic and hydroclimatic model validation. *Water Resources Research*, 35: 233–241.
- Lide, D. R., editor (2004). *CRC Handbook of Chemistry and Physics 2004-2005: A Ready-Reference Book of Chemical and Physical Data*. CRC press.
- Liebenthal, C. and Foken, T. (2007). Evaluation of six parameterization approaches for the ground heat flux. *Theoretical and Applied Climatology*, 88: 43–56.
- Liu, C., Zhang, X., and Zhang, Y. (2002). Determination of daily evaporation and evapotranspiration of winter wheat and maize by large-scale weighing lysimeter and micro-lysimeter. *Agricultural and Forest Meteorology*, 111: 109–120.
- Lloyd, J. and Taylor, J. (1994). On the temperature dependence of soil respiration. *Functional Ecology*, 315–323.
- Lüers, J., Detsch, F., and Zhao, P. (2014). Application of a multi-step error filter for post-processing atmospheric flux and meteorological basic data. *Universität Bayreuth, Abt. Mikrometeorologie*, in print, ISSN 1614-8916, Arbeitsergebnisse 58, 22 pp.
- Mauder, M. and Foken, T. (2004). Documentation and instruction manual of the eddy covariance software package TK2. *Univ., Abt. Mikrometeorologie, Universität Bayreuth, Abt. Mikrometeorologie, Print*, ISSN 1614-8916, Arbeitsergebnisse 26. 43 pp.
- Mauder, M. and Foken, T. (2006). Impact of post-field data processing on eddy covariance flux estimates and energy balance closure. *Meteorologische Zeitschrift*, 15: 597–609.
- Mauder, M. and Foken, T. (2011). Documentation and instruction manual of the eddy covariance software package TK3. *Universität Bayreuth, Abt. Mikrometeorologie, Print*, ISSN 1614-8916, Arbeitsergebnisse 46. 58 ppm.
- Mauder, M., Liebenthal, C., Göckede, M., Leps, J., Beyrich, F., and Foken, T. (2006). Processing and quality control of flux data during LITFASS-2003. *Boundary-Layer Meteorology*, 121: 67–88.
- Mauder, M., Desjardins, R., Oncley, S. P., and MacPherson, I. (2007). Atmospheric response to a partial solar eclipse over a cotton field in central California. *Journal of Applied Meteorology and Climatology*, 46: 1792–1803.

- McCuen, R. H. (1974). A sensitivity and error analysis of procedures used for estimating evaporation¹. *JAWRA Journal of the American Water Resources Association*, 10: 486–497.
- Mercado, L. M., Bellouin, N., Sitch, S., Boucher, O., Huntingford, C., Wild, M., and Cox, P. M. (2009). Impact of changes in diffuse radiation on the global land carbon sink. *Nature*, 458: 1014–1017.
- Michaelis, L. and Menten, M. (1913). Die kinetik der invertinwirkung. *Biochemische Zeitschrift*, 49: 352.
- Millennium Ecosystem Assessment (2005). *Ecosystems and Human Well-being: Synthesis*. Island Press, Washington, DC., 137 pp.
- Miyata, A., Leuning, R., Denmead, O., Kim, J., and Harazono, Y. (2000). Carbon dioxide and methane fluxes from an intermittently flooded paddy field. *Agricultural and Forest Meteorology*, 102: 287–303.
- Miyata, A., Iwata, T., Nagai, H., Yamada, T., Yoshikoshi, H., Mano, M., Ono, K., Han, G., Harazono, Y., Ohtaki, E., Baten, M. A., Inohara, S., Takimoto, T., and Saito, M. (2005). Seasonal variation of carbon dioxide and methane fluxes at single cropping paddy fields in central and western Japan. *Phyton*, 45: 89–97.
- Moffat, A. M., Papale, D., Reichstein, M., Hollinger, D. Y., Richardson, A. D., Barr, A. G., Beckstein, C., Braswell, B. H., Churkina, G., Desai, A. R., Falge, E., Gove, J. H., Heimann, M., Hui, D., Jarvis, A. J., Kattge, J., Noormets, A., and Stauch, V. J. (2007). Comprehensive comparison of gap-filling techniques for eddy covariance net carbon fluxes. *Agricultural and Forest Meteorology*, 147: 209–232.
- Moffat, A. M., Beckstein, C., Churkina, G., Mund, M., and Heimann, M. (2010). Characterization of ecosystem responses to climatic controls using artificial neural networks. *Global Change Biology*, 16: 2737–2749.
- Monteith, J. (1965). Evaporation and environment. In *Symposia of the Society for Experimental Biology*, volume 19, 205 pp.
- Montgomery, R. (1948). Vertical eddy flux of heat in the atmosphere. *Journal of Atmospheric Sciences*, 5: 265–274.

- Moon, B., Hong, J., Lee, B., Yun, J., Park, E., and Kim, J. (2003). CO₂ and energy exchange in a rice paddy for the growing season of 2002 in Hari, Korea. *Korean Journal of Agricultural and Forest Meteorology*, 5: 51–60.
- Nash, J. and Sutcliffe, J. (1970). River flow forecasting through conceptual models. Part I — a discussion of principles. *Journal of Hydrology*, 10: 282 – 290.
- Nemani, R. R. and Running, S. W. (1989). Testing a theoretical climate-soil-leaf area hydrologic equilibrium of forests using satellite data and ecosystem simulation. *Agricultural and Forest Meteorology*, 44: 245–260.
- Niyogi, D., Chang, H.-I., Saxena, V. K., Holt, T., Alapaty, K., Booker, F., Chen, F., Davis, K. J., Holben, B., Matsui, T., Meyers, T., Oechel, W. C., Pielke, R. A., Wells, R., Wilson, K., and Xue, Y. (2004). Direct observations of the effects of aerosol loading on net ecosystem CO₂ exchanges over different landscapes. *Geophysical Research Letters*, 31.
- Noormets, A., Chen, J., and Crow, T. R. (2007). Age-dependent changes in ecosystem carbon fluxes in managed forests in northern Wisconsin, USA. *Ecosystems*, 10: 187–203.
- Oliphant, A. J. (2012). Terrestrial ecosystem-atmosphere exchange of CO₂, water and energy from FLUXNET: Review and meta-analysis of a global in-situ observatory. *Geography Compass*, 6: 689–705.
- Onckley, S. P., Foken, T., Vogt, R., Kohsiek, W., DeBruin, H., Bernhofer, C., Christen, A., Gorsel, E., Grantz, D., Feigenwinter, C., Lehner, I., Liebethal, C., Liu, H., Mauder, M., Pitacco, A., Ribeiro, L., and Weidinger, T. (2007). The energy balance experiment EBEX-2000. Part I: overview and energy balance. *Boundary-Layer Meteorology*, 123: 1–28.
- Oren, R., Sperry, J., Katul, G., Pataki, D., Ewers, B., Phillips, N., and Schäfer, K. (1999). Survey and synthesis of intra-and interspecific variation in stomatal sensitivity to vapour pressure deficit. *Plant, Cell and Environment*, 22: 1515–1526.
- Osborne, B., Saunders, M., Walmsley, D., Jones, M., and Smith, P. (2010). Key questions and uncertainties associated with the assessment of the cropland greenhouse gas balance. *Agriculture, Ecosystems and Environment*, 139: 293–301.
- Osborne, T., Lawrence, D., Challinor, A., Slingo, J., and Wheeler, T. (2007). Development and assessment of a coupled crop-climate model. *Global Change Biology*, 13: 169–183.

- Otieno, D., Wartinger, M., Nishiwaki, A., Hussain, M., Muhr, J., Borken, W., and Lischeid, G. (2009). Responses of CO₂ exchange and primary production of the ecosystem components to environmental changes in a mountain peatland. *Ecosystems*, 12: 590–603.
- Papale, D. (2012). Data gap filling. In Aubinet, M., Vesala, T., and Papale, D., editors, *Eddy Covariance*, Springer Atmospheric Sciences. Springer, Dordrecht, 159-172.
- Papale, D., Reichstein, M., Aubinet, M., Canfora, E., Bernhofer, C., Kutsch, W., Longdoz, B., Rambal, S., Valentini, R., Vesala, T., and Yakir, D. (2006). Towards a standardized processing of net ecosystem exchange measured with eddy covariance technique: algorithms and uncertainty estimation. *Biogeosciences*, 3: 571–583.
- Parent, A. and Anctil, F. (2012). Quantifying evapotranspiration of a rainfed potato crop in South-eastern Canada using eddy covariance techniques. *Agricultural Water Management*, 113: 45–56.
- Pauwels, V. and Samson, R. (2006). Comparison of different methods to measure and model actual evapotranspiration rates for a wet sloping grassland. *Agricultural Water Management*, 82: 1–24.
- Penman, H. (1948). Natural evaporation from open water, bare soil and grass. *Proceedings of the Royal Society of London. Series A. Mathematical and Physical Sciences*, 193: 120–145.
- Perez, P. J., Lecina, S., Castellvi, F., Martínez-Cob, A., and Villalobos, F. (2006). A simple parameterization of bulk canopy resistance from climatic variables for estimating hourly evapotranspiration. *Hydrological Processes*, 20: 515–532.
- Prescher, A., Grünwald, T., and Bernhofer, C. (2010). Land use regulates carbon budgets in eastern Germany: From NEE to NBP. *Agricultural and Forest Meteorology*, 150: 1016–1025.
- Rana, G. and Katerji, N. (2000). Measurement and estimation of actual evapotranspiration in the field under Mediterranean climate: a review. *European Journal of Agronomy*, 13: 125–153.
- Rana, G., Katerji, N., Mastrorilli, M., and El Moujabber, M. (1994). Evapotranspiration and canopy resistance of grass in a Mediterranean region. *Theoretical and Applied Climatology*, 50: 61–71.

- Rana, G., Katerji, N., Mastrorilli, M., and El Moujabber, M. (1997a). A model for predicting actual evapotranspiration under soil water stress in a Mediterranean region. *Theoretical and Applied Climatology*, 56: 45–55.
- Rana, G., Katerji, N., Mastrorilli, M., El Moujabber, M., and Brisson, N. (1997b). Validation of a model of actual evapotranspiration for water stressed soybeans. *Agricultural and Forest Meteorology*, 86: 215–224.
- Rana, G., Katerji, N., and Perniola, M. (2001). Evapotranspiration of sweet sorghum: A general model and multilocal validity in semiarid environmental conditions. *Water Resources Research*, 37: 3237–3246.
- Rana, G., Katerji, N., and de Lorenzi, F. (2005). Measurement and modelling of evapotranspiration of irrigated citrus orchard under Mediterranean conditions. *Agricultural and Forest Meteorology*, 128: 199–209.
- Rannik, Ü., Aubinet, M., Kurbanmuradov, O., Sabelfeld, K., Markkanen, T., and Vesala, T. (2000). Footprint analysis for measurements over a heterogeneous forest. *Boundary-Layer Meteorology*, 97: 137–166.
- Reichstein, M., Falge, E., Baldocchi, D., Papale, D., Aubinet, M., Berbigier, P., Bernhofer, C., Buchmann, N., Gilmanov, T., Granier, A., Grünwald, T., Havránková, K., Ilvesniemi, H., Janous, D., Knohl, A., Laurila, T., Lohila, A., Loustau, D., Matteucci, G., Meyers, T., Miglietta, F., Ourcival, J.-M., Pumpanen, J., Rambal, S., Rotenberg, E., Sanz, M., Tenhunen, J., Seufert, G., Vaccari, F., Vesala, T., Yakir, D., and Valentini, R. (2005). On the separation of net ecosystem exchange into assimilation and ecosystem respiration: review and improved algorithm. *Global Change Biology*, 11: 1424–1439.
- Richardson, A. and Hollinger, D. (2007). A method to estimate the additional uncertainty in gap-filled NEE resulting from long gaps in the CO₂ flux record. *Agricultural and Forest Meteorology*, 147: 199–208.
- Roderick, M. L., Farquhar, G. D., Berry, S. L., and Noble, I. R. (2001). On the direct effect of clouds and atmospheric particles on the productivity and structure of vegetation. *Oecologia*, 129: 21–30.
- Ruidisch, M., Kettering, J., Arnhold, S., and Huwe, B. (2013). Modeling water flow in a plastic mulched ridge cultivation system on hillslopes affected by South Korean summer monsoon. *Agricultural Water Management*, 116: 204–217.

- Ruppert, J., Mauder, M., Thomas, C., and Lüers, J. (2006). Innovative gap-filling strategy for annual sums of CO₂ net ecosystem exchange. *Agricultural and Forest Meteorology*, 138: 5–18.
- Ryan, M. (1990). Growth and maintenance respiration in stems of *pinus contorta* and *picea engelmannii*. *Canadian Journal of Forest Research*, 20: 48–57.
- Saito, M., Miyata, A., Nagai, H., and Yamada, T. (2005). Seasonal variation of carbon dioxide exchange in rice paddy field in Japan. *Agricultural and Forest Meteorology*, 135: 93–109.
- Sakai, R. K., Fitzjarrald, D. R., Moraes, O. L., Staebler, R. M., Acevedo, O. C., Czikowsky, M. J., Silva, R. d., Brait, E., and Miranda, V. (2004). Land-use change effects on local energy, water, and carbon balances in an Amazonian agricultural field. *Global Change Biology*, 10: 895–907.
- Savelyev, S. A. and Taylor, P. A. (2005). Internal boundary layers: I. height formulae for neutral and diabatic flows. *Boundary-Layer Meteorology*, 115: 1–25.
- Saxe, H., Cannell, M., Johnsen, Ø., Ryan, M., and Vourlitis, G. (2002). Tree and forest functioning in response to global warming. *New Phytologist*, 149: 369–399.
- Shi, T., Guan, D., Wang, A., Wu, J., Jin, C., and Han, S. (2008). Comparison of three models to estimate evapotranspiration for a temperate mixed forest. *Hydrological Processes*, 22: 3431–3443.
- Sonntag, D. (1990). Important new values of the physical constants of 1986, vapour pressure formulations based on the ITS-90, and psychrometer formulae. *Zeitschrift für Meteorologie*, 70: 340–344.
- Steduto, P., Todorovic, M., Caliendo, A., and Rubino, P. (2003). Daily reference evapotranspiration estimates by the Penman-Monteith equation in Southern Italy. constant vs. variable canopy resistance. *Theoretical and Applied Climatology*, 74: 217–225.
- Stoy, P., Katul, G., Siqueira, M., Juang, J., Novick, K., Uebelherr, J., and Oren, R. (2006). An evaluation of models for partitioning eddy covariance-measured net ecosystem exchange into photosynthesis and respiration. *Agricultural and Forest Meteorology*, 141: 2–18.
- Sumner, D. and Jacobs, J. (2005). Utility of Penman-Monteith, Priestley-Taylor, reference evapotranspiration, and pan evaporation methods to estimate pasture evapotranspiration. *Journal of Hydrology*, 308: 81–104.

- Tabbal, D., Bouman, B., Bhuiyan, S., Sibayan, E., and Sattar, M. (2002). On-farm strategies for reducing water input in irrigated rice: case studies in the Philippines. *Agricultural Water Management*, 56: 93–112.
- Taylor, K. (2001). Summarizing multiple aspects of model performance in a single diagram. *Journal of Geophysical Research*, 106: 7183–7192.
- Tolk, J. A., Howell, T. A., and Evett, S. R. (1998). Evapotranspiration and yield of corn grown on three high plains soils. *Agronomy Journal*, 90: 447–454.
- Tsai, J., Tsuang, B., Lu, P., Yao, M., and Shen, Y. (2007). Surface energy components and land characteristics of a rice paddy. *Journal of Applied Meteorology and Climatology*, 46: 1879–1900.
- Tsai, J., Tsuang, B., Lu, P., Chang, K., Yao, M., and Shen, Y. (2010). Measurements of aerodynamic roughness, Bowen ratio, and atmospheric surface layer height by eddy covariance and tethersonde systems simultaneously over a heterogeneous rice paddy. *Journal of Hydrometeorology*, 11: 452–466.
- Twine, T. E., Kustas, W., Norman, J., Cook, D., Houser, P., Meyers, T., Prueger, J., Starks, P., and Wesely, M. (2000). Correcting eddy-covariance flux underestimates over a grassland. *Agricultural and Forest Meteorology*, 103: 279–300.
- Walker, W. (1989). Guidelines for designing and evaluating surface irrigation systems. FAO irrigation and drainage paper 45. Food and Agriculture Organization of the United Nations, 137 pp.
- Wang, J., Rich, P., and Price, K. (2003). Temporal responses of NDVI to precipitation and temperature in the central Great Plains, USA. *International Journal of Remote Sensing*, 24: 2345–2364.
- Wang, K. and Dickinson, R. E. (2012). A review of global terrestrial evapotranspiration: Observation, modeling, climatology, and climatic variability. *Reviews of Geophysics*, 50: RG2005.
- Willmott, C. J. (1981). On the validation of models. *Physical Geography*, 2: 184–194.
- Wu, J., der Linden, L., Lasslop, G., Carvalhais, N., Pilegaard, K., Beier, C., and Ibrom, A. (2012). Effects of climate variability and functional changes on the interannual variation of the carbon balance in a temperate deciduous forest. *Biogeosciences*, 9: 13–28.

- Xing, Z., Bourque, C., Meng, F., Zha, T., Cox, R., and Swift, D. (2007). A simple net ecosystem productivity model for gap filling of tower-based fluxes: An extension of Landsberg's equation with modifications to the light interception term. *Ecological Modelling*, 206: 250–262.
- Yun, K., Shin, S., Ha, K., Kitoh, A., and Kusunoki, S. (2008). East Asian precipitation change in the global warming climate simulated by a 20-km mesh AGCM. *Asia-Pacific Journal of Atmospheric Sciences*, 44: 233–247.
- Zhao, P., Lüers, J., Olesch, J., and Foken, T. (2011). Complex TERRain and ECOlogical heterogeneity (TERRECO): WP 1-02: Spatial assessment of atmosphere-ecosystem exchanges via micrometeorological measurements, footprint modeling and mesoscale simulations ; documentation of the observation period May 12th to Nov. 8th, 2010, Haean, South Korea. Universität Bayreuth, Abt. Mikrometeorologie, Print, ISSN 1614-8916, Arbeitsergebnisse 45. 43 pp.
- Zhao, W., Liu, B., and Zhang, Z. (2010). Water requirements of maize in the middle Heihe River basin, China. *Agricultural Water Management*, 97: 215–223.
- Zhao, X., Huang, Y., Jia, Z., Liu, H., Song, T., Wang, Y., Shi, L., Song, C., and Wang, Y. (2008). Effects of the conversion of marshland to cropland on water and energy exchanges in northeastern China. *Journal of Hydrology*, 355: 181–191.
- Zhou, L.-M., Li, F.-M., Jin, S.-L., and Song, Y. (2009). How two ridges and the furrow mulched with plastic film affect soil water, soil temperature and yield of maize on the semiarid loess Plateau of China. *Field Crops Research*, 113: 41–47.

(Eidesstattliche) Versicherungen und Erklärungen

(§ 8 S. 2 Nr. 6 PromO)

Hiermit erkläre ich mich damit einverstanden, dass die elektronische Fassung meiner Dissertation unter Wahrung meiner Urheberrechte und des Datenschutzes einer gesonderten Überprüfung hinsichtlich der eigenständigen Anfertigung der Dissertation unterzogen werden kann.

(§ 8 S. 2 Nr. 8 PromO)

Hiermit erkläre ich eidesstattlich, dass ich die Dissertation selbständig verfasst und keine anderen als die von mir angegebenen Quellen und Hilfsmittel benutzt habe.

(§ 8 S. 2 Nr. 9 PromO)

Ich habe die Dissertation nicht bereits zur Erlangung eines akademischen Grades anderweitig eingereicht und habe auch nicht bereits diese oder eine gleichartige Doktorprüfung endgültig nicht bestanden.

(§ 8 S. 2 Nr. 10 PromO)

Hiermit erkläre ich, dass ich keine Hilfe von gewerbliche Promotionsberatern bzw. -vermittlern in Anspruch genommen habe und auch künftig nicht nehmen werde.

Ort, Datum, Unterschrift